COMMITTEE CERTIFICATION OF APPROVED VERSION

The committee for Payal R. Sheth certifies that this is the approved version of the following dissertation:

A MECHANISM OF ACTIVATION OF C-MET RECEPTOR TYROSINE KINASE

Committee:

Stanley J. Watowich, Ph.D.

Lisa A. Elferink, Ph.D.

Rolf Konig, Ph.D.

Bing Su, Ph.D.

Vincent J. Hilser , Ph.D.

James C. Lee, Ph.D.

Dean, Graduate School

A MECHANISM OF ACTIVATION OF C-MET RECEPTOR TYROSINE KINASE

by

Payal R. Sheth, B.E.

Dissertation
Presented to the Faculty of the University of Texas Graduate School of
Biomedical Sciences at Galveston
in Partial Fulfillment of the Requirements
for the Degree of

Doctor of Philosophy

Approved by the Supervisory Committee

Stanley J. Watowich, Ph.D.
Lisa A. Elferink, Ph.D.
Rolf Konig, Ph.D.
Bing Su, Ph.D.
Vincent J. Hilser, Ph.D.
James C. Lee, Ph.D.

July 2006
Galveston, Texas

Key Words: cell signaling, cancer

Dedicated to my grandparents, Rameshchandra Vrajlal Sheth and Prabhavati Premchand Shah , who are and will always be my biggest fans

ACKNOWLEDGMENTS

I wish to thank Dr. Stan Watowich for his steadfast support and encouragement during the course of my graduate tenure. He has been extremely supportive and has always challenged me to do my very best and produce the best science possible. I thank my committee members Drs Lisa Elferink, James Lee, Vincent Hilser, Rolf Konig, and Bing Su for their ideas and suggestions for my project. I would especially like to acknowledge Drs Lee and Elferink, who have been like my co-mentors during the past few years, giving me extra encouragement when I truly needed it. I would like to thank Dr. Lynn Soong and the members of the McLaughlin Committee for choosing me as a recipient of the James W. McLaughlin fellowship. Special thanks to the members of Watowich laboratory, past and present, for being excellent colleagues and good friends, especially John Hays, who helped me during the early stages of this project. Yvette Boyd has been a phenomenal support-system for me, helping me with anything and everything, administration-related or otherwise. I would also like to acknowledge the excellent support that I have received from the Biochemistry and Molecular Biology department especially from the director Dr. Lillian Chan and coordinator Debora Botting.

One of the most admirable aspects of working in UTMB is the camaraderie we share with our neighboring labs. The Watowich lab have been extremely fortunate to share the floor with some of the nicest PIs including Drs Papaconstantinou and Srivastava, whose labs and the equipments therein are always accessible to us for our research. We have also been very fortunate to have collaborations with some of the best labs in the country for our project (Lisa Elferink (UTMB), Morag Park (McGill University), and George Vande Woude (Van Andel Research Institute)).

I am truly lucky to have the love and support of my dear husband, Kunal Ashar, who has been my lifeline throughout these years. He has provided the balance I have needed during the stressful times, and without him, I doubt if I would have been able to go through this journey by myself. I would also like to thank my parents Dipika and Rajiv Sheth, without whom I would never have been able to achieve so much. My friends Marta Lorinczi, Lokesh Rao, Lakshmi Pillai, Sujal Deshmukh, Jen Crawford, and everyone at the BCSO, thank you for being there for me and keeping me sane!

A MECHANISM OF ACTIVATION OF C-MET RECEPTOR TYROSINE KINASE

Publication No. _____
Payal R. Sheth, Ph.D.
The University of Texas Medical Branch at Galveston, July 2006

Supervisor: Stanley J. Watowich

c-MET receptor tyrosine kinase-mediated signaling governs numerous important cellular responses including cellular proliferation, differentiation, migration and apoptosis. Deregulation of these signals result in malignant behaviors, often leading to cancers. While the identity of the many signaling molecules that are activated following hepatocyte-growth factor (HGF)-induced activation of c-MET had been established, little was known about the mechanism of activation of c-MET. From a therapeutic perspective, it is necessary to understand the detailed molecular mechanisms regulating c-MET activation to selectively target these molecules. c-MET, in presence of its cognate ligand, is oligomerized, and is autophosphorylated on specific tyrosines on its cytoplasmic domain. The phosphorylated tyrosines in specific sub-domains of c-MET cytoplasmic region perform specific functions including increase in catalytic activity and recruitment of effector molecules. Classically, it has been believed that the sole role of ligand-induced oligomerization was to autophosphorylate the receptor, thereby switching the receptor's kinase activity on. However, in light of a recent body of evidence suggesting that certain RTKs are kinase active on cell surface in absence of ligand-induced oligomerization, we hypothesized that oligomerization could be important for other aspects of RTK activation. Using c-MET as our model system, we investigated the role of oligomerization, irrespective of its role in autophosphorylation, in regulating c-MET activation. Previous studies from our laboratory have conclusively shown that oligomerization increases c-MET's substrate binding affinity and substrate phosphorylation k_{cat}. The work presented here addresses the role of oligomerization in regulating c-MET's susceptibility to dephosphorylation, another important regulator of c-MET activation. The biochemical parameters measured for c-MET are used to build a unified kinetic model for c-MET activation. The model building and its subsequent validation using cell culture experiments are described here. Furthermore, the model is probed using parameter sensitivity analyses to understand how oligomerization-induced changes in the kinetic, thermodynamic and dephosphorylation properties of c-MET work synergistically to selectively induce specific signaling from the dimeric and not the monomeric receptor. Using these data, we propose an alternative feed-forward model for c-MET activation mechanism differs from the traditional view of the RTK activation.

TABLE OF CONTENTS

Page

LIST OF TABLES

Page

LIST OF FIGURES

Page

LIST OF ABBREVIATIONS

AL- Activation loop
ATP- Adenosine triphosphate
CHAPS- 3-[(3-cholamideopropyl) dimethylammoniol-1-propanesulfonic acid
CIAP- Calf intestinal alkaline phosphatase
Crk- Regulator of kinase
DTT- Dithiothreitol
EGF- Epidermal growth factor
FGF- Fibroblast growth factor
Gab1- Grb2-associated binder
Grb2- Growth factor receptor bound protein
HGF- Hepatocyte growth factor
InlB- Internalin B
IR- Insulin receptor
LAR- leukocyte common antigen-related
PDGF- Platelet-derived growth factor
PI3K- Phosphatidyl inositol 3-kinase
PKB- PI3K protein kinase B
PLC- Phospholipase C
PTB- Protein tyrosine binding
PTP- Protein tyrosine phosphatase
pTyr- phosphorylated tyrosine-containing effector
pY- phosphotyrosine
SF- Scatter factor
SH2- Src homology 2
Shc- SH2 containing protein
RTK- Receptor tyrosine kinase
Tyr- Tyrosine-containing effector
VEGF- Vascular endothelial growth factor
Y- Tyrosine amino acid

INTRODUCTION

Reversible phosphorylation is one of the most common post-translational modifications that proteins undergo. Since the discovery of protein phosphorylation (Fischer and Krebs 1955), several decades of work has been focused on trying to characterize this event, and its role as a 'biological-switch'. Kinases are the enzymes that catalyze the transfer of γ-phosphate from ATP to an amino acid on the proteins. Thus, kinases are the positive regulators of this biological switch. Kinases are further characterized into distinct sub-classes (tyrosine, serine-threonine) depending on their amino-acid specificity. The tyrosine kinase sub-family of kinases is further sub-divided into receptor and non-receptor tyrosine kinases. Receptor tyrosine kinases (RTK) have been extensively characterized with respect to their role in cell signaling.

The strength and duration of numerous intracellular signaling responses are dependent on c-MET RTK activation, defined as sustained c-MET phosphorylation and subsequent downstream signaling. c-MET activation is a critical and tightly regulated process in normal functioning of cells; aberrant signaling has been linked to pathological conditions including tumorigenesis and metastasis. Recently, much effort in academia as well as pharmaceutical industry has been focused on trying to develop therapeutic strategies that can result in blocking of RTK activation. However, in order to effectively block these molecules, we first need to gain a detailed mechanistic understanding of how they function. Unfortunately, little was known about the biochemical basis of activation of c-MET or other RTKs, in general. In this work, we highlight some of our significant advances towards understanding c-MET activation, with particular emphasis on the role of dimerization in this process.

CHAPTER 1:
C-MET RECEPTOR TYROSINE KINASE -STRUCTURE FUNCTION AND ENZYMATIC REGULATION[1]

C-MET RECEPTOR TYROSINE KINASE & HEPATOCYTE GROWTH FACTOR/SCATTER FACTOR

c-MET structure

c-MET, the receptor tyrosine kinase (RTK) for hepatocyte growth factor (HGF)/scatter factor (SF), was first identified as an oncogene mediating the chemically induced transformation of a human osteogenic sarcoma cell line (Cooper *et al.* 1984). Cellular physiological functions of c-MET include, but are not limited to, proliferation, differentiation, motility and survival. c-MET is single-pass transmembrane glycoprotein that consists of an extracellular region that possesses the specificity for the ligands, and a cytoplasmic region that harbors the tyrosine kinase catalytic activity (Hubbard and Till 2000; Pazin and Williams 1992; Ullrich and Schlessinger 1990). Related members of the RTK family include receptors for epidermal growth factor (EGF), platelet-derived growth factor (PDGF), fibroblast growth factor (FGF) and insulin. While the intracellular domains of different RTKs are highly conserved, the extracellular domains contain multiple structurally distinct regions that form the basis of further classification of RTKs (Blume-Jensen and Hunter 2001; Hubbard and Till 2000).

c-MET sub-family of RTKs includes MET, RON, and SEA. These receptors have a short α-chain and a longer β-chain linked together by a disulfide bond (Huff *et al.* 1993; Ronsin *et al.* 1993).

---

[1] Reproduced with permission from the following source: Gene Therapy Press (http://www.cancer-therapy.org); Sheth P. R., Watowich, S. J. 2006. Biochemical ground-rules regulating c-MET receptor tyrosine kinase activation. *Cancer Ther*. Jan 26;4 (A):1-15

This heterodimeric structure results from furin cleavage of a single-chain precursor. The mature form of c-MET constitutes an extracellular 45kDa α-chain and a 190kDa membrane-spanning β-chain. The β-chain consists of an extracellular region, a membrane spanning region and a cytoplasmic region containing the signaling elements - the juxtamembrane element, the catalytic domain and the carboxy-terminal tail (**Fig. 1.1**). The extracellular region contains a *sema* domain with marked structural similarity to extracellular domains of semaphorins and plexins (Winberg *et al.* 1998), a small cysteine rich PSI domain similar to those found in plexins, semaphorins and integrins (Bork *et al.* 1999) and four IgG-like domains with similarity to the IgG domains present in plexins and transcription factors (Ohta *et al.* 1995). Structural and biochemical studies have shown that c-MET *sema* domain forms a high-affinity binding site for HGF (Gherardi *et al.* 2003; Stamos *et al.* 2004). The residues critical for HGF binding in c-MET have been mapped and are contained within the α-chain and 212 residues of the β-chain (Gherardi *et al.* 2003). Recent structural studies have revealed the domain architecture of the c-MET extracellular region, and have shed light on the mechanism of HGF-c-MET interactions (Kozlov *et al.* 2004; Stamos *et al.* 2004).

The cytoplasmic catalytic domain of c-MET is highly conserved amongst RTKs. Several structures of this domain in an unphosphorylated and phosphorylated state have been determined (Hubbard 1997; Hubbard *et al.* 1994; Mohammadi *et al.* 1998; Mohammadi *et al.* 1996; Schiering *et al.* 2003). The catalytic domain folds into distinct N-terminal and C-terminal lobes, connected via a flexible polypeptide linker. The N-terminal and C-terminal lobes are formed predominantly by β-sheets and α-helices respectively. The ATP substrate binds within a cleft formed between the two lobes, and the peptide substrate binds to the C-terminal lobe. Crystal structure of insulin receptor (IR) catalytic domain in the phosphorylated and unphosphorylated state provided a structural basis of the observed increase in the catalytic activity upon activation loop (AL) phosphorylation (Hubbard 1997; Hubbard *et al.* 1994). The activation loop is a segment of amino acids in the catalytic domain that contains one or more tyrosine residues that are autophosphorylated (**Fig. 1.2).** Within apo IR, the AL traverses the cleft

between the N-terminal and the C-terminal lobes, thus obstructing the ATP binding site (Hubbard *et al.* 1994). The AL conformation in the unphosphorylated and phosphorylated forms in IR, showed dramatic differences, which impact the ability of ATP to access the kinase catalytic site (Hubbard 1997).

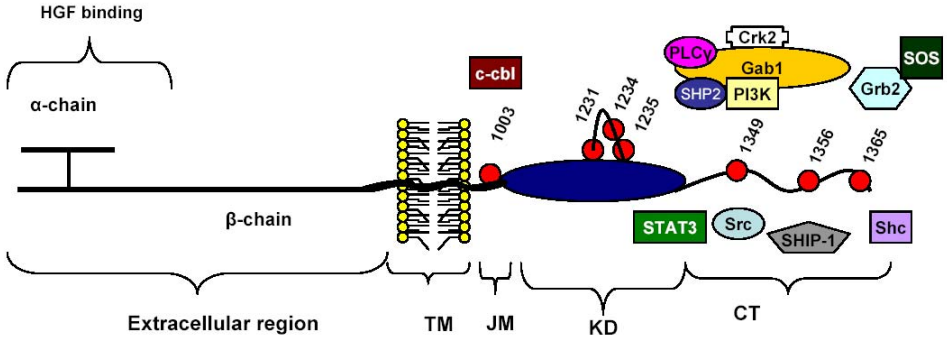

Fig. 1.1. Domain map of c-MET.

c-MET is composted of an α and β chain linked together via a single disulfide bond. The β chain includes the extracellular, transmembrane (TM), and the cytoplasmic regions. The cytoplasmic region contains the signaling apparatus consisting of the juxtamembrane region (JM), the kinase domain (KD), and carboxy-terminal tail (CT). HGF binds to the extracellular region of c-MET and signal transduction is mediated in part by the phosphorylation of residues in the multifunctional docking sites (Y1349, Y1356 and Y1365). c-MET catalytic activity is positively regulated by the phosphorylation of tyrosine residues 1231, 1234 and 1235 in the catalytic domain. Phosphorylation of juxtamembrane residue Y1003 is important for c-MET degradation. The important effectors of c-MET are also shown.

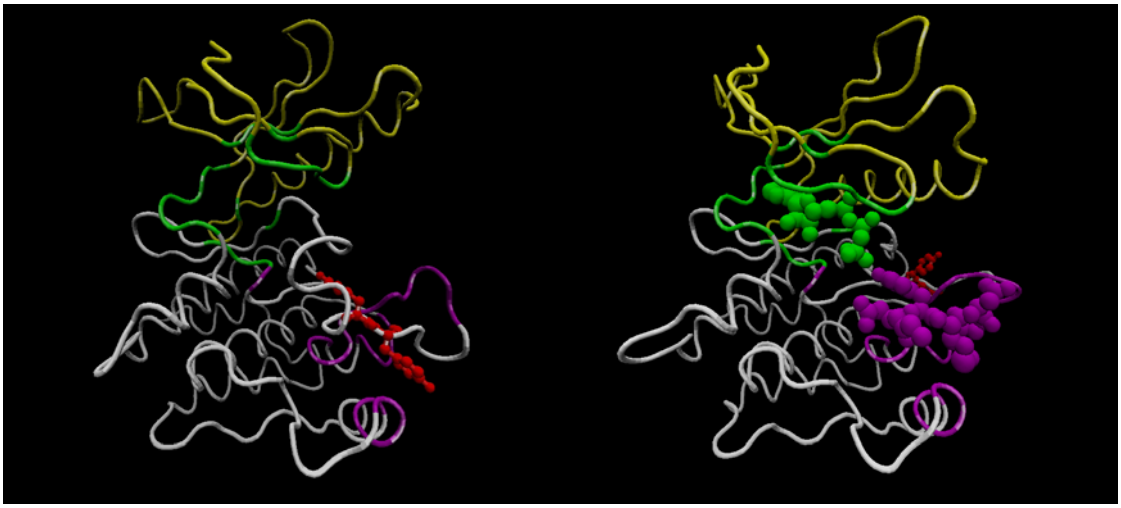

Fig. 1.2. Kinase domain structure of Insulin Receptor (IR).
The structure for IRK in its apo and in ternary complex with ATP and substrate is shown. The autophosphorylation of the AL tyrosines increases the receptor's kinase catalytic activity.

In FGFR, autoinhibition occurs via a different mechanism: a proline residue in the AL together with flanking residues occlude the substrate binding site (Mohammadi *et al.* 1996). Crystal structures of apo and inhibitor-bound forms of the c-MET catalytic domain showed the characteristic kinase bilobal structure described above (**Fig. 1.3)** (Schiering *et al.* 2003). The AL loop residues in the apo c-MET were disordered. However, the structure of the c-MET: inhibitor binary complex showed a unique AL conformation. This conformation may represent a quasi-stable intermediate state along the transition pathway between phosphorylated and unphosphorylated AL conformations, although it is possible this conformation is an artifact arising from mutations to the conserved residues within the AL.

HGF structure

The ligand for c-MET was independently identified by two different laboratories as a mitogen for hepatocytes (hepatocyte growth factor, HGF) and a scatter factor (SF) in fibroblasts (Nakamura *et al.* 1989; Stoker *et al.* 1987; Stoker and Perryman 1985). Since

Fig. 1.3. Kinase domain structure of c-MET.
The kinase domain of c-MET adopts the canonical bilobular fold, with the N-terminal and C-terminal lobes linked together by a single polypeptide linker. The activation loop, in this structure, was seen to adapt a different conformation than that seen in apo forms of the kinase domains of other RTKs (Schiering *et al.* 2003).

its discovery, HGF has been shown to elicit pleotropic cellular responses including mitogenesis, motility and morphogenesis. HGF/SF is synthesized as an inactive single-chain precursor that is proteolytically cleaved to form an active disulfide-linked heterodimer. Both the single-chain precursor as well as disulfide-linked heterodimer appear to bind c-MET with high affinity, however, c-MET activation occurs only by the cleaved mature form of the ligand (Lokker *et al.* 1992).

HGF shows sequence homology to the plasminogen-related growth factor family: these proteins have a similar cleavage-mediated activation mechanism. The 69 kDa α-chain of HGF consists of an N-terminal domain (N), followed by four kringle domains

(K1-K4) **(Fig. 1.4)** (Lokker *et al.* 1992). The 34 kDa β-chain forms a conserved protease-like domain; this domain is inactive due to substitution of required active site serine and histidine residues. The HGF residues that form the receptor binding site are unknown, although a number of studies indicate that the α- and β-chains have distinct roles in c-MET binding, and subsequent dimerization (Gherardi *et al.* 2003; Lietha *et al.* 2001; Stamos *et al.* 2004; Ultsch *et al.* 1998). Several truncated forms of the α-chain region, including NK1 (**Fig. 1.4)**, bind c-MET with high affinity. HGF is also a high-affinity ligand for heparan sulfate proteoglycans. However, unlike fibroblast growth factor receptor (FGFR), this interaction does not appear to be critical for c-MET activation (DiGabriele *et al.* 1998; Hartmann *et al.* 1998; Lokker *et al.* 1992). The β-chain of HGF (**Fig. 1.4)**, which harbors the serine-protease-like catalytic domain, has also been shown to bind the *sema* domain within c-MET, albeit with relatively lower affinity (Stamos *et al.* 2004).

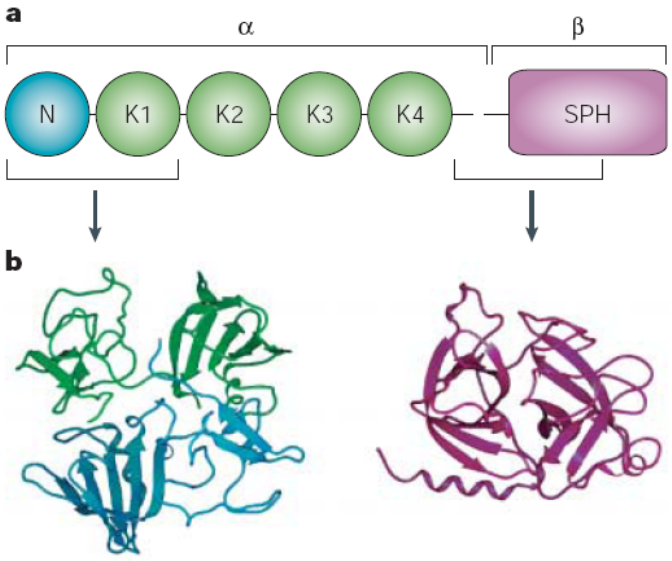

Fig. 1.4. Domain structure of hepatocyte growth factor (HGF)/ scatter factor (SF).
The solved structures of the NK1 domain and a construct of the protease domain of HGF are shown from a recent c-MET review paper (Birchmeier *et al.* 2003). HGF consists of an N-terminal domain (N), 4 kringle domains (K1-K4), and protease like domain (SPH). The structures of the NK1 domain and the protease domain has been solved and shown above.

HGF-INDUCED C-MET DIMERIZATION AND ACTIVATION

Normal signaling by RTKs requires ligand-induced receptor oligomerization and tyrosine phosphorylation of the cytoplasmic domains of the receptor. Although ligand-mediated receptor dimerization appears to be a common event preceding RTK activation, structures of several receptor ectodomains bound to their cognate ligands showed RTKs used different binding modes to accomplish dimerization. In vascular endothelial growth factor receptor (VEGFR), dimerization was induced by binding of dimeric ligand (Wiesmann *et al.* 1997), whereas fibroblast growth factor receptor (FGFR) bound monomeric FGF and the dimeric complex was stabilized by heparin cofactors (Mohammadi *et al.* 2005; Schlessinger *et al.* 2000). Recent crystallographic studies of epidermal growth factor receptor (EGFR) showed that the binding stoichiometry of EGF to receptor was 1:1, and the dimeric complex was stabilized solely through receptor-receptor interactions formed upon ligand binding (Ogiso *et al.* 2002). The mechanism utilized by HGF to induce c-MET dimerization remained largely elusive until recently, when the crystal structure of the HGF β-chain and c-MET *sema* domain highlighted a possible dimer interface between the ligand-receptor pair, and suggested a potential 2:2 HGF:c-MET complex (Stamos *et al.* 2004). Future structural studies on intact HGF and c-MET ectodomain would shed light on the structural-basis of recruitment of HGF by c-MET, and subsequent c-MET dimerization induced by HGF. Interestingly, crosslinking c-MET receptors by specific antibodies to the extracellular domain can trigger c-MET signaling implying that dimerization is sufficient to activate c-MET (Prat *et al.* 1998).

Irrespective of its mode of dimerization, autophosphorylation of c-MET tyrosines necessary for signaling occurs after dimerization and presumably, by transphosphorylation between the catalytic domains of dimeric c-MET. The biochemical events regulating c-MET signaling have been recently elucidated (as discussed below), although, the structural basis for c-MET autophosphorylation upon HGF binding remains largely unclear. Tyrosines Y1231, Y1234 and Y1235 in the AL of the c-MET catalytic domain have been shown to be phosphorylated in response to HGF-induced c-MET

dimerization (**Fig. 1.1**). The presence of three phosphotyrosine sites in the AL is also a characteristic of the insulin receptor, a disulfide-linked constitutive dimer. While the phosphorylation of AL tyrosines is important for increased c-MET kinase activity (Rodrigues and Park 1994), the phosphorylation of carboxy-terminal tail tyrosines Y1349, Y1356 and Y1365 (Birchmeier *et al.* 2003) is required for the recruitment of cytoplasmic signaling proteins with Src homology-2 (SH2) and protein tyrosine binding (PTB) domains. Phenylalanine substitution at residues Y1349 and Y1356 render c-MET functionally impaired in its ability to induce proliferation, motility, differentiation and survival (Weidner *et al.* 1995). In addition, phosphorylation of Y1003 within the juxtamembrane region appears to be critical for receptor degradation (Preschard *et al.* 2001; Preschard *et al.* 2004).

C-MET FUNCTIONS

c-MET signaling

Functional genetic studies of c-MET and HGF have conclusively revealed an indispensable role of these molecules in mammalian development. *HGF* $^{-/-}$ and *c-MET* $^{-/-}$ mice die *in utero* after incurring severe placental and live defects, along with disruption in the migration of myogenic precursors into the limb bud (Bladt *et al.* 1995; Schmidt *et al.* 1995; Uehara *et al.* 1995). Furthermore, in adults, c-MET and HGF are widely expressed, and c-MET signaling has been shown to be important for tissue repair and organ regeneration (Matsumoto and Nakamura 2001; Michalopoulos and DeFrances 1997). In the recent years, extensive studies have been conducted to elucidate the mechanism by which HGF/c-MET regulate such diverse physiological responses. HGF-activated c-MET recruits cytoplasmic signaling molecules such as Grb2-associated binder 1 (Gab1), growth factor receptor-bound protein (Grb2), phosphatidylinositol 3-kinase (PI3K), SH2-containing protein (Shc) (**Fig. 1.5)** via a unique multisubstrate

docking site that is conserved in the c-MET family of RTKs (Ponzetto *et al.* 1994). This docking site encompasses phosphorylated Y1349, Y1356 and adjacent residues. Y1365 has also been implicated in the c-MET-initiated morphogenesis, although the signaling molecules that interact with this c-MET site are largely unknown (Weidner *et al.* 1995). Recruitment of the signaling molecules results in the activation of specific signaling pathways that regulate multiple cellular processes including proliferation, disruption of intracellular junctions, migration and survival. Furthermore, c-MET signaling is also involved in complex processes such as cellular differentiation and formation of branching tubules. Some of the well-characterized signaling pathways activated by c-MET are Ras-MAPK, PI3K, Src and Stat3 (Bertotti and Comoglio 2003; Birchmeier *et al.* 2003). Although several researchers have tried to link individual effector molecules and/or specific signaling pathways to a particular cellular response, it is becoming increasingly apparent that HGF-induced c-MET signaling is complex and branches into distinct but interacting cascades.

The multi-adapter Gab1 plays a critical role in mediating c-MET signaling by providing a scaffold for simultaneous binding several signaling molecules. The central role of Gab1 in c-MET signaling is evident from the phenotype of *Gab1* $^{-/-}$ mice, which show the characteristic placental, liver and muscle defects seen in c-MET null mice (Sachs *et al.* 2000). Upon HGF stimulation, Gab1 directly interacts with phosphorylated c-MET, via a unique Met-binding domain, which is not present in other members of the Gab family, and indirectly interacts with phosphorylated c-MET via Grb2 (Lock *et al.* 2000). The c-MET-Gab1 interaction appears to be critical for stimulating branching morphogenesis (Maroun *et al.* 1999). Phosphorylation of specific Gab1 tyrosines creates sites for binding the SH2 domain of Shp2, a protein-tyrosine phosphatase (PTP) (Gu and Neel 2003). The Shp2-Gab1 interaction plays an important role in activating the Erk/MAPK pathway (Gu and Neel 2003; Schaeper *et al.* 2000). Mutations that disrupt Gab1-Shp2 binding result in a phenotype incapable of activating the Erk/MAPK pathway. Although Shp2 is believed to act upstream of Ras and Raf, the direct effectors of Shp2 are currently unknown. Interestingly, recent studies show that Gab1 can directly

interact with Erk1/2 via its Met-binding domain and this interaction is critical for transporting Erk1/2 to the nucleus (Osawa *et al.* 2004). However, the significance of this interaction for c-MET signaling is unclear. Upon HGF stimulation, Gab1 also interacts with CT10 regulator of kinase (Crk), phospholipase C (PLC), PI3K and Shc (**Fig. 1.4)**. Signaling from Gab1 and Crk appears to be important for motility (Schaeper *et al.* 2000), whereas the Gab1-PLC and Gab1-Shp2 interactions have been shown to be important for branching morphogenesis (Gual *et al.* 2000; Maroun *et al.* 2000)

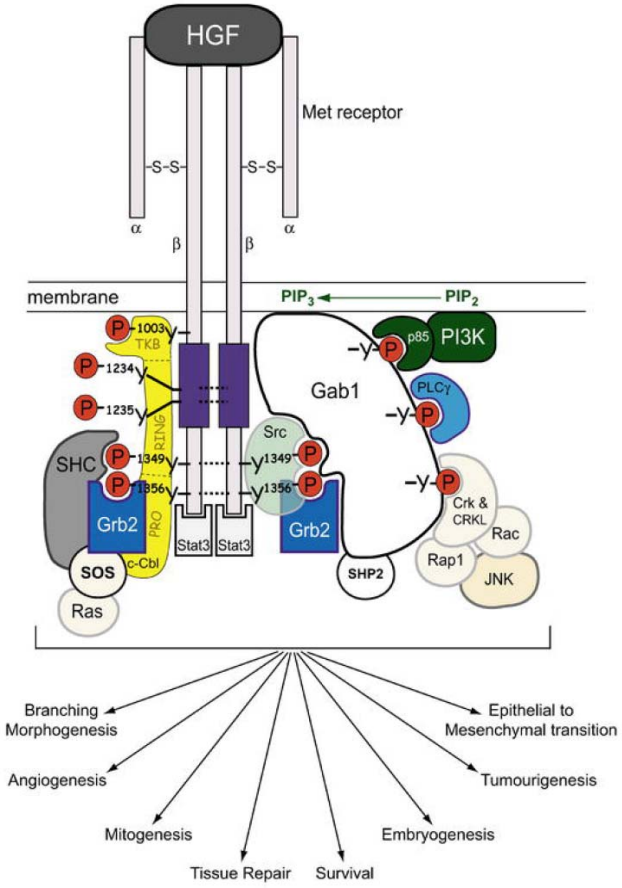

Fig. 1.5. c-MET signaling.

A schematic representation of the c-MET in complex with its effectors and downstream effects of c-MET signaling is depicted (Hammond *et al.* 2004).

Another important adapter molecule for c-MET is Grb2, which possesses a SH2 domain and multiple SH3 domains. Grb2 constitutively associates with Sos, a Ras-specific guanine nucleotide exchange factor. Grb2 binds phosphorylated RTKs via its SH2 domain, thereby shuttling the Sos to the plasma membrane, where Ras is localized (Ponzetto *et al.* 1994). This sequence of events activates Ras, which then activates the Raf1 serine threonine kinase. Raf1 activates the MAPK signaling pathway by phosphorylating MEK, which in turn phosphorylates the MAP kinase (Campbell *et al.* 1998). As mentioned earlier, Grb2 also provides a high-affinity binding site for Gab1. Grb2 has been implicated in c-MET-mediated proliferation, transformation and motility. Upon its phosphorylation Grb2 is also able to interact with Shc, which can also directly bind c-MET (Pelicci *et al.* 1995).

The SH2 domain of the effector protein PI3K has been shown to bind phosphorylated c-MET (Ponzetto *et al.* 1994). In addition, PI3K indirectly interacts with c-MET via Gab1 (Holgado-Madruga *et al.* 1996). Several studies have concluded that PI3K mediates most of the MET-induced signaling responses namely- mitogenesis, motility, and morphogenesis (Khwaja *et al.* 1998; Potempa and Ridley 1998; Royal *et al.* 1997; Royal and Park 1995). Furthermore the PI3K-protein kinase B(PKB)/Akt pathway, which mediates MET-induced scattering and branching morphogenesis (Royal *et al.* 1997), is also the main mediator for cell survival (Xiao *et al.* 2001).

Other proteins reportedly recruited to c-MET phosphotyrosine docking sites include Shc, Src and Stat3. Shc and Src are involved in cellular proliferation and motility, Stat3 is involved in branching morphogenesis, and Stat3 and Src are also involved in cellular transformation (Boccaccio *et al.* 1998; Pelicci *et al.* 1995; Ponzetto *et al.* 1993; Rahimi *et al.* 1998; Zhang *et al.* 2002). Phosphorylation of c-MET Y1003 is important for recruitment of c-Cbl, a member of the E3 ubiquitin ligase family (Preschard *et al.* 2001). c-Cbl has also shown to be recruited indirectly to the MET-signaling complex via interactions with Grb2. The c-Cbl-c-MET interaction appears to be critical for MET ubiquitination and degradation. Finally, several transmembrane proteins namely α6β4 integrin (Trusolino *et al.* 2001), Plexin B1 (Basile *et al.* 2005; Giordano *et al.* 2002), and

CD44 (Orian-Rousseau *et al.* 2002) have also been shown to associate with c-MET, although the significance of these interactions for c-MET signaling *in vivo* is unclear. Thus HGF-activated c-MET triggers complex cellular responses by activating interacting signaling pathways.

Aberrant c-MET regulation and human malignancies

Aberrant regulation of c-MET signaling has emerged as a likely causative element for a number of human malignancies. Abnormal activation of c-MET can occur via different mechanisms, some of the reported mechanisms include c-MET or HGF overexpression, and c-MET mutations (**Fig. 1.6**). c-MET activation and signaling is clearly deregulated in several osteosarcomas, glioblastomas and melanoma, where c-MET and HGF have been observed to be constitutively overexpressed (Birchmeier *et al.* 2003; Fukuda *et al.* 1998; Hendrix *et al.* 1998; Koochekpour *et al.* 1997). These observations are further strengthened by the evidence of c-MET and/or HGF expression in carcinomas, and other types of human solid tumors and their metastasis (Birchmeier *et al.* 2003). Furthermore, mouse and human cells that ectopically overexpress HGF or c-MET become tumorigenic and metastatic in athymic nude mice (Rong *et al.* 1994). A large number of sporadic and germline mutations of c-MET have been identified in human renal papillary carcinomas (Danilkovitch-Miagkova and Zbar 2002) and homologous c-MET mutations produce distinct tumor profiles in mice (Graveel *et al.* 2004). These mutations occur within the c-MET kinase domain, often making it capable of constitutive signaling. In addition, mutations in the c-MET juxtamembrane residues important for c-Cbl binding have been detected in gastric and lung cancers (Lee *et al.* 2000; Ma *et al.* 2003). The role of c-MET in physiological processes such as proliferation, survival, invasion and angiogenesis could point to its involvement in corresponding stages during tumor progression.

c-MET signaling has also repeatedly emerged as a pathway that is exploited by several pathogens including *Listeria monocytogenes*, *Plasmodium spp.* and *Helicobacter pylori* (**Fig. 1.6**) (Carrollo *et al.* 2003; Churin *et al.* 2003; Shen *et al.* 2000). InlB, a

listerial protein was identified as a bacterial agonist for c-MET and shown to mimic HGF-induced c-MET activation, endocytosis (Ireton *et al.* 1999; Li *et al.* 2005) and signaling (Shen *et al.* 2000). *H. pylori* CagA protein also activated c-MET, although by a distinct mechanism. The CagA- induced c-MET signaling could be important for *H. pylori*-induced cancer onset and tumor progression (Churin *et al.* 2003). Contrary to *Listeria* and *H pylori*, *Plasmodium*, the causative agent for malaria, did not directly interact with c-MET, but exploited HGF-c-MET signaling to make the host cell susceptible to infection (Carrollo *et al.* 2003).

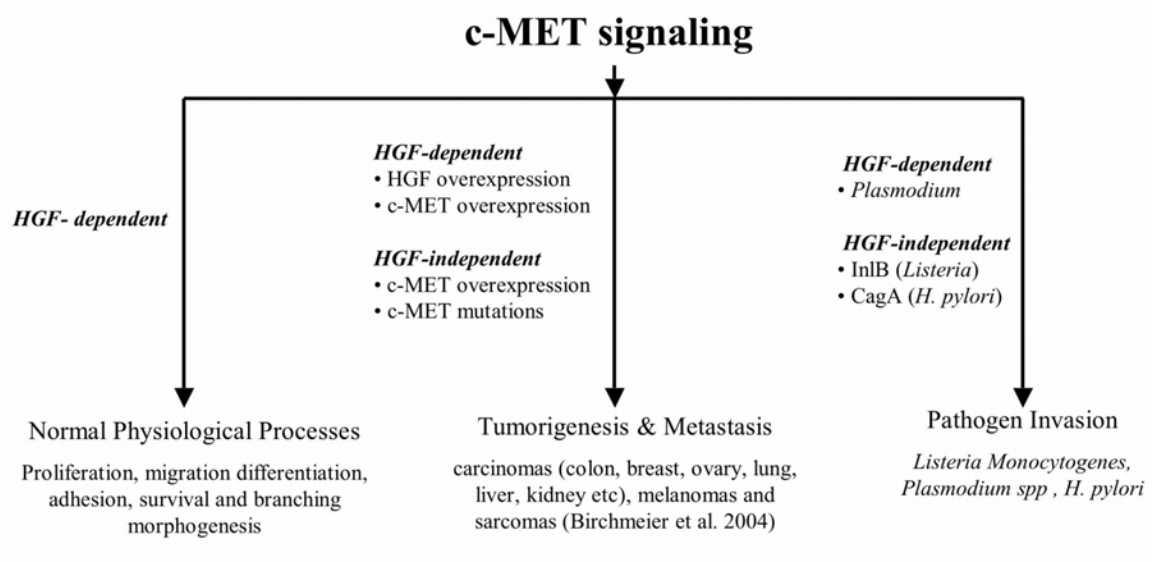

Fig. 1.6. c-MET signaling malignancies.

HGF-mediated c-MET signaling is important for several physiological processes including cell proliferation, differentiation and survival. Aberrant regulation of c-MET signaling by HGF/c-MET overexpression or c-MET mutations is associated with tumorigenesis and metastasis. c-MET signaling has been shown to be exploited by several pathogens, including *Listeria monocytogenes*, *Helicobacter pylori* and malarian parasite *Plasmodium spp* for tissue invasion and pathogen dissemination.

REGULATING C-MET ENZYMATIC ACTIVITY

Regulation by autophosphorylation

HGF-mediated dimerization facilitates c-MET autophosphorylation. The kinetics of c-MET autophosphorylation has not been extensively studied, although the phosphotyrosine sites and their role in c-MET signaling are well-characterized (as reviewed above). Phosphorylation of Y1231, Y1234 and Y1235 in the kinase domain AL has been reported to modulate c-MET catalytic activity (Rodrigues and Park 1994). The correlation between the AL phosphorylation and increased kinase catalytic activity has been extensively documented in a number of RTKs (Cobb *et al.* 1989; Murray *et al.* 2001; Parast *et al.* 1998). In IR, where insulin binding induces receptor activation of a constitutive dimeric receptor, autophosphorylation kinetics were observed to follow a two phase model where the ligand activated receptor had a prolonged fast phase compared to the non-ligand stimulated receptor (Kohanski 1993b). Murray *et al.* determined the kinetic parameters for phosphorylated and unphosphorylated Tie2 cytoplasmic kinase domain and showed that phosphorylation resulted in a 2-5 fold decrease in substrate K_M relative to the unphosphorylated kinase (Murray *et al.* 2001). Parast *et al* also showed an order of magnitude increase in the catalytic activity of the phosphorylated VEGFR2 tyrosine kinase domain versus unphosphorylated receptor (Parast *et al.* 1998).

The crystal structure of IR (**Fig. 1.2)** in its phosphorylated and unphosphorylated forms provided a structural basis for how AL phosphorylation might modulate kinase activity (Hubbard 1997; Hubbard *et al.* 1994). In the phosphorylated state the AL adopted a conformation that was more amenable to binding ATP and tyrosine-containing peptide substrate (Hubbard 1997). These studies demonstrated the importance of the phosphorylation state of RTKs in modulating their kinase activity. However, these studies but did not address whether oligomerization could impact these parameters, although Hubbard *et al* hypothesized that dimer formation could stabilize the "flipped out" activation loop conformation in a catalysis favorable position (Hubbard 1997).

The mechanism of autophosphorylation within the oligomeric RTK is still elusive, although evidence for both intramolecular (i.e. *cis*) (Bertics *et al.* 1985; Biswas *et al.* 1985; Villalba *et al.* 1989; Weber *et al.* 1984) and intermolecular (i.e. *trans*) mechanism (Cobb *et al.* 1989; Sherrill 1997; Treadway *et al.* 1991; Yarden and Schlessinger 1987) as well as sequential *cis/trans* mechanisms (Iwasaki *et al.* 1997) exist. Structural studies support a *trans* mechanism of AL autophosphorylation within IR. In this system the AL tyrosine is believed to bind to the kinase catalytic site in a *cis* fashion (**Fig. 1.2)**, but cannot be phosphorylated due to steric constraints that prevent simultaneous binding of MgATP when the tyrosine is bound to the IR active site (Hubbard *et al.* 1994). The kinetic properties of several RTKs have been characterized and the reaction model is dependent on the purification process and the constructs used. Both the EGF receptor (Posner *et al.* 1992; Ward *et al.* 1994) and the IR (Walker *et al.* 1987; Yuan *et al.* 1990) were consistent with a rapid equilibrium random order mechanism, while the TrkA receptor showed an ordered sequential scheme (Angeles *et al.* 1998). In contrast, kinetic studies on the Rous sarcoma virus pp60src supported a steady state ordered bi-bi mechanism with ATP binding occurring first (Wong and Goldberg 1984). The VEGFR was characterized as a hybrid of the rapid equilibrium random order and sequential mechanisms (Parast *et al.* 1998). Unfortunately, in some studies, an isolated kinase domain was used and in other studies, an immunoprecipitated whole receptor or kinase domain was used, making the direct comparison between these studies difficult. This difficulty was highlighted by Cheng and Koland, who showed that the binding properties of the EGF receptor were dependent on the form of the receptor studied, as the whole cytoplasmic domain had 10-fold greater affinity for ATP relative to the isolated kinase domain (Cheng and Koland 1996).

Regulation by dephosphorylation

Protein tyrosine phosphatases (PTPs) catalyze dephosphorylation of ligand-stimulated and unstimulated c-MET (Sheth and Watowich 2005; Villa-Moruzzi *et al.* 1993). Recent studies have shown that RTK phosphorylation was dynamically regulated

by competing autophosphorylation and dephosphorylation rates (Baxter *et al.* 1998; Bohmer *et al.* 1995; Posner *et al.* 1994; Sheth and Watowich 2005). Regulation of c-MET by PTPs is poorly understood, although studies using substrate trapping mutants, antisense RNA, and phosphotyrosine peptides have proposed DEP-1 (CD148/PTP-η), PTP-S and leukocyte common antigen-related (LAR) to be potentially involved in c-MET dephosphorylation (Kulas *et al.* 1996; Palka *et al.* 2003; Villa-Moruzzi *et al.* 1998). Moreover, DEP-1 was observed to preferentially dephosphorylate the carboxyl-terminal Y1349 and Y1365 in c-MET, suggesting that phosphatase site-specific preferences might be an additional mechanism for regulating receptor signaling (Palka *et al.* 2003). Detailed animal model or cell culture studies have yet to substantiate a role of these putative PTPs in c-MET signaling.

Regulation by dimerization

The classical RTK activation model consists of dimerization-mediated RTK autophosphorylation, which in turn activates kinase activity of the receptor (**Fig. 1.7**). Thus, activation of the kinase activity of RTKs has been synonymously used for RTK activation. However, *in vitro* studies using isolated kinase domains and *ex vivo* studies using phosphatase inhibitors have shown conclusively that monomeric receptors can be rapidly phosphorylated on tyrosine residues involved in intracellular signal propagation (Baxter *et al.* 1998; Posner *et al.* 1994; Sheth and Watowich 2005). Thus, it is clear that ligand-induced receptor oligomerization is not necessary for kinase activity. There has been limited number of studies addressing the role of dimerization on the biochemistry of RTK activation. This has in part been due to the lack of an appropriate model system to study dimerization. We have recently employed a well-characterized *in vitro* system, consisting of functional monomeric and dimeric forms of c-MET to develop a detailed understanding of how oligomerization state modulates c-MET's biochemical and conformational properties and thus contributes to receptor activation. TPR-MET, a naturally occurring oncoprotein resulting from fusion of the TPR region of nuclear pore complex and the cytoplasmic domain of c-MET recapitulated many of the molecular and

cellular properties of ligand-activated c-MET. Specifically, TPR-MET has been shown to be an active kinase both *in vitro* and *in vivo*, and it activated c-MET signaling pathways in transformed cells (Rodrigues and Park 1993; Rodrigues and Park 1994). Thus, it is an established model system for the ligand-dependent oligomeric state of c-MET (**Fig. 3.1**). The isolated cytoplasmic domain of c-MET (cytoMET; **Fig. 3.1**) served as a functional analog of monomeric c-MET. Detailed comparative kinetic analysis of similarly phosphorylated TPR-MET and cytoMET showed that their catalytic efficiency for substrate phosphorylation differed several-fold (Hays and Watowich 2003). In addition, TPR-MET showed significantly lower K_D for peptide substrates as compared to cytoMET (Hays and Watowich 2004). These results clearly showed that the RTK oligomeric state substantially influenced its kinetic and thermodynamic properties, implying that functionally necessary conformational changes accompanied receptor oligomerization.

In this study, we used the TPR-MET and cytoMET model system to dissect the role of dimerization in regulating c-MET's susceptibility to dephosphorylation, a critical regulator of RTK activation process. The measured biochemical parameters from our *in vitro* studies were used to build a unified mathematical model for c-MET activation. The model predictions for c-MET activation were faithfully reproduced in intact cells. The model was used to dissect the mechanism of activation of c-MET. Based on our work, we propose a novel feed-forward model for activation of c-MET, and conclude that this may be a general mechanism utilized by many oligomeric RTKs to regulate their activity.

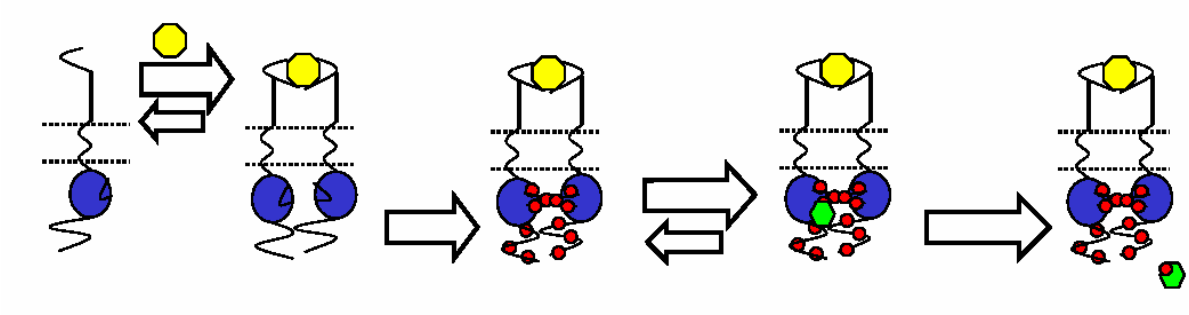

Fig. 1.7. Classical model for RTK activation.

The RTK in presence of its cognate ligand was thought to follow a linear sequence of events highlighted above resulting in their activation. Although the mode of dimerization in RTKs differs (discussed at length in the text), dimerization was thought to result in autophosphorylation, which in turn increased the kinase activity of these receptors. Increase in kinase activity was thought to be necessary and sufficient for RTK activation.

CHAPTER 2:
MATERIALS AND METHODS

Cell culture

Vero cells (African Green Monkey kidney cells) were obtained from the American Tissue Culture Collection. Cells were grown at 37^{o}C in 5% CO_2 and Minimum Essential Medium (MEM) supplemented with glutamine and 5% FBS.

Protein expression and purification

TPR-MET and cytoMET (cytoplasmic domain of the c-MET receptor; **Fig. 3.1**) expression and purification has been described previously (Hays and Watowich 2003). Briefly, both proteins were cloned into the Bac-to-Bac baculovirus expression system (Invitrogen) with a carboxy-terminal hexahistidine sequence. For expression, Sf-9 insect cells were infected with recombinant baculovirus, cells were harvested 72 hrs post-infection, and lysed in TBSC lysis buffer (50 mM Tris, pH 7.5, 150 mM NaCl, 0.5% CHAPS) supplemented with 1 mM DTT and 1X Complete Protease Inhibitor Cocktail (Roche). TPR-MET and cytoMET were separately purified from the cleared lysate by binding and elution from Ni-NTA beads (Qiagen). Purified protein was dialyzed into PBSC (50 mM Sodium phosphate pH 6.5, 150 mM NaCl, 0.5% CHAPS, 1 mM DTT) supplemented with 50 μM ATP, 25 mM $MgCl_2$, and 5 mM $MnCl_2$ to ensure complete autophosphorylation. Excess ATP, ADP, $MgCl_2$, and $MnCl_2$ were removed by successive dialysis against PBSC. The proteins were further purified with gel filtration column (Phenomenex BIOSEP SEC-3000 column) chromatography. Protein concentrations were determined by absorbance at A_{280} with molar extinction coefficients calculated based on the aromatic content of the proteins.

Western blot analysis

c-Met anti-phospho $Y^{1234,1235}$, mouse monoclonal anti-phosphotyrosine clone 4G10, anti-MET DO-24, anti-MET DO-21, Protein A agarose were obtained from Upstate Biotechnology, Inc. c-Met anti-phospho Y^{1349} and anti-phospho Y^{1365} were obtained from Cell Signaling Technology and Biosource International, respectively. Anti-c-MET SC-161 was obtained from SantaCruz Biotechnology. Anti-rabbit and anti-mouse HRP linked conjugates were obtained from Southern Biotechnology Associates, Inc. and Amersham Biosciences, respectively. For western blot analyses, proteins were separated on 10% polyacrylamide gels and transferred to PVDF membrane using standard procedures. After incubation overnight in blocking buffer (1% BSA in TBST) at 4^{o}C, the membranes were incubated with appropriate antibodies (typically at 1:1000 dilution), washed in TBST, and incubated with HRP-coupled secondary antibody (typically at 1:10000 dilution). Antibodies were detected using ECL Plus chemiluminescent kit (Amersham) and exposure to film (Kodak X-OMAT AR). Whenever required, antibodies were removed from the membranes in stripping buffer (100 mM 2-mercaptoethanol, 2% SDS in 62.5 mM Tris-HCl pH 6.7) at 65°C for 45 min, and the membranes were reblocked, and reprobed with anti-MET antibody. X-ray films containing the protein bands were imaged with a MultiImage Light Cabinet (Alpha Innotech Corp.) and densitometry performed using ChemiImager® software (Alpha Innotech Corp).

Immunoprecipitation

The cells were grown as required and serum-starved for several hours prior to stimulation with pervandate or ligand, depending on the experiments. Subsequent to desired treatment, the cells were washed with ice-cold PBS and lysed in Triton X-100 lysis buffer (50 mM Tris pH 7.5, 150 mM NaCl, 1% Triton X-100, 3 mM Na_3VO_4, 2 mM EDTA, 2 mM NaF, and protease inhibitor cocktail). Protein concentrations in each lysate were determined using BioRad DC Assay. Lysates containing 1 mg protein were used for immunoprecipitation of c-MET with DO-24 antibody, which recognizes c-MET

extracellular region. Briefly, lysate was incubated with the antibody overnight at 4°C, after which ~100 µl of Protein A agarose in PBS was added to the mixture for 3-4 hrs at 4°C to capture the immune complex. The lysate and beads were centrifuged, supernatant was removed, and beads were washed extensively in lysis buffer before resuspending in SDS-PAGE buffer. Samples were separated on 7.5% polyacrylamide gels and immunoblotting was performed as described above with blocking buffer 3% BSA in TBST.

In-vitro dephosphorylation assay

Fixed concentrations of phosphorylated TPR-MET or cytoMET were separately incubated with recombinant PTPβ (2 units/µl final concentration) in the dephosphorylation reaction buffer (25 mM HEPES pH 7.2, 50 mM NaCl, 5 mM dithiothreitol, 2.5 mM EDTA) at 37^{o}C. At specified time points reaction aliquots were removed and quenched in SDS PAGE buffer. Proteins were separated on 10% polyacrylamide gels and transferred to PVDF membrane using standard procedures. After incubation overnight in blocking buffer (1% BSA in TBST) at 4^{o}C, the membranes were incubated with phosphotyrosine specific antibodies (typically at 1:1000 dilution, except in anti-phospho $Y^{1234,1235}$ where 1:500 dilution was used), washed in TBST, and incubated with HRP-coupled secondary antibody (1:10000 dilution). Antibodies were detected using ECL Plus chemiluminescent kit (Amersham) and exposure to film (Kodak X-OMAT AR). Antibodies were removed from the membranes in stripping buffer (100 mM 2-mercaptoethanol, 2% SDS in 62.5 mM Tris-HCl pH 6.7) at 65°C for 45 min, reblocked, and reprobed with anti-MET antibody. X-ray films containing the protein bands were imaged with a MultiImage Light Cabinet (Alpha Innotech Corp.) and densitometry performed using ChemiImager® software (Alpha Innotech Corp). Experiments were performed within the dynamic range of the antibody signal and the exposure time. Similar protocol was used for dephosphorylation with PTP1B and CIAP.

GraphPad Prism® was used for data fitting and statistical analysis. Unless otherwise mentioned all experiments were done in triplicate.

Pervanadate-induced c-MET phosphorylation in cells

The cells were grown to confluency and serum starved for 12-24 hrs. Pervanadate was prepared by mixing 500 µl of 100 mM Na_3VO_4 with 500 µl of 100 mM H_2O_2 and incubating at room temperature for 20 min. The solution was cooled on ice and added to cell medium to yield a final concentration of 50 µM pervanadate as denoted by vanadate concentration in the medium. Stimulation was done at room temperature with pervanadate-containing media and at indicated time points the cells were washed with ice-cold PBS and lysed in Triton X-100 lysis buffer (50 mM Tris pH 7.5, 150 mM NaCl, 1% Triton X-100, 3 mM Na_3VO_4, 2 mM EDTA, 2 mM NaF, and protease inhibitor cocktail). Protein concentrations in each lysate were determined using BioRad DC Assay. Lysates containing 1 mg protein were used for immunoprecipitation of c-MET with DO-24 antibody, which recognizes c-MET extracellular region. Briefly, lysate was incubated with the antibody overnight at 4°C, after which ~100 µl of Protein A agarose in PBS was added to the mixture for 3-4 hrs at 4°C to capture the immune complex. The lysate and beads were centrifuged, supernatant was removed, and beads were washed extensively in lysis buffer before resuspending in SDS-PAGE buffer. Samples were separated on 7.5% polyacrylamide gels and immunoblotting was performed as described above with blocking buffer 3% BSA in TBST.

Building feed-forward model for c-MET activation

A differential equation framework was built using Mathematica 4.1 to express the time-dependent concentrations of reaction intermediates and products shown in Figure 1B. Given initial conditions, rate constants for the forward and reverse reactions (k_{on} and k_{off}, respectively), catalytic efficiencies for the enzymatic reactions, and the time interval,

Mathematica was used to solve our set of simultaneous differential equations to obtain concentrations of any species at any given time point.

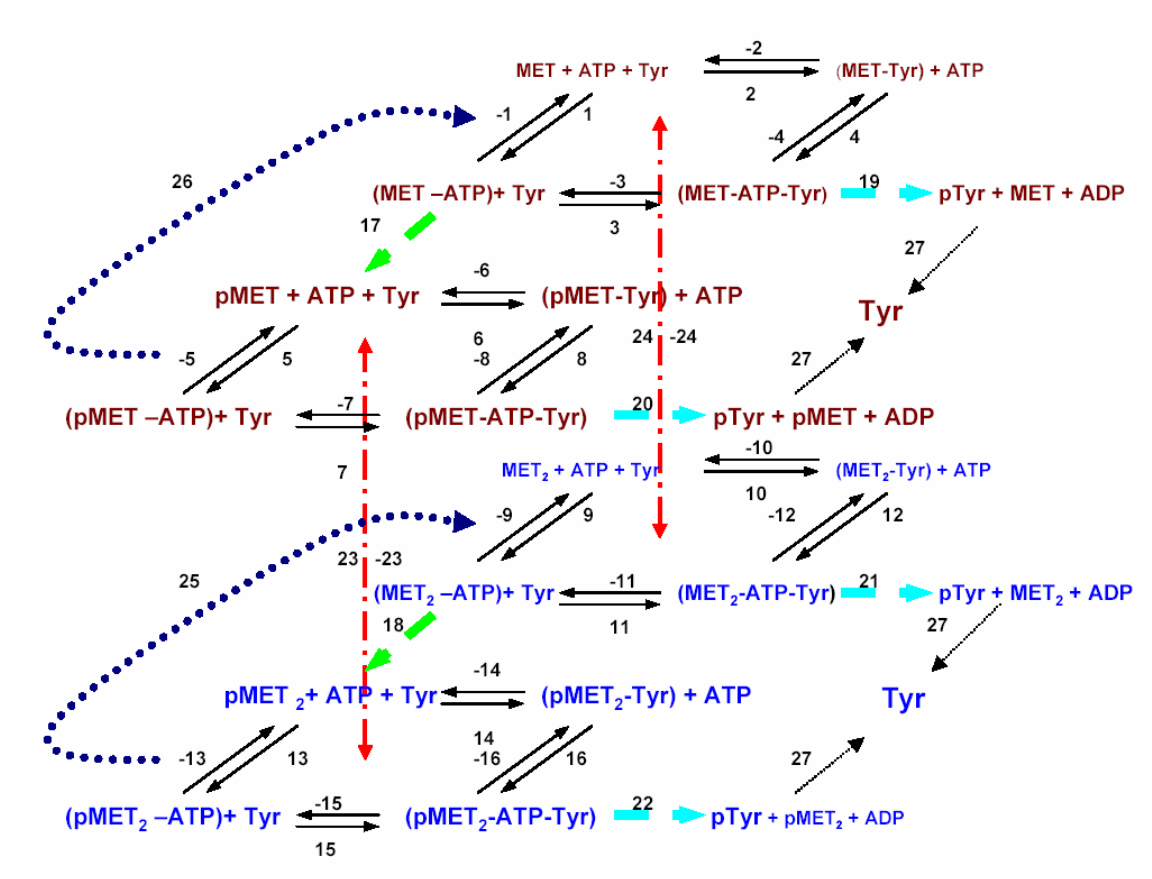

Fig. 2.1. c-MET activation model.

Schematic representation of reactions necessary for c-MET activation. The numbering of the reactions was consistent with equations in **Table 2.1** and **Table 2.2**. Thermodynamic interactions (1-16, solid lines) were described by on/off rates and the concentration of dependent species. The kinetic reactions (17-24, green and blue dashed lines) were described by the catalytic efficiency of the enzyme species for autophosphorylation and effector phosphorylation, respectively, and concentrations of reactants. The extracellular ligand-mediated dimerization process (23-24, red hatched line) was described by on/off rate constants and the concentrations of extracellular ligand MET, c-MET monomer (MET); c-MET dimer (MET_2), ATP, and tyrosine containing effector (Tyr). The p-suffix defined the phosphorylated form of molecule. Reactions associated with c-MET monomer and dimer were colored brown and blue, respectively.

Table 2.1. Rate equations describing the c-MET activation pathway

$\nu_1 = k_1 \cdot [MET] \cdot [ATP]$; $k_1 = 0.01$
$\nu_2 = k_2 \cdot [MET] \cdot [Tyr]$; $k_2 = 0.001$
$\nu_3 = k_3 \cdot [MET\text{-}ATP] \cdot [Tyr]$; $k_3 = 0.001$
$\nu_4 = k_4 \cdot [MET\text{-}Tyr] \cdot [ATP]$; $k_4 = 0.01$
$\nu_5 = k_5 \cdot [pMET] \cdot [ATP]$; $k_5 = 0.1$
$\nu_6 = k_6 \cdot [pMET] \cdot [Tyr]$; $k_6 = 0.00032$
$\nu_7 = k_7 \cdot [pMET\text{-}ATP] \cdot [Tyr]$; $k_7 = 0.0015$
$\nu_8 = k_8 \cdot [pMET\text{-}Tyr] \cdot [ATP]$; $k_8 = 0.1$
$\nu_9 = k_9 \cdot [MET_2] \cdot [ATP]$; $k_9 = 0.01$
$\nu_{10} = k_{10} \cdot [MET_2] \cdot [Tyr]$; $k_{10} = 0.001$
$\nu_{11} = k_{11} \cdot [MET_2\text{-}ATP] \cdot [Tyr]$; $k_{11} = 0.001$
$\nu_{12} = k_{12} \cdot [MET_2\text{-}Tyr] \cdot [ATP]$; $k_{12} = 0.01$
$\nu_{13} = k_{13} \cdot [pMET_2] \cdot [ATP]$; $k_{13} = 0.1$
$\nu_{14} = k_{14} \cdot [pMET_2] \cdot [Tyr]$; $k_{14} = 0.001$
$\nu_{15} = k_{15} \cdot [pMET_2\text{-}ATP] \cdot [Tyr]$; $k_{15} = 0.001$
$\nu_{16} = k_{16} \cdot [pMET_2\text{-}Tyr] \cdot [ATP]$; $k_{16} = 0.1$
$\nu_{17} = k_{17} \cdot [MET\text{-}ATP]$; $k_{17} = 0.0008$
$\nu_{18} = k_{18} \cdot [MET_2\text{-}ATP]$; $k_{18} = 0.24$
$\nu_{19} = k_{19} \cdot [MET\text{-}ATP\text{-}Tyr]$; $k_{19} = 0.0008$
$\nu_{200} = k_{20} \cdot [pMET\text{-}ATP\text{-}Tyr]$; $k_{20} = 0.008$
$\nu_{21} = k_{21} \cdot [MET_2\text{-}ATP\text{-}Tyr]$; $k_{21} = 0.0024$
$\nu_{22} = k_{22} \cdot [pMET_2\text{-}ATP\text{-}Tyr]$; $k_{22} = 0.024$
$\nu_{23} = k_{23} \cdot [MET] \cdot [GF]$; $k_{23} = 10$
$\nu_{24} = k_{24} \cdot [pMET] \cdot [GF]$; $k_{24} = 10$
$\nu_{25} = (V_{25} \cdot [pMET_2]) / (K_{25} + [pMET_2])$; $V_{25} = 0.045$, $K_{25} = 0.01$
$\nu_{26} = (V_{26} \cdot [pMET]) / (K_{26} + [pMET])$; $V_{26} = 0.45$, $K_{26} = 0.01$
$\nu_{27} = (V_{27} \cdot [pTyr]) / (K_{27} + [pTyr])$; $V_{27} = 0.001$, $K_{27} = 0.1$

$\nu_{-1} = k_{-1} \cdot [MET\text{-}ATP]$; $k_{-1} = 0.34$
$\nu_{-2} = k_{-2} \cdot [MET\text{-}Tyr]$; $k_{-2} = 0.3$
$\nu_{-3} = k_{-3} \cdot [MET\text{-}ATP\text{-}Tyr]$; $k_{-3} = 0.18$
$\nu_{-4} = k_{-4} \cdot [MET\text{-}ATP\text{-}Tyr]$; $k_{-4} = 0.29$
$\nu_{-5} = k_{-5} \cdot [pMET\text{-}ATP]$; $k_{-5} = 1.7$
$\nu_{-6} = k_{-6} \cdot [pMET\text{-}Tyr]$; $k_{-6} = .045$
$\nu_{-7} = k_{-7} \cdot [pMET\text{-}ATP\text{-}Tyr]$; $k_{-7} = 0.10$
$\nu_{-8} = k_{-8} \cdot [pMET\text{-}ATP\text{-}Tyr]$; $k_{-8} = 1.43$
$\nu_{-9} = k_{-9} \cdot [MET_2\text{-}ATP]$; $k_{-9} = 0.114$
$\nu_{-10} = k_{-10} \cdot [MET_2\text{-}Tyr]$; $k_{-10} = 0.024$
$\nu_{-11} = k_{-11} \cdot [MET_2\text{-}ATP\text{-}Tyr]$; $k_{-11} = 0.018$
$\nu_{-12} = k_{-12} \cdot [MET_2\text{-}ATP\text{-}Tyr]$; $k_{-12} = 0.166$
$\nu_{-13} = k_{-13} \cdot [pMET_2\text{-}ATP]$; $k_{-13} = 0.57$
$\nu_{-14} = k_{-14} \cdot [pMET_2\text{-}Tyr]$; $k_{-14} = 0.013$
$\nu_{-15} = k_{-15} \cdot [pMET_2\text{-}ATP\text{-}Tyr]$; $k_{-15} = 0.016$
$\nu_{-16} = k_{-16} \cdot [pMET_2\text{-}ATP\text{-}Tyr]$; $k_{-16} = 0.87$
$\nu_{-23} = k_{-23} \cdot [MET_2]$; $k_{-23} = 0.01$
$\nu_{-24} = k_{-24} \cdot [pMET_2]$; $k_{-24} = 0.01$

All rate constants (k) are given in s-1 (1st order) and in μM-1·s-1 (2nd order). All catalytic efficiencies (V) are given in μM·s-1, and Michaelis-Menten constants (K, reactions 25-27) are in μM. For reaction 23, -23, 24, and –24 only one example is given, although the dimerization could occur between any two matching species.

The model describes the minimal number of reactions required to generate a downstream signal (**Fig. 2.1, Appendix B**). In its simplest form, the c-MET receptor is at the cell surface as a non-signaling monomer that can bind ATP and a tyrosine-containing effector molecule (Tyr) (reactions 1-4). The monomeric, non-phosphorylated receptor can either become autophosphorylated (reaction 17) or may phosphorylate the Tyr effector (reaction 19). Similarly, the phosphorylated monomer can bind ATP and Tyr to form a ternary complex (reaction 5-8, **Fig. 2.1**). The phosphorylated and non-

phosphorylated c-MET may dimerize in response to extracellular ligand binding (reactions 23, -23, 24, and -24). Also, the phosphorylated receptor can be dephosphorylated (reactions 25 and 26) by cellular protein tyrosine phosphatases (PTP). Dephosphorylation of Tyr effector is included in the model as this down-regulatory reaction is present in cells. Not included in the current model is the formation of multiple phosphorylated c-MET species, although the addition of multiple reactions and catalytic efficiencies can be easily done when experimental data becomes available for these reactions. The kinetic and thermodynamic parameters are for fully phosphorylated c-MET, as that is the data currently available either from our lab or the literature as described below.

A complete set of the kinetic equations used to describe the activation of the c-MET receptor can be found in **Table 2.2**. For example, the concentration of the binary complex [MET-ATP] at any given time is equal to the rate of production of the binary complex less its consumption. The production of binary complex can be described by the rate of formation from free MET and free ATP, the rate of dissociation of the ternary complex [MET-ATP-Tyr] into [MET-ATP] and free Tyr, the rate of monomerization of [MET_2-ATP] into [MET-ATP] and the dephosphorylation of [pMET-ATP] into [MET-ATP]. The rate of consumption of the binary [MET-ATP] complex is equal to the reverse of the reactions mentioned above with the loss due to the kinetic autophosphorylation reaction instead of the dephosphorylation reaction. Mathematically this can be expressed as:

$$d[\text{MET-ATP}]/dt = \nu_1+\nu_{-3}+\nu_{-24}+\nu_{26}-\nu_{-1}-\nu_3-\nu_{24}-\nu_{17},$$

where, d_x is the rate of reaction x from **Fig. 2.1**. The exact values of the rate equations are enumerated in **Table 2.1**. In the overall activation process, the receptor concentration is assumed conserved such that $[\text{MET}]_{total} = [\text{MET}]_{free}$ + [MET] + [MET-ATP] + [MET-Tyr] + [MET-ATP-Tyr] + [pMET] + [pMET-ATP] + [pMET-Tyr] + [pMET-ATP-Tyr] + [MET_2] + [MET_2-ATP] + [MET_2-Tyr] + [MET_2-ATP-Tyr] + [$pMET_2$] + [$pMET_2$-ATP] + [$pMET_2$-Tyr] + [$pMET_2$-ATP-Tyr] = Constant. This assumption is easily accounted for

in the initial response in the computer model. In cells, c-MET is internalized and degraded through endosomal trafficking, each of which occur in the time-frame of minutes (Hammond *et al.* 2003; Li *et al.* 2005). Since we focus on initial activation of the receptor which occurs within ~200 secs, the contribution of receptor internalization and degradation is assumed to be negligible.

Parameter values for feed-forward model for c-MET activation

In our model, we used k_{on} and k_{off} values that had been previously determined in our laboratory for reactions 5-8 and 13-16 (Hays and Watowich 2004). Similarly, the kinetic catalytic efficiencies for reactions 20 and 22 were described by our lab (Hays and Watowich 2003). Although we have not directly measured k_{on} and k_{off} values for the dephosphorylated forms of c-MET, other groups showed that equilibrium dissociation constants between phosphorylated and dephosphorylated RTK catalytic domains differ by a factor of 2 (Murray *et al.* 2001). Thus, it was reasonable to assume that the on and off rates for the ATP and effector to the dephosphorylated c-MET were of the same order of magnitude as the c-MET phosphorylated form. This assumption was tested with the model, and order of magnitude changes to on and off rates for substrate binding to dephosphorylated c-MET did not affect the shape of the response curves for total phosphorylated receptor and pTyr.

Naldini et al. measured the phosphorylation of exogenous substrates by phosphorylated and dephosphorylated c-MET immunoprecipitated from cell lysates, and observed the phosphorylated receptor had ~10-fold higher kinase activity than the dephosphorylated receptor (Naldini *et al.* 1991a). Our kinetic constants for phosphorylated active dimeric TPR-MET were similar to the values obtained by Naldini et al. for the phosphorylated immunoprecipitated c-MET; therefore we assumed a 10-fold difference in catalytic efficiencies for the dephosphorylated c-MET to phosphorylate exogenous tyrosine substrates compared to phosphorylated c-MET (reactions 19 and 21 vs. 20 and 22). Similarly, the ability of unstimulated c-MET to undergo autophosphorylation was assumed to mimic monomer's ability to phosphorylate

exogenous effectors. Therefore, reactions 17 and 19 were assumed to have similar catalytic rates. The mechanism of c-MET autophosphorylation is unknown, however evidence for both inter and intramolecular phosphorylation exists for different RTKs (Bertics *et al.* 1985; Biswas *et al.* 1985; Cobb *et al.* 1989; Iwasaki *et al.* 1997; Sherrill 1997; Treadway *et al.* 1991; Villalba *et al.* 1989; Weber *et al.* 1984; Yarden and Schlessinger 1987). For our model, as a starting point, monomer autophosphorylation was assumed to be an intramolecular reaction. Preliminary computation analyses using the autophosphorylation k_{cat} used for monomeric c-MET, but assuming a *trans* mode of autophosphorylation, predicted similar levels of c-MET phosphorylation. The catalytic efficiency of dephosphorylated dimeric c-MET was unknown; however, extracellular ligand stimulation induced an ~10-fold increase in the autophosphorylation catalytic activity of the IR hence the increased activity assumed for reaction 18 vs. 22 (Kohanski 1993a). Since the on/off rate constants for c-MET interactions with its target proteins were unavailable, these rate constants were assumed to be similar to those reported for other RTKs (Kholodenko *et al.* 1999). Dephosphorylation rate constants for Shc and EGFR were used to approximate the dephosphorylation rates of exogenous Tyr effectors and c-MET (Kholodenko *et al.* 1999). Shimizu et al. (Shimizu *et al.* 2001) described an ~10-fold increase in the sensitivity of monomeric vs. dimeric PDGFR towards dephosphorylation by recombinant phosphatases. Our studies measured a 10-fold decreased substrate specificity of recombinant PTPβ for phosphorylated dimeric TPR-MET as compared to phosphorylated monomeric cytoMET (Sheth and Watowich 2005). We included a 10-fold difference in V_{max} between the two c-MET dephosphorylation reactions while keeping the K_m equal. The number of c-MET molecules present on Vero cells is unknown; however, related studies with EGFR showed that the EGFR concentrations can be estimated as ~100 nM (Kholodenko *et al.* 1999). Therefore, we estimated c-MET and EGFR concentrations to be similar. Furthermore, the concentration of Tyr-containing effector molecules that were phosphorylated by c-MET were taken from previously published results to be 150 nM (Kholodenko *et al.* 1999). ATP concentration was assumed to be 1 mM (Posner *et al.* 1992). Concentrations of c-MET

and Tyr were assumed to be constant throughout the early time points investigated in our model. We assumed that ternary complexes of c-MET, ATP, and tyrosine containing substrate or effector (Tyr) were the necessary intermediate complex leading to effector phosphorylation. The actual mechanistic details of this phosphorylation reaction does not change the time-dependent buildup of phosphorylated c-MET and Tyr. All enzymatic reactions were assumed be irreversible, and PTPs were assumed to follow Michealis-Menten kinetics. The activation model used first-order mass-action kinetics and sets of differential equations described by specific kinetic and thermodynamic parameters.

Internalin B (InlB) was used as the extracellular ligand to activate c-MET in computer simulations and corresponding cell culture experiments. InlB was recently identified as a bacterial agonist for c-MET RTK, and was shown to mimic c-MET activation and endocytosis following stimulation with cognate HGF ligand (Ireton *et al.* 1999; Li *et al.* 2005). Furthermore, InlB initiated c-MET signaling as measured by phosphorylation of Gab1, Cbl and Shc along with activation of the PI3K pathway (Shen *et al.* 2000). K_d values for InlB binding to the extracellular domain of c-MET was measured to be ~20-30 nM (Machner *et al.* 2003). On/off rates for InlB-Met binding, which were more crucial for developing time-dependent models, were unknown. Thus, we used InlB on and off rates consistent with the equilibrium binding constant and the time constraints of the signaling process (Wiley *et al.* 2003). With $k_{on} = 10\ \mu M^{-1} \cdot s^{-1}$ and $k_{off} = 0.01\ s^{-1}$, the receptor reached a steady state value within 2 minutes. Increasing or decreasing the on and off rates by a factor of 10 did not significantly affect the response curves that described build up of phosphorylated c-MET or pTyr.

Table 2.2. Kinetic equations describing the c-MET activation pathway

$$d[MET]/dt = \nu_{-1}+\nu_{-2}+\nu_{-24}+\nu_{26}+\nu_{19}-\nu_{1}-\nu_{2}-\nu_{24}$$

$$d[ATP]/dt = \nu_{-1}+\nu_{-4}+\nu_{-5}+\nu_{-8}+\nu_{-9}+\nu_{-12}+\nu_{-13}+\nu_{-16}-\nu_{1}-\nu_{4}-\nu_{5}-\nu_{8}-\nu_{9}-\nu_{12}-\nu_{13}-\nu_{16}$$

$$d[Tyr]/dt = \nu_{-2}+\nu_{-3}+\nu_{-6}+\nu_{-7}+\nu_{-10}+\nu_{-11}+\nu_{-14}+\nu_{-15}-\nu_{2}-\nu_{3}-\nu_{6}-\nu_{7}-\nu_{10}-\nu_{11}-\nu_{14}-\nu_{15}$$

$$d[MET\text{-}Tyr]/dt = \nu_{2}+\nu_{-4}+\nu_{-24}+\nu_{26}-\nu_{-2}-\nu_{4}-\nu_{24}$$

$$d[MET\text{-}ATP]/dt = \nu_{1}+\nu_{-3}+\nu_{-24}+\nu_{26}-\nu_{-1}-\nu_{3}-\nu_{24}-\nu_{17}$$

$$d[MET\text{-}ATP\text{-}Tyr]/dt = \nu_{3}+\nu_{4}+\nu_{-24}+\nu_{26}-\nu_{-3}-\nu_{-4}-\nu_{24}-\nu_{19}$$

$$d[pMET]/dt = \nu_{-5}+\nu_{-6}+\nu_{-23}+\nu_{17}-\nu_{5}-\nu_{6}-\nu_{23}-\nu_{26}$$

$$d[pMET\text{-}ATP]/dt = \nu_{5}+\nu_{-7}+\nu_{-23}-\nu_{26}-\nu_{-5}-\nu_{7}-\nu_{23}$$

$$d[pMET\text{-}Tyr]/dt = \nu_{6}+\nu_{-8}+\nu_{-23}-\nu_{26}-\nu_{-6}-\nu_{8}-\nu_{23}$$

$$d[pMET\text{-}ATP\text{-}Tyr]/dt = \nu_{7}+\nu_{8}+\nu_{-23}-\nu_{26}-\nu_{-7}-\nu_{-8}-\nu_{24}-\nu_{20}$$

$$d[MET_2]/dt = \nu_{-9}+\nu_{-10}+\nu_{24}+\nu_{25}-\nu_{9}-\nu_{10}-\nu_{24}$$

$$d[MET_2\text{-}ATP]/dt = \nu_{9}+\nu_{-11}+\nu_{24}+\nu_{25}-\nu_{-9}-\nu_{11}-\nu_{-24}-\nu_{18}$$

$$d[MET_2\text{-}Tyr]/dt = \nu_{10}+\nu_{-12}+\nu_{24}+\nu_{25}-\nu_{-10}-\nu_{12}-\nu_{-24}$$

$$d[MET_2\text{-}ATP\text{-}Tyr]/dt = \nu_{11}+\nu_{12}+\nu_{24}+\nu_{25}-\nu_{-11}-\nu_{-12}-\nu_{-24}-\nu_{21}$$

$$d[pMET_2]/dt = \nu_{-13}+\nu_{-14}+\nu_{23}+\nu_{18}-\nu_{13}-\nu_{14}-\nu_{25}-\nu_{-23}$$

$$d[pMET_2\text{-}ATP]/dt = \nu_{13}+\nu_{-15}+\nu_{23}-\nu_{25}-\nu_{1}-\nu_{2}-\nu_{-23}$$

$$d[pMET_2\text{-}Tyr]/dt = \nu_{14}+\nu_{-16}+\nu_{23}-\nu_{25}-\nu_{-14}-\nu_{16}-\nu_{-23}$$

$$d[pMET_2\text{-}ATP\text{-}Tyr]/dt = \nu_{15}+\nu_{16}+\nu_{23}-\nu_{25}-\nu_{-15}-\nu_{-16}-\nu_{-23}-\nu_{22}$$

$$d[pTyr]/dt = \nu_{19}+\nu_{20}+\nu_{21}+\nu_{22}-\nu_{27}$$

Each reaction *j* in **Fig. 2.1** has an associated concentration-dependence rate vj expression described in Table 2.1. Reactions 23, 24, 25, 26, and 27 have identical rate constants, but differ in the concentration of their reactants.

InlB-induced c-MET phosphorylation

The quantitative and qualitative predictions of the activation model were tested experimentally. The Vero cells (ATCC) used for these studies endogenously expressed c-MET. Prior to any stimulation with extracellular ligand, the cells were grown to ~60%

confluency and serum-starved for 12-24 hours. For ligand stimulation experiments, cells were stimulated with 1, 5 and 20nM InlB. At 0, 15, 60, 120 and 300 seconds post InlB stimulation, the cells were washed twice with ice-cold PBS for 3 minutes and subsequently lysed in Triton X-100 lysis buffer (50mM Tris pH 7.5, 150 mM NaCl, 1% Triton X-100, 3 mM Na_3VO_4, 2 mM EDTA, 2 mM NaF, and protease inhibitor cocktail). Protein concentration in the lysates were determined using BioRad DC Assay, and 500-1000 μgs of total protein was used for c-MET immunoprecipitation with primary antibody to the c-MET extracellular region (antibody DO-24, Upstate, NY). Quantitative analyses to determine the percentage of total receptor that was phosphorylated used the strategy described by Kholodenko *et al.* (Kholodenko *et al.* 1999). Briefly, cell lysates at each time point were divided into equal parts for parallel immunoprecipitation with anti-phospho tyrosine (PY)-agarose conjugate and anti-MET (Upstate). The anti-PY immunoprecipitates and the c-MET immunoprecipitates at indicated time points post ligand-stimulation were run on the same gel for immunoblotting with anti-MET antibody. InlB-induced c-MET phosphorylation was measured at early time points where internalization is negligible (Li *et al.* 2005). Immunoprecipitation was performed according to standard protocols. Briefly, lysates were incubated with primary antibody overnight at 4°C, and then incubated with 100 μLs of Protein A agarose in PBS for 3-4 hours at 4°C to capture the immune complex. The tubes were spun, beads washed 3-4 times in the lysis buffer, and then resuspended in SDS-PAGE buffer. Samples were separated with 7.5% polyacrylamide gels and SDS-PAGE for subsequent immunoblotting. After an overnight incubation in blocking buffer (1% BSA in TBST) at 4°C, the membranes were incubated with anti-MET antibody (typically at 1:1000 dilution) for 1 hour at room temperature. After 3 successive 10 minute washes in TBST, the membranes were incubated with secondary antibody (1:10000 dilution) for 45 minutes. The proteins were visualized with ECL Plus chemiluminescent kit (Amersham) and exposure to film (Kodak X-OMAT AR). The fraction of total c-MET phosphorylated in Vero cells was determined from the quantified blots as the ratio of signal from anti-MET antibody in precipitates from PY antibody to that from the anti-MET antibody for

each time points (Kholodenko *et al.* 1999). X-ray films containing the protein bands were imaged in a MultiImage Light Cabinet (Alpha Innotech Corp.) and densitometry performed using ChemiImager® software provided by the manufacturer. Experiments were performed within the dynamic range of the antibody signal and the exposure time.

The pervanadate stimulation experiments have been previously described (Sheth and Watowich 2005). Briefly, cells were stimulated with the addition of pervanadate-containing media. At specific time points post stimulation, the cells were lysed and subjected to immunoprecipitation with anti-MET antibody. The precipitated proteins were separated on denaturing polyacrylamide gels and transferred to a PVDF membrane using protocols outlined above. The membranes were probed with anti-PY antibody and reprobed with anti-MET antibody. Quantitative analyses was used to obtain the fraction of c-MET phosphorylated, At PY signal saturation, it was assumed that all active c-MET receptors were fully phosphorylated. In that case, the fraction of phosphorylated receptor would be the ratio of signal at any time point to the signal measured at saturation.

CHAPTER 3:
OLIGOMERIZATION-INDUCED DIFFERENTIAL DEPHOSPHORYLATION OF C-MET RECEPTOR TYROSINE KINASE[2]

INTRODUCTION

The importance of dephosphorylation in regulating RTK activation has been demonstrated by ligand-independent platelet derived growth factor receptor (PDGFR) and IR autophosphorylation following pervanadate treatment in cultured cells (Baxter *et al.* 1998; Posner *et al.* 1994). These studies implied that RTK phosphorylation was dynamically regulated by the combined action of kinase and phosphatase activity. A recent study has suggested that oligomerization might modulate RTK dephosphorylation (Shimizu *et al.* 2001). Unfortunately, the chemical cross-linking step used in that study made it difficult to accurately correlate differences in dephosphorylation to a unique receptor oligomeric state, and cellular cofactors coimmunoprecipitating with different receptor oligomeric states may have also contributed to the observed differential dephosphorylation (Shimizu *et al.* 2001).

We have recently utilized a well-defined *in vitro* system, consisting of functional monomeric and dimeric forms of c-MET, to develop a detailed understanding of how oligomerization state modulates a receptor's biochemical and conformational properties and thus contributes to receptor activation (Hays and Watowich 2003; Hays and Watowich 2004). c-MET, the RTK for hepatocyte growth factor/scatter factor (HGF/SF), is responsible for cell proliferation, differentiation, branching morphogenesis, and protein synthesis associated with an invasive cell phenotype (Birchmeier *et al.* 2003). Sustained

[2] Reproduced with permission from the following source: ACS Publications (http://pubs.acs.org/journals/bichaw/index.html); Sheth P. R., Watowich, S. J. 2005. Oligomerization-induced differential dephosphorylation in c-MET receptor tyrosine kinase. *Biochemistry*. July 26;44(33):10984-93.

c-MET signaling, caused by c-MET overexpression, HGF overexpression, or activating c-MET mutations, has been linked to solid tumor growth and metastasis (Birchmeier *et al.* 2003; Trusolino and Comoglio 2002). TPR-MET, a naturally occurring oncoprotein resulting from fusion of the TPR region of nuclear pore complex and the cytoplasmic domain of c-MET, recapitulated many of the molecular and cellular properties of ligand-activated c-MET. Specifically, TPR-MET has been shown to be an active kinase both *in vitro* and *in vivo*, and it activated c-MET signaling pathways in transformed cells (Rodrigues and Park 1993; Rodrigues and Park 1994). Thus, it is an established model system for the ligand-dependent oligomeric state of c-MET (**Fig. 3.1**). The isolated cytoplasmic domain of c-MET (cytoMET; **Fig. 3.1**) served as a functional analog of monomeric c-MET. Detailed comparative kinetic analysis of similarly phosphorylated TPR-MET and cytoMET showed that their catalytic efficiency for substrate phosphorylation differed several-fold (Hays and Watowich 2003). In addition, TPR-MET showed significantly lower K_D for peptide substrates as compared to cytoMET (Hays and Watowich 2004). These results clearly showed that the RTK oligomeric state substantially influenced its kinetic and thermodynamic properties, implying that functionally necessary conformational changes accompanied receptor oligomerization.

Regulation of c-MET by protein tyrosine phosphatases (PTPs) is poorly understood, although studies using substrate trapping mutants, antisense RNA, and phosphotyrosine peptides have proposed DEP-1 (CD148/PTP-η), PTP-S and leukocyte common antigen-related (LAR) to be potentially involved in c-MET regulation (Kulas *et al.* 1996; Palka *et al.* 2003; Villa-Moruzzi *et al.* 1998). Detailed animal model or cell culture studies have yet to substantiate a role of these indicated PTPs in c-MET signaling. Moreover, DEP-1 was observed to preferentially dephosphorylate the carboxyl-terminal tyrosines Y^{1349} and Y^{1365} in c-MET (Palka *et al.* 2003), suggesting that phosphatase site-specific preferences might be an additional mechanism for regulating receptor signaling.

To better understand the relationship between RTK oligomerization, dephosphorylation, and receptor regulation, we now present convincing data showing the RTK dephosphorylation can be modulated by its oligomeric state. These studies used the

well-behaved TPR-MET/cytoMET system to represent ligand-stimulated oligomeric and unactivated monomeric forms of c-MET (Hays and Watowich 2003; Hays and Watowich 2004; Rodrigues and Park 1993) and demonstrated that oligomerization interfered with receptor dephosphorylation. This observation held for all examined phosphorylated tyrosines, although the degree to which oligomerization interfered with dephosphorylation was quantitatively different for tyrosines located in the activation loop and carboxy-terminal tail of the receptor. Cell culture studies showed rapid and complete c-MET phosphorylation following phosphatase inhibition. Our results clearly revealed a "protective" role for oligomerization in dephosphorylation of c-MET RTK, which could be crucial for proper activation and regulation of the receptor. Furthermore, our data suggests a dynamic flux balance exists between the kinase and phosphatase activities associated with RTKs, and when these fluxes are differentially perturbed by oligomerization then tyrosines necessary for RTK signaling are rapidly phosphorylated.

RESULTS

TPR-MET and cytoMET phosphorylation

Both TPR-MET (~60 kD) and cytoMET (~44 kD) were separately purified from Sf9 cells to >90% homogeneity (Hays and Watowich 2003). Quantitative western blot analysis of purified TPR-MET and cytoMET using antibodies against phosphorylated tyrosines (4G10), activation loop $Y^{1234,1235}$, and carboxy-terminal tail Y^{1349} and Y^{1365} showed the same tyrosines on both proteins were phosphorylated to identical levels (**Fig. 3.2**). Furthermore, incubation of phosphorylated TPR-MET or cytoMET with ^{32}P-γ-ATP revealed no further incorporation of phosphate into either TPR-MET or cytoMET, indicating both kinases were completely phosphorylated (Hays and Watowich 2003). No dephosphorylation was observed over time in stored solutions of purified kinases prior to dephosphorylation assay (**Fig. 3.3B**).

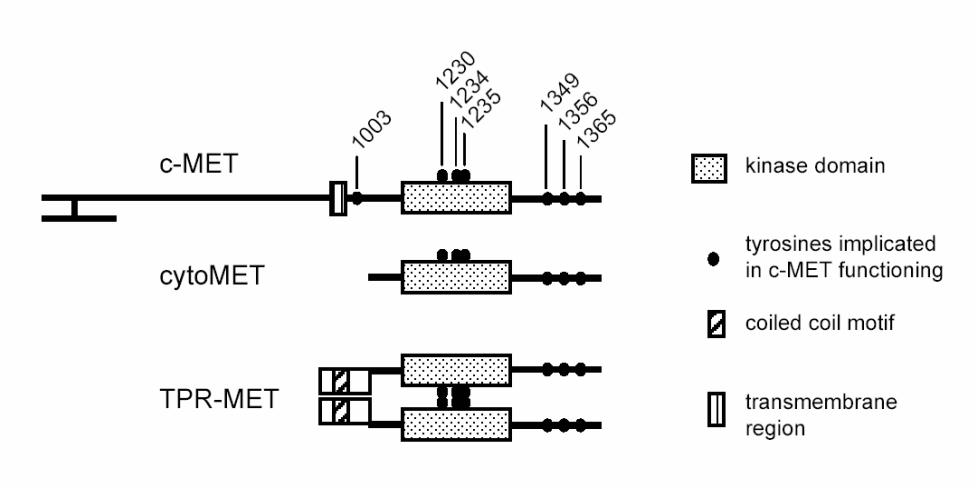

Fig. 3.1. Domain organization of c-MET, cytoMET and TPR-MET.

CytoMET corresponds to the cytoplasmic portion of c-MET contained within TPR-MET. TPR-MET corresponds to a fusion between the cytoplasmic domain of c-MET and TPR, a coiled-coil domain from the nuclear pore complex. The coiled-coil interactions within the TPR domain render TPR-MET a constitutive dimer (Rodrigues and Park 1993). Tyrosines that have been implicated in c-MET functioning are marked. Both cytoMET and TPR-MET proteins contain all known phosphorylation sites within the activation loop (corresponding to c-MET Y^{1230}, Y^{1234}, Y^{1235}) and the carboxy-terminal tail (corresponding to c-MET Y^{1349}, Y^{1356}, and Y^{1365}).

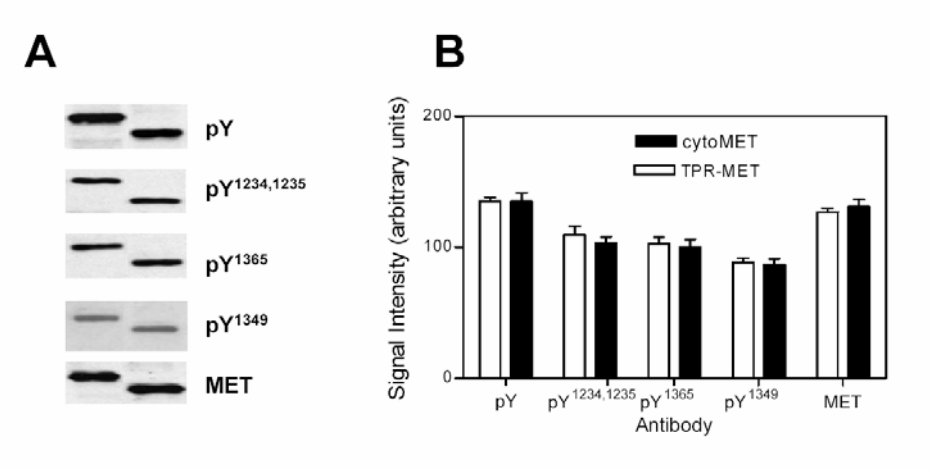

Fig. 3.2. Phosphorylation levels in cytoMET and TPR-MET.

The phosphorylation levels in cytoMET and TPR-MET were measured using different phospho-specific antibodies. Equimolar quantities of purified cytoMET and TPR-MET proteins were separated on polyacrylamide gels and subjected to Western blot analyses using anti-PY (4G10). The membranes were stripped and reprobed with anti-phospho-$Y^{1234,\ 1235}$, anti-phospho-Y^{1349}, anti-phospho-Y^{1365}, and anti-MET antibody as a loading control (*Panel A*). The higher molecular weight band corresponds to TPR-MET (~60 KD) and the lower molecular weight band corresponds to cytoMET (~40 KD). X-ray films containing the protein bands were imaged in a MultiImage Light Cabinet (Alpha Innotech Corp.) and densitometry was performed using ChemiImager® software provided by the manufacturer. Experiments were performed within the dynamic range of the antibody signal and the exposure time. The data from the densitometry analyses for cytoMET and TPR-MET is depicted as a bar graph in *Panel B*. The data is presented as mean of three different experiments with error bars representing standard deviations. Comparable levels of phosphorylation were seen at two different protein concentrations.

Differential dephosphorylation of oligomeric TPR-MET and monomeric cytoMET by PTPβ

To test the effects of oligomerization on dephosphorylation, we compared the overall dephosphorylation rates of equimolar quantities of phosphorylated cytoMET and TPR-MET. The rate and extent of dephosphorylation in each protein was examined using commercially available recombinant PTPβ catalytic domain. This phosphatase belongs to the receptor-like protein tyrosine phosphatases (RPTP) sub-family, which includes DEP-1, a reported physiological phosphatase for c-MET. Approximately 50% overall sequence

identity existed between PTPβ and DEP-1 and ~60% sequence identity and 80% sequence similarity was found between their catalytic domains.

Equimolar amounts (1 μM) of fully phosphorylated TPR-MET and cytoMET were separately incubated with PTPβ. Preliminary studies showed that TPR-MET consistently required more phosphatase than cytoMET to achieve comparable dephosphorylation between the two proteins. No significant dephosphorylation of TPR-MET was observed at low PTPβ concentrations. No dephosphorylation was observed for either TPR-MET or cytoMET when PTPβ was not included in the reaction. Aliquots were removed from each phosphatase reaction mixture at fixed times and the reactions were quenched by addition of SDS-PAGE buffer. The degree of tyrosine phosphorylation in each reaction aliquot was examined by phosphotyrosine immunoblotting (**Fig. 3.3A**). All immunoblotting experiments were performed within the linear dynamic range of the antibody signal and the exposure time. Both TPR-MET and cytoMET were dephosphorylated during the 120 min reaction period examined, within which, cytoMET was dephosphorylated more rapidly and to a greater extent than TPR-MET (**Fig. 3.3A**). Although the comprehensive studies discussed in this paper utilized PTPβ for reasons cited above, preliminary experiments with other commercially available phosphatases yielded similar results, with cytoMET clearly dephosphorylated more rapidly and to a greater extent than TPR-MET (**Fig. 3.4**). No significant differences in the dephosphorylation reactions were observed when the above reactions were performed with the addition of 1 μM of the generic kinase inhibitor staurosporine in the dephosphorylation buffers (**Fig. 3.3B**). This control eliminated the possibility that the observed differences in global dephosphorylation rates and phosphotyrosine levels were due to the differences in re-autophosphorylation rates of the purified proteins that were induced by possible residual ATP in the storage buffers.

The global dephosphorylation reaction data for each receptor were fit to exponential decay equations. Analyses of the curves clearly showed that cytoMET dephosphorylation occurred rapidly, and was essentially complete within 30 min (**Fig. 3.3B**). Under similar reaction conditions, the dephosphorylation rate of TPR-MET was

substantially slower. Significant differences in the extent of dephosphorylation were also observed between the monomeric and dimeric form of the MET receptor. Although the global dephosphorylation reaction kinetics were fit to one-phase exponential decay models (**Fig. 3.3B**) with an excellent goodness-of-fit obtained for both reactions ($R^2 >$ 0.9), the reaction times were very long, which could result in potential loss of PTPβ activity. If this occurred, it might adversely affect the accuracy of our quantitative exponential decay analysis and comparisons based on this analysis. Thus, quantitative comparisons between the two oligomeric states of the MET receptor relied on initial rates of dephosphorylation measured within time intervals where no loss of PTPβ activity was observed. The slope of the lines plotted in insets of **Fig. 3.3B** provided initial dephosphorylation rates for the monomeric and dimeric receptor; the dephosphorylation rate of dimeric TPR-MET was ~4-fold slower rate than the dephosphorylation rate of its monomeric counterpart, cytoMET (**Fig. 3.3B**, **Table 3.1**). Dephosphorylation rates calculated from parameters derived from exponential curves for data between 0-120 minutes gave similar results, with a 6-fold difference in dephosphorylation rates calculated for cytoMET and TPR-MET. To make certain that this difference in dephosphorylation rates was not dependent upon a singular receptor concentration, we performed dephosphorylation reactions at additional cytoMET and TPR-MET concentrations ultimately spanning a 100-fold concentration range for the receptors. The data at these concentrations were qualitatively similar to our findings at 1 μM receptor concentrations, consistently showing that TPR-MET dephosphorylated slower than cytoMET (**Fig. 3.3C**). There are six possible phosphorylated tyrosine sites in TPR-MET and cytoMET, corresponding to Y^{1231}, Y^{1234}, Y^{1235}, Y^{1349}, Y^{1356} and Y^{1365} in c-MET (**Fig. 3.1**). Fit to the global dephosphorylation data could indicate two equally possible scenarios, either the dephosphorylation rate at each phosphotyrosine sites were independent of the phosphorylation state of the other sites, or different multi-phase exponential functions corresponding to different site dephosphorylation rates were too close to one another for us to deconvolute the separate exponentials from our data. Detailed kinetic analyses with site-specific antibodies (described in the next section),

more sensitive probes, or site-specific mutants would be expected to differentiate between these models.

Estimations of K_m and V_{max} of PTPβ for cytoMET and TPR-MET substrates were derived by fitting the velocity data at different receptor concentrations to the Michealis-Menten (M-M) equation (**Fig. 3.3C**). The experimental data for cytoMET and TPR-MET fit the M-M equation with goodness of fit $R^2 > 0.97$. Significantly, different K_m and V_{max} values were calculated for TPR-MET and cytoMET as PTPβ substrates; PTPβ had ~7-fold greater K_m and ~2-fold smaller V_{max} for TPR-MET compared to cytoMET (**Table 3.2**). Interestingly, the observed PTPβ K_m values measured with the Met substrates were comparable to the micromolar K_m values observed for PTPβ reacting with several phosphotyrosine peptide substrates (Cho *et al.* 1993). Coupling the low K_M and increased V_{max} yielded a 10-fold decreased substrate specificity of PTPβ for TPR-MET relative to cytoMET. Based on these experiments, we concluded that the dephosphorylation profiles of similarly phosphorylated TPR-MET and cytoMET differed significantly, such that TPR-MET had a slower rate of dephosphorylation and lower substrate specificity relative to cytoMET.

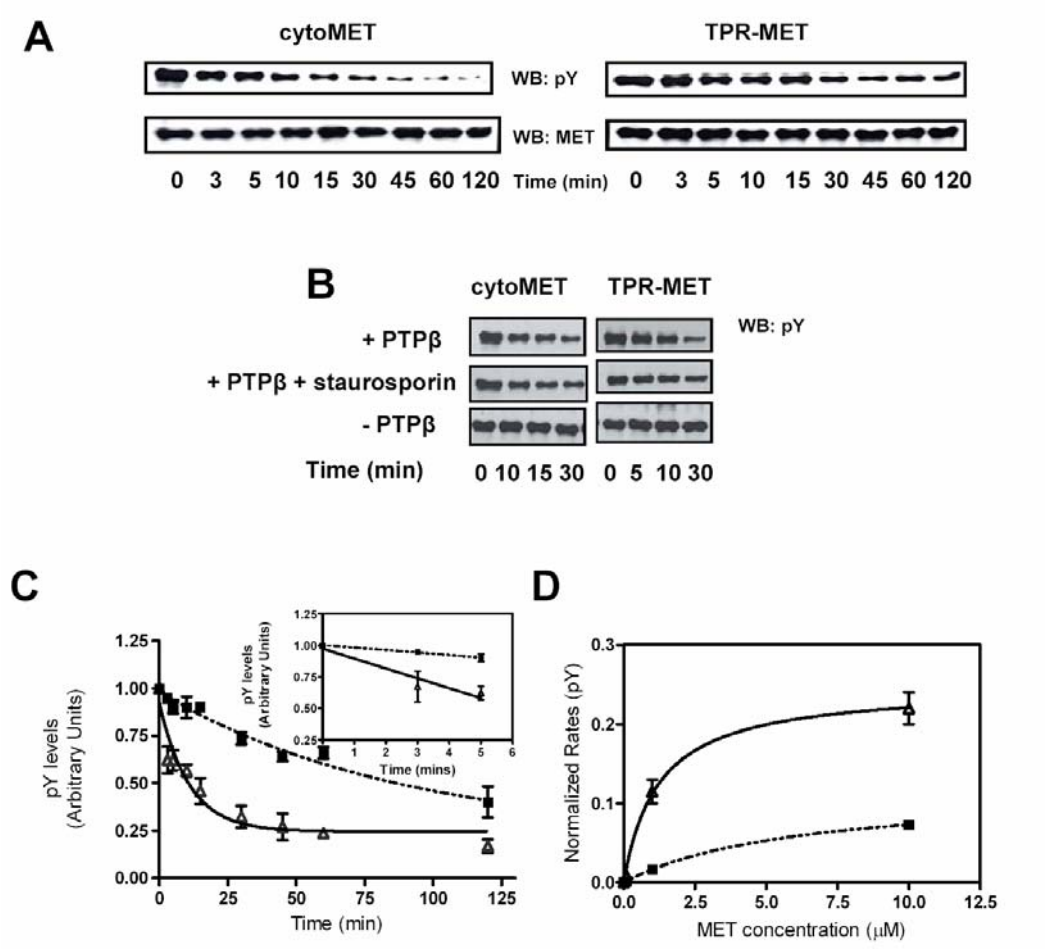

Fig. 3.3. Global dephosphorylation in cytoMET and TPR-MET.

1μM of purified phosphorylated protein was incubated in phosphatase buffer with PTPβ, and aliquots removed at indicated times. The proteins separated on polyacrylamide gels, transferred to PVDF membrane and probed with phosphotyrosine antibody. The blots were stripped and re-probed with anti-MET antibody. Control experiments were performed in presence of staurosporine in the MET-PTPβ mixture and in absence of PTPβ. The representative immunoblots for dephosphorylation and controls are shown in *Panel A and B* respectively, and quantitative representation of normalized phosphorylation levels at different time points subsequent to addition of PTPβ are shown in *Panel C*. The data was fitted to one-phase exponential decay for TPR-MET (■) and cytoMET (Δ) using GraphPad Prism®. Each point in *Panel B* plots represent three independent experiments done in duplicate at a fixed concentration. The insets in *Panel B* represent the data at early times, and the slope of the line depicted in the insets represents the initial velocity of dephosphorylation for cytoMET (Δ) and TPR-MET (■) at 1μM concentration. Data was fit to Michealis-Menten curves (*Panel D*). The fits for cytoMET and TPR-MET are indicated by solid lines and dotted lines, respectively in *Panels B* and *C*.

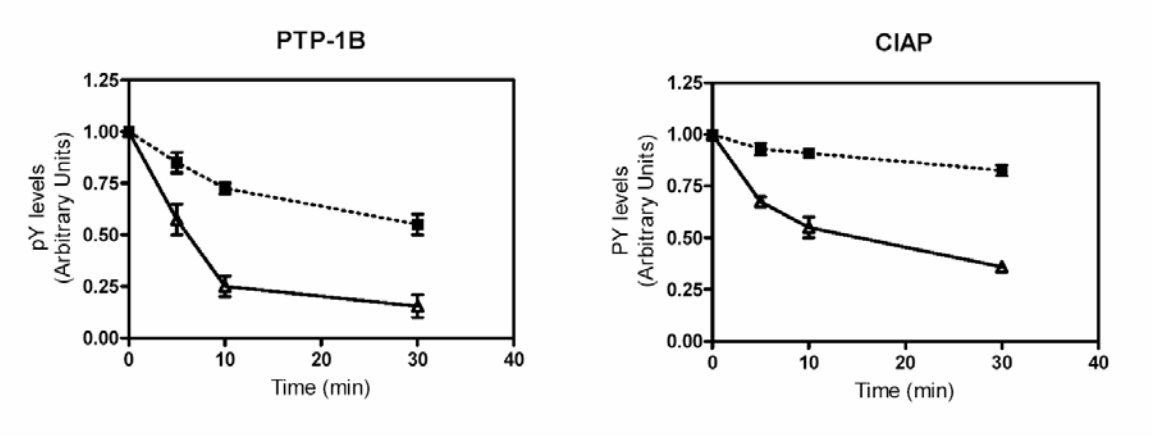

Fig. 3.4. PTP1B and CIAP induced dephosphorylation of cytoMET and TPR-MET.

1μM of purified phosphorylated protein was incubated in phosphatase buffer with PTPIB and Alkaline phosphatase, and aliquots removed at indicated times. The assay was performed as described for global dephosphorylation. The quantitative representation of normalized phosphorylation levels at different time points subsequent to addition of PTP1B and alkaline phosphatase are shown. The data for TPR-MET (■) and cytoMET (Δ) represent two independent experiments done in duplicate at a fixed concentration.

Table 3.1. Dephosphorylation velocities for TPR-MET and cytoMET

Sites	V_0 (units/min) cytoMET	V_0(units/min) TPR-MET	V_0 cytoMET/TPR-MET
All	0.0783 ± 0.022	0.0194 ± 0.002	~ 4 (*p=0.0053*)
$Y^{1234,1235}$	0.0902 ± 0.002	0.038 ± 0.012	~ 2.5 *(p=0.0074)*
Y^{1349}	0.110 ±0.021	0.017 ± 0.01	~ 7 (*p=0.0003*)
Y^{1365}	0.095 ± 0.036	0.014 ± 0.011	~ 6.5 *(p=0.0004)*

Dephosphorylation of equimolar quantities of similarly phosphorylated cytoMET and TPR-MET was analyzed as described under "Experimental Procedures". The V0 values represent V0 ± SE (units/min) for unweighted nonlinear least square regression analyses of the data from figure 2. Two-tailed p-values were calculated using paired t-tests.

Table 3.2. Kinetic data for PTPβ using TPR-MET and cytoMET as substrates

Sites	TPR-MET			cytoMET		
	K_M (μM)	V_{MAX} (units/min)	V_{MAX}/K_M	K_M (μM)	V_{MAX} (units/min)	V_{MAX}/K_M
All	6.184 (± 1.547)	0.132 (± 0.024)	0.021	1.219 (± 0.297)	0.247 (± 0.016)	0.20
$Y^{1234,1235}$	4.544 (± 1.442)	0.202 (± 0.036)	0.044	1.550 (± 0.528)	0.271 (± 0.026)	0.17
Y^{1349}	5.172 (± 1.721)	0.102 (± 0.010)	0.019	*	*	
Y^{1365}	4.184 (± 1.470)	0.093 (± 0.011)	0.022	*	*	

*** data did not fit Michealis-Menten equation**

Dephosphorylation of cytoMET and TPR-MET was analyzed as described under "Materials and Methods". The values reported represent V_{max} ± SE (units/min) and K_m ± SE (μM) for unweighted nonlinear least square regression analyses of the data from figures 2 and 3. Two-tailed p-values were calculated using paired t-tests**.**

Dephosphorylation kinetics of activation loop and carboxy-terminal tyrosines

Wild type c-MET contains three phosphotyrosine sites within its activation loop (Y^{1230}, Y^{1234}, Y^{1235}) and three phosphotyrosine sites within its carboxy-terminal tail (Y^{1349}, Y^{1356}, and Y^{1365}). These phosphorylation sites were present in both cytoMET and TPR-MET (**Fig. 3.1**). Phosphorylation of activation loop tyrosines 1234 and 1235 has been shown to be important for increased kinase activity of the receptor (Rodrigues and Park 1994). Phosphorylation of carboxy-tail tyrosine 1349 and 1356 has been shown to be necessary for recruitment of downstream effector molecules Gab1 and Grb2, respectively (Birchmeier *et al.* 2003). Although proteins that interact with phosphorylated tyrosine 1365 have not been identified, mutation analyses have indicated that this site was involved in morphogenesis (Weidner *et al.* 1995). To probe the impact of oligomerization on the structural and functional properties of the activation loop and carboxy-tail sub-domains, site-specific antibodies were used to compare dephosphorylation rates of specific phosphotyrosines in cytoMET and TPR-MET.

Purified cytoMET and TPR-MET were separately dephosphorylated with PTPβ under similar conditions as used for the global dephosphorylation assay. The membranes were sequentially probed with anti-phospho- $Y^{1234,\ 1235}$, anti-phospho-Y^{1365}, and anti-MET antibodies with the membranes extensively stripped between each primary antibody. CytoMET and TPR-MET showed clear differences in the intensity patterns of the antibody response from the activation loop and carboxy-tail regions (**Fig. 3.5A**). Detailed comparative quantitative analysis of the digitized antibody signals showed cytoMET was dephosphorylated at a faster rate than TPR-MET on both its activation loop tyrosines $Y^{1234,1235}$ and its carboxy-tail tyrosine Y^{1365} (**Fig. 3.5B**) The initial dephosphorylation rate for the activation loop calculated from the linear response region of the dephosphorylation reaction (inset **Fig. 3.5B** *left-hand panel*) was ~2.5 fold larger for cytoMET relative to TPR-MET (**Table 3.1**) The data for cytoMET and TPR-MET activation loop dephosphorylation were separately fit to one-phase exponential decay curves ($R^2 > 0.95$; **Fig. 3.5B**, *left-hand panel*) and comparable differences in dephosphorylation rates for dimeric TPR-MET and monomeric cytoMET were independently calculated from these curve fits. In contrast, the dephosphorylation rate of the carboxy-tail phosphotyrosine was ~6-fold slower in TPR-MET compared to cytoMET based on initial dephosphorylation rates (**Table 3.1**; **Fig. 3.5B** *right-hand panel*). The dephosphorylation data for the carboxy-tail Y^{1365} was fit to a two-phase exponential for cytoMET ($R^2 = 0.95$) and one-phase exponential for TPR-MET ($R^2 = 0.93$) and rate constants calculated from these fits gave a ~10-fold difference in the dephosphorylation rates for carboxy-tail site. Interestingly, the second exponential term of the cytoMET Y^{1365} dephosphorylation curve had a decay constant that was not significantly different than the decay constant calculated for the TPR-MET dephosphorylation exponential curve. The two-phase exponential observed for cytoMET carboxy-tail dephosphorylation could imply changes in local conformational environment of Y^{1365} due to dephosphorylation at distant sites. The decreased slope and decay constant observed in the second phase (late reaction times) of the cytoMET dephosphorylation curve relative to the first phase (early reaction times) of the curve implied that the dephosphorylation

rate of Y^{1365} slowed as additional cytoMET sites were dephosphorylated. The initial dephosphorylation rates and curves measured in cytoMET and TPR-MET for another carboxy-tail phosphotyrosine site, Y^{1349}, were very similar to those values measured for the carboxy-tail site Y^{1365}, and the dephosphorylation rate at Y^{1349} was ~7-fold slower in TPR-MET relative to cytoMET (**Table 3.1**). Similar qualitative differences in the activation loop and carboxy-tail phosphotyrosine dephosphorylation rates of cytoMET and TPR-MET were measured at several receptor concentrations covering a 100-fold receptor concentration range (**Fig. 3.5C**). The initial velocities computed from the straight line slopes (insets, **Fig. 3.5B**) at different receptor concentrations fit the M-M equation well for cytoMET and TPR-MET activation loop phosphotyrosine dephosphorylation (**Fig. 3.5C**, *left-hand panel*). PTPβ showed ~3-fold difference in the K_M and not a statistically significant difference in V_{max} for activation loop dephosphorylation between the different oligomeric states of the receptor. The M-M parameter comparison between cytoMET and TPR-MET carboxy-tail phosphotyrosine dephosphorylation was not made since the cytoMET data did not fit the M-M equation well (R^2 = 0.85). However, dephosphorylation rates at all examined substrate concentrations clearly showed dephosphorylation was significantly faster for the carboxy-tail tyrosines in cytoMET compared to TPR-MET (**Fig. 3.5C**, *right-hand panel*, and **Table 3.2**).

Our kinetic analyses consistently showed that TPR-MET activation loop and carboxy-tail phosphotyrosines had reduced susceptibility relative to cytoMET to phosphatase-catalyzed dephosphorylation. Interestingly, while the activation loop dephosphorylation rates between monomeric cytoMET and dimeric TPR-MET differed by at least 3-fold, there was an even greater ~7-fold difference in the carboxy-tail dephosphorylation rates between these two receptor states. This implied that oligomerization impacted the two domains of the receptors to different extents.

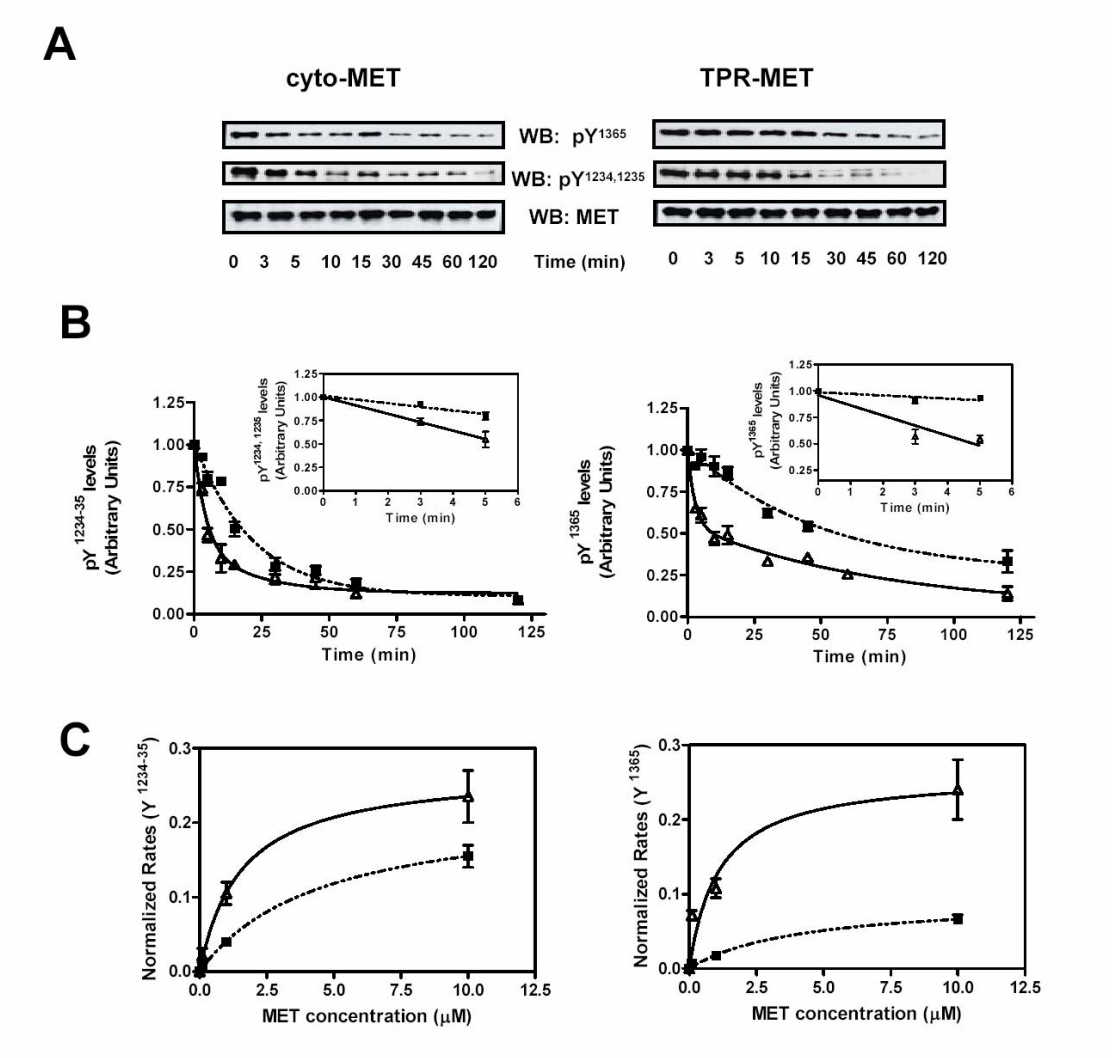

Fig. 3.5. Site-specific dephosphorylation in cytoMET and TPR-MET.
1μM of purified phosphorylated proteins were incubated in phosphatase buffer with PTPβ and aliquots removed at indicated times. The proteins separated on polyacrylamide gels, transferred to PVDF membrane and probed with different site-specific antibodies. The blots were stripped and re-probed with anti-MET antibody. The representative immunoblots are shown in *Panel A*, and quantitative representation of normalized phosphorylation levels at different time points subsequent to addition of PTPβ is shown in *Panel B*. The data was fitted to one-phase ($Y^{1234,1235}$ cytoMET (Δ), $Y^{1234,1235}$ TPR-MET (■), Y^{1365} TPR-MET (■)) or two-phase (Y^{1365}, cytoMET (Δ)) exponential decay using GraphPad Prism®. The insets in *Panel B* represent the data at early time points, and the slope of the line depicted in the insets represents the initial velocity of dephosphorylation for cytoMET (Δ) and TPR-MET (■).Each point in *Panel B* represents three independent experiments done in duplicate and error bars represent standard error. Data was fit to Michealis- Menten curves (*Panel C*). The fits for cytoMET and TPR-MET are indicated by solid lines and dotted lines, respectively in *Panels B* and *C*.

Pervandate-induced phosphorylation of WT unligated c-MET in intact cells

Our studies using the well-defined TPR-MET/cytoMET system showed that cytoMET functioned as a better phosphatase substrate than TPR-MET. Increased sensitivity to dephosphorylation in cytoMET compared to TPR-MET implied that phosphatase might efficiently dephosphorylate monomeric unstimulated c-MET on the cell surface, thereby providing an additional mechanism of regulating receptor signaling. Since direct comparison of dephosphorylation rates between monomeric and dimeric receptor states in intact cells were problematic, due in part to difficulties in determining receptor oligomerization levels and obtaining phosphorylated monomeric receptor, we monitored phosphorylation of unstimulated c-MET upon PTP inhibition. This process could be clearly followed, and served as a probe for phosphatase activity directed against monomeric c-MET. Although PTP-inhibition by pervanadate has resulted in PDGFR and IR phosphorylation (Baxter *et al.* 1998; Posner *et al.* 1994), it was unknown whether analogous receptor phosphorylation would occur for c-MET. Also unknown were the identities of sites that are phosphorylated in RTKs upon PTP inhibition.

Serum-starved confluent Vero cells were treated with pervanadate, lysed at various times post-treatment and c-MET was immunoprecipitated and immunoblotted with phosphotyrosine antibodies. The blots were stripped and reprobed with site-specific antibodies to monitor specific phosphotyrosine sites. Although similar amounts of c-MET were immunoprecipitated at each time post-treatment, a time-dependent increase in c-MET phosphorylation levels was observed upon pervanadate stimulation (**Fig. 3.6**). Immunoblots with phosphotyrosine antibody showed buildup of phosphorylated c-MET occurred within 2 min post-treatment and phosphotyrosine levels peaked at ~30 min post-treatment. (**Fig. 3.6A**) Reprobing the blot with anti-phospho Y^{1365}, anti-phospho Y^{1349}, and anti-phospho $Y^{1234, 1235}$ antibodies showed c-MET phosphorylation on all examined c-MET functionally important sites occurred within 5 min post-pervanadate treatment. Notably, the carboxy-tail phosphotyrosine sites clearly showed a delay in phosphorylation relative to the activation loop phosphotyrosine sites (**Fig. 3.6B**). Interestingly, both the amount of total c-MET and phosphorylated c-MET recovered from

cells decreased ~30 min post-treatment implying c-MET degradation was likely occurring at this time. Cells stimulated with sodium-orthovanadate also triggered buildup of phosphorylated c-MET, although to a lesser extent than that observed with the more potent PTP inhibitor pervandate. No phosphorylation of unstimulated c-MET occurred when cells were treated with buffer lacking PTP inhibitor. These results conclusively showed that rapid phosphorylation of c-MET functionally important tyrosines occurred when PTP activity was blocked, thus implying that PTPs play an important role in eliminating phosphorylation of unstimulated c-MET.

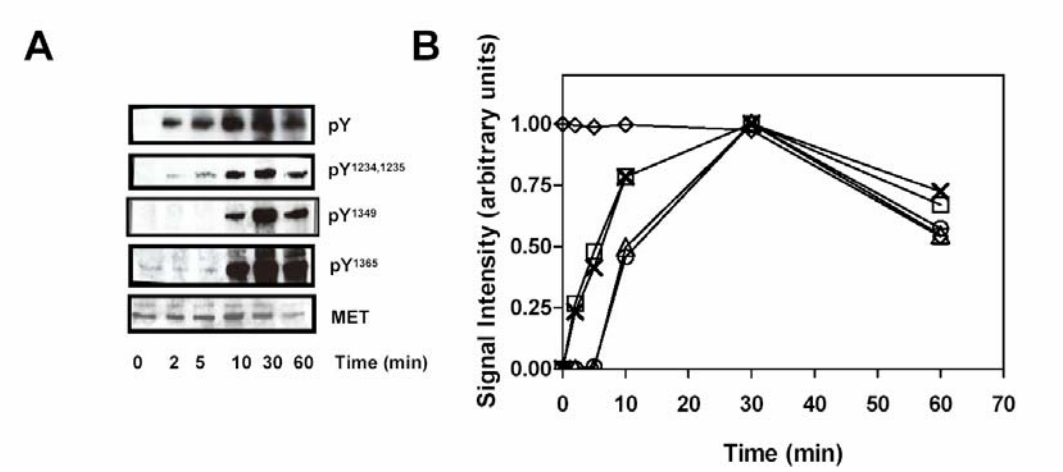

Fig. 3.6. Effect of phosphatase inhibition on c-MET monomer phosphorylation.

Vero cells were grown to near confluency and serum starved for 12-24 hours. Cells were treated with pervanadate and lysed at indicated times. c-MET was immunoprecipitated using antibody to the extracellular region (DO-24). The receptor was then separated by SDS-PAGE and transferred to PVDF membrane. The membrane was probed with phosphotyrosine antibody and stripped and reprobed with different c-MET phosphosite-specific antibodies. The blots were stripped and re-probed with anti-MET antibody. The representative immunoblots are shown in *Panel A*, and quantitative representation of normalized signal intensities are depicted in *Panel B* for $Y^{1234,1235}$ (X), Y^{1365} (Δ), Y^{1349} (O), PY (□) and MET (◊). Each point in *Panel B* represents three independent experiments done in duplicate. The error bars representing standard error are smaller than symbol size and hence not included in the figure for clarity.

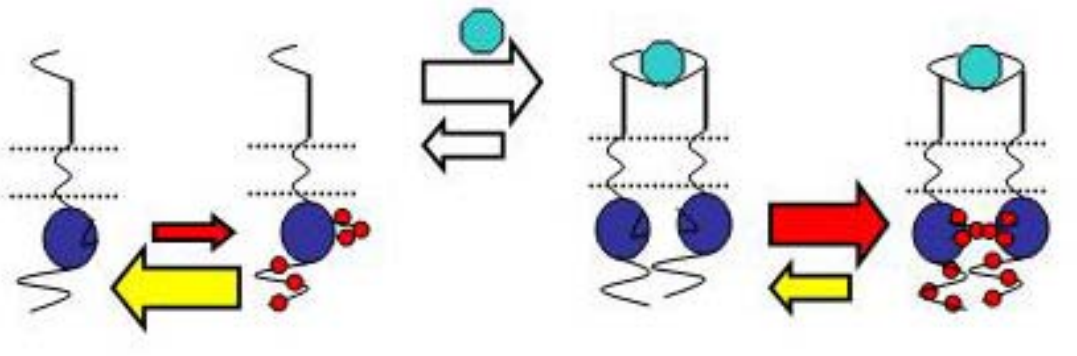

Fig. 3.7. Model for c-MET regulation by dephosphorylation and dimerization upon ligand binding.

In absence of any ligand, monomeric receptor resides on the cell membrane tightly regulated by the action of phosphatases. Upon ligand binding, the receptors dimerize and the system shifts to a different equilibrium state. Accumulation of phosphorylated receptor occurs due to the synergistic combination of increased kinase activity, resulting from oligomerization-dependent catalytic changes and activation loop phosphorylation and decreased dephosphorylation rates associated with the dimeric species. The equilibrium established by the autophosphorylation (red arrows) and dephosphorylation (yellow arrows) reactions for the tyrosines is depicted for monomeric unstimulated and ligand-stimulated receptors on the cell surface.

DISCUSSION

The importance of c-MET signaling is highlighted by its function in angiogenesis, placental and liver development, B-cell differentiation, embryogenesis, and dysregulation in multiple neoplastic disorders (van der Voort *et al.* 2000). The molecular mechanism regulating c-MET activation and signaling are not completely understood. The activation process of RTKs such as c-MET has typically been described as a series of sequential steps involving cognate ligand binding, receptor dimerization, receptor autophosphorylation, substrate recruitment and phosphorylation, and eventual downregulation of the receptor activity mediated by ligand dissociation, dephosphorylation and/or degradation. To provide a more detailed and quantitative model

of receptor activation, previous studies from our laboratory examined how oligomerization modulated receptor kinase activity (Hays and Watowich 2003; Hays and Watowich 2004). These studies used phosphorylated TPR-MET and cytoMET, well-defined functional surrogates for signaling-competent dimeric and inactive monomeric c-MET, and showed that the oligomeric state of the receptor markedly changed its kinetic and thermodynamic properties. In this paper, we sought to extend our understanding of receptor activation and regulation by investigating the impact of oligomerization on c-MET dephosphorylation.

Consistent with preliminary dephosphorylation studies on PDGFR (Shimizu *et al.* 2001), dimeric TPR-MET displayed increased resistance to dephosphorylation as compared to monomeric cytoMET. Significantly, the oligomerization-dependent changes in dephosphorylation rates were different for the activation loop and carboxy-terminal sub-domains of the receptor. Dimerization of the receptor reduced the susceptibility of its activation loop and carboxy-tail phosphotyrosines to dephosphorylation by ~3-fold and ~7-fold, respectively at 1 μM MET. Two possible explanations are consistent with these observations, namely dimerization induces conformational changes in the MET receptor that make it less susceptible to dephosphorylation relative to the monomeric MET receptor, or dimerization produces steric effects that "shield" the phosphotyrosine sites from phosphatases. The differences in K_m values for overall phosphorylation could support the hypotheses stated above, however, differences in V_{max} imply a possible structural reorganization of substrate site as opposed to a mere "shielding effect". In addition, the switch between non-Michealis-Menten and Michealis-Menten kinetics observed for the cytoMET and TPR-MET carboxy-tail phosphotyrosine supports a model of structural reorganization occurring during receptor oligomerization. The differences between cytoMET and TPR-MET in dephosphorylation rates for activation loop as well as carboxy-tail phosphotyrosines suggest that upon oligomerization conformational changes occur in several domains within the receptor. The precise understanding of the nature of these dimerization-induced conformational and/or possible dynamics changes awaits further studies. The different reaction kinetics shown by PTPβ towards protein

substrates in different oligomerization states indicates that PTPβ-catalyzed dephosphorylation is more complex for protein substrates than for phosphotyrosylpeptide substrates.

Classically, it was believed that the sole role of ligand-induced receptor oligomerization was to autophosphorylate the receptor's activation loop, which in turn was believed necessary to activate the receptor's kinase function. *In vitro* studies using isolated kinase domains (Baxter *et al.* 1998; Rodrigues and Park 1993), and *ex vivo* studies using phosphatase inhibitor have shown conclusively that monomeric receptors can be rapidly phosphorylated on tyrosine residues involved in intracellular signal propagation (Baxter *et al.* 1998; Posner *et al.* 1994). Thus, it is clear that ligand-induced receptor oligomerization is not necessary for kinase activity.

Alternatively, our work and that of others (Hubbard *et al.* 1998; Rodrigues and Park 1993) suggests that RTK oligomerization is necessary to rapidly switch the receptor between distinct signaling incompetent and signaling competent states. In this model, a RTK is in a signaling competent state when it is phosphorylated at specific tyrosine residues and capable of binding and activating immediate down-stream effectors (e.g. PI3K, Gab1, Grb2). The receptor is in a signaling incompetent state when it is dephosphorylated and unable to bind and activate immediate downstream effectors. Neither functional state is restricted to a particular oligomeric state; it is possible to observe monomeric signaling competent states and oligomeric signaling incompetent states. As shown in our previous studies, oligomerization modifies the thermodynamic and kinetic properties of the MET kinase domain, such that dimeric phosphorylated MET more efficiently phosphorylates substrate molecules than the monomeric phosphorylated MET (Hays and Watowich 2003; Hays and Watowich 2004). It is likely, though not yet proven, that oligomerization causes similar changes in unphosphorylated MET kinase activity. Several studies have also shown that receptor autophosphorylation occurs more rapidly for oligomeric receptors relative to monomeric receptors ((Baer *et al.* 2001; Posner *et al.* 1992); Watowich unpublished data), although kinetic parameters associated with monomer and dimer receptor autophosphorylation have only been quantitatively

measured for IR (Baer *et al.* 2001). Kinase activity is additionally regulated by phosphorylation levels, in particular the phosphorylation state of tyrosines within the receptor activation loop. Thus, both receptor phosphorylation and receptor oligomeric states clearly modulate receptor kinase activity. Moreover, the extent of receptor phosphorylation is regulated by competing autophosphorylation and dephosphorylation reactions which in turn are modulated by receptor oligomeric state. Thus, receptor oligomerization can either directly modulate kinase activity, or can indirectly modulate kinase activity by modulating autophosphorylation and dephosphorylation rates which impact receptor phosphorylation levels and in turn affect kinase activity (**Fig. 3.7)**. The inter-dependency between phosphorylation state, oligomerization state, and kinase activity enables receptor oligomerization to amplify the sharp separation between signaling competent and signaling incompetent states.

A mechanistic model of receptor signaling that incorporates the multiple regulatory effects of receptor oligomerization is shown in **Fig. 3.7**. In absence of ligand stimulation, monomeric receptors reside at the cell membrane. The autophosphorylation of unstimulated monomeric receptor is balanced by cellular phosphatases present either on cell surface on in the cytoplasm of the cells, such that the monomeric receptor remains phosphorylated. Tight regulation of monomeric receptor by phosphatases could function to prevent non-specific signaling. Extracellular ligand stimulation causes receptor dimerization, which changes the equilibrium state of the system. Accumulation of phosphorylated dimeric receptor results from the synergistic combination of properties associated with this dimeric state, i.e. an increased kinase activity (resulting from oligomerization-dependent catalytic changes and activation loop phosphorylation) and decreased susceptibility to dephosphorylation. These properties produce the signaling competent state observed for the dimeric receptor, which is capable of producing specific and sustained signaling responses.

The results presented in this paper directly demonstrate for the first time the effects of oligomerization in modifying the dephosphorylation rates of c-MET substrate. We have shown that phosphorylated TPR-MET dephosphorylates at a slower rate

compared to phosphorylated cytoMET. Site- specific dephosphorylation measurements corroborated the overall dephosphorylation data, with TPR-MET displaying resistance to dephosphorylation on its activation loop and increased resistance on the carboxy-tail phosphotyrosines required for signaling. The implications of these findings are particularly important in furthering our understanding of the activation mechanism of RTK.

CHAPTER 4:
A FEED-FORWARD LOOP PROVIDES THE FUNCTIONAL SWITCH FOR C-MET ACTIVATION[3]

INTRODUCTION

The observed nonlinearity of intracellular signaling pathways is believed to enable small changes in reaction kinetics or input signals to be highly amplified, and thus generate large changes in downstream signaling responses necessary for cell proliferation, differentiation, migration, and motility (Asthagiri and Lauffenburger 2000; Hubbard and Till 2000; Hunter 1997; Kholodenko *et al.* 1999; Moehren *et al.* 2002; Pazin and Williams 1992; Schlessinger 2000). The amplitude, duration and strength of many intracellular signaling responses is dependent on activation of receptor tyrosine kinases (RTKs), defined as receptor phosphorylation and subsequent downstream signaling, suggesting RTK activation is a critical and tightly regulated process in normal functioning cells (Hubbard *et al.* 1998; Hubbard and Till 2000; Schlessinger and Ullrich 1992). Our work and that of others suggests that oligomerization may be necessary to rapidly and selectively switch the RTK between distinct inactive and active states (Baer *et al.* 2001; Baxter *et al.* 1998; Hays and Watowich 2003; Hays and Watowich 2004; Kohanski 1993b; Rodrigues and Park 1993; Shimizu *et al.* 2001), where the active state exists when the RTK is autophosphorylated and capable of binding and signaling through immediate down-stream effectors (e.g. PI3K, Gab1, Grb2) (Birchmeier *et al.* 2003; Hubbard and Till 2000; Pazin and Williams 1992; Schlessinger 2000; Ullrich and Schlessinger 1990). The inactive state exists when the RTK is unphosphorylated and

[3] Sheth P. R., Hays J. L., Elferink L. A., Watowich, S. J. 2006. A feed-forward loop provides a functional switch for c-MET activation. (*Submitted)*

unable to bind and/or phosphorylate immediate downstream effectors. Neither functional state is restricted to a particular oligomeric state; it is possible to observe monomeric active states and oligomeric inactive states (Baxter *et al.* 1998; Posner *et al.* 1994; Sheth and Watowich 2005).

As described in the earlier chapters, activation of hepatocyte growth factor receptor (c-MET) triggers complex intracellular signaling responses leading to cell proliferation, differentiation, branching morphogenesis, motility, and invasion (Birchmeier *et al.* 2003; Zhang *et al.* 2004). Our previous studies showed that MET oligomerization modified its thermodynamic, kinetic and catalytic properties (Hays and Watowich 2003; Hays and Watowich 2004), and phosphorylation of the MET activation loop modified its kinase catalytic activity (Rodrigues and Park 1994). In addition, oligomerization modulated MET susceptibility to dephosphorylation (Sheth and Watowich 2005). Thus, a feed-forward loop exists between c-MET phosphorylation state, oligomerization state, and kinase catalytic activity, which effectively amplifies and sharpens the separation between c-MET active and inactive states **Fig. 4.1**. Central to this reaction network is the prevalence of two c-MET species- the unligated monomer and ligand-bound dimer. (Birchmeier *et al.* 2003; Bottaro *et al.* 1992; Naldini *et al.* 1991b; Naldini *et al.* 1991c). Our model of c-MET activation is described by a differential equations framework that allows time-dependent quantification of all c-MET intermediates and their contribution to c-MET activation, which occurs as the system shifts from an inactive state to an active state. The relative importance of the biochemical processes involved in regulating c-MET activation can be clearly understood with this model. Such in-depth understanding could promote development of novel therapeutic approaches to treat c-MET-mediated tumorigenesis and metastasis.

RESULTS

Development of the kinetic model

To quantitatively study c-MET activation, a detailed mathematical model was developed that incorporated the dynamical processes associated with c-MET dimerization and signaling **Fig. 4.1 and Fig. 2.1**. Where available, our model used published kinetic and thermodynamic parameters for monomeric cytoMET and dimeric TPR-MET (Hays and Watowich 2003; Hays and Watowich 2004; Sheth and Watowich 2005). A few rate constants in our model were not available for c-MET interactions; in these cases constants measured for related RTKs were used (Kholodenko *et al.* 1999; Kohanski 1993b; Moehren *et al.* 2002; Naldini *et al.* 1991a; Shimizu *et al.* 2001). Protein-protein interaction kinetics were described by mass action equations. Rate equations used for generating our c-MET activation model are listed in **Table 2.1**. Starting concentrations of c-MET and Tyr-containing effectors were taken from published results (Kholodenko *et al.* 1999). ATP concentration was set at 1 mM (Posner *et al.* 1992). Activation of c-MET occurs in response to binding the physiological ligand HGF or the Internalin B (InlB) protein of *Listeria monocytogenes*. InlB has been shown to mimic HGF-induced c-MET activation, endocytosis (Ireton *et al.* 1999; Li *et al.* 2005) and signaling (Shen *et al.* 2000). Accordingly, InlB was used as the c-MET agonist for the simulations and cell culture studies.

c-MET phosphorylation in absence of ligand stimulus.

We determined the population distribution of different c-MET species in absence of extracellular ligand. Assuming millimolar ATP cellular concentrations and no external ligand stimulus, our model predicted c-MET would exist predominantly as an ATP-bound unphosphorylated monomeric receptor (denoted MET-ATP in **Fig. 4.1B**). In addition, since c-MET monomer has kinase activity (Hays and Watowich 2003; Hays and Watowich 2004; Rodrigues and Park 1993; Sheth and Watowich 2005), we tested

whether significant levels of phosphorylated c-MET monomers would accumulate in absence of extracellular ligand. Our model predicted a small steady state concentration (~0.1% of total c-MET) of phosphorylated c-MET monomers, defined as [pMET] + [pMET-ATP] + [pMET-Tyr] + [pMET-ATP-Tyr], would be present in cells in the absence of extracellular ligand. Significantly, this level of monomeric phosphorylated receptor was at least two orders of magnitude smaller than the steady-state levels of phosphorylated dimeric receptor generated in response to added extracellular ligand (**Fig. 4.2A**). We could not detect the predicted very low basal level of c-MET phosphorylation in unstimulated serum-starved Vero cells using immunoblotting. However, EGFR basal phosphorylation in unstimulated cells has been reported using a more sensitive FRET-based detection system (Offterdinger *et al.* 2004).

The basal level of c-MET phosphorylation in absence of extracellular ligand stimulation was directly correlated with changes to the modeled c-MET monomer autophosphorylation (reaction 17) and dephosphorylation (reaction 26) rates. We examined the impact of setting the c-MET monomer dephosphorylation rate (**Fig. 2.1)**, reaction 26) to zero. In this extreme case, our model predicted a relatively slow, but substantial, buildup of phosphorylated c-MET (**Fig. 4.2C**). This prediction has been confirmed in cell culture, where the buildup of phosphorylated PDGFR (Baxter *et al.* 1998), IR (Posner *et al.* 1994), and c-MET (Sheth and Watowich 2005) was observed in the presence of phosphatase inhibitors. Our experimental data on c-MET phosphorylation kinetics in presence of the PTP inhibitor pervanadate (**Fig. 4.3B**) correlated qualitatively and quantitatively with our model's prediction (**Fig. 4.2C**). Moreover, our model predicted that the rate of phosphorylated monomeric c-MET accumulation upon inhibition of receptor dephosphorylation was directly related to c-MET autophosphorylation k_{cat} (reaction 17). Thus, our model clearly showed c-MET phosphorylation and dephosphorylation processes were balanced to establish a dynamic equilibrium.

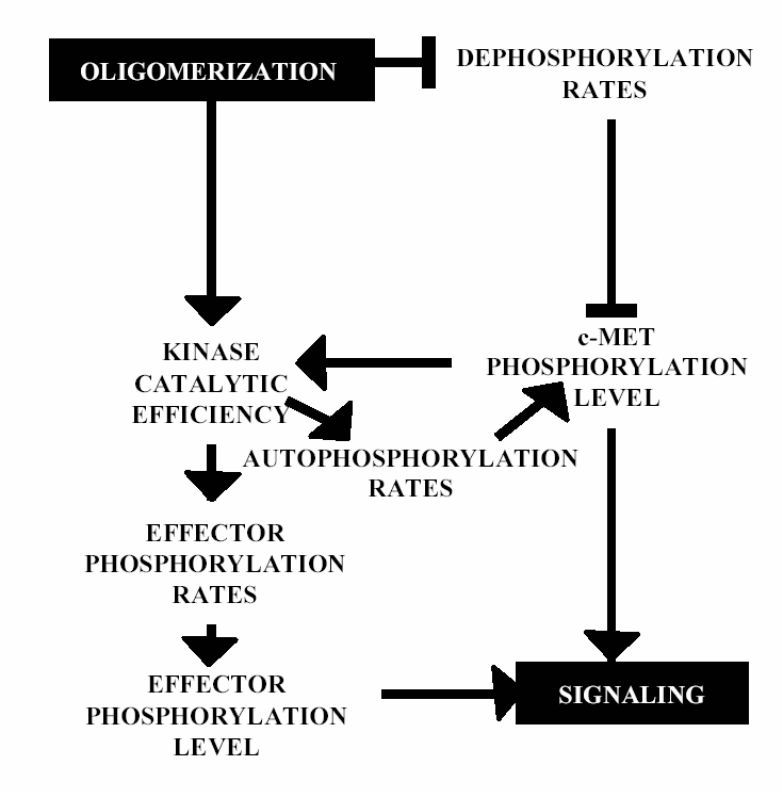

Fig. 4.1. Feed-forward loop results in c-MET activation.
Ligand-induced c-MET oligomerization increases kinase activity of the receptor, which results in buildup of phosphorylated c-MET by autophosphorylation. Oligomerization reduces c-MET's susceptibility to PTP-catalyzed dephosphorylation, which negatively regulates c-MET phosphorylation. Thus, oligomerization amplifies the buildup of phosphorylated c-MET via a feed-forward loop. The increased kinase catalytic efficiency also increases effector phosphorylation rates, which controls the buildup of activated effector. Phosphorylated c-MET and effector buildup are critical determinants of c-MET activation.

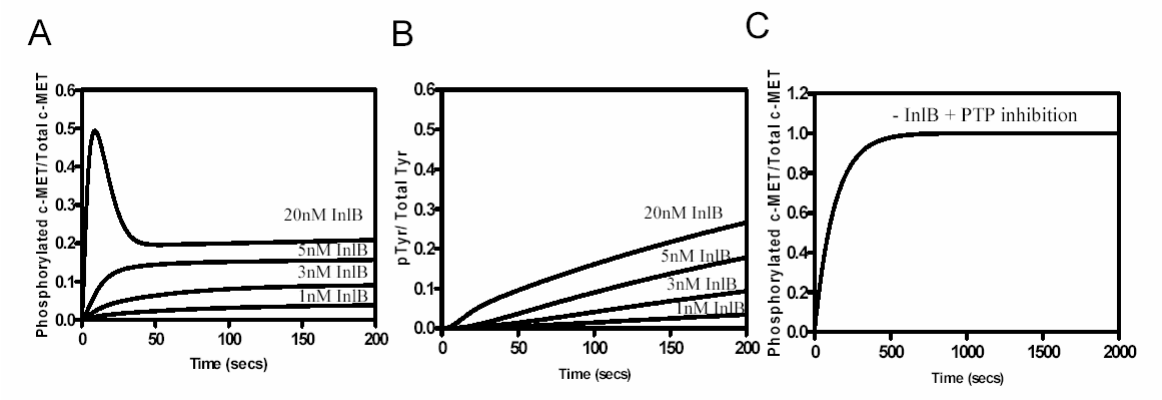

Fig. 4.2. Model predictions.
(**A**) The predicted kinetics of c-MET phosphorylation in presence of 1, 3, 5 and 20nM InlB. (**B**) The predicted kinetics of effector phosphorylation (pTyr) in presence 1, 3, 5 and 20nM InlB. The y-axis on the graphs represents the fraction of total c-MET and Tyr containing effector phosphorylated. (**C**) Model prediction of fraction of c-MET phosphorylated as a result of blocking PTP activity associated with monomeric c-MET and no InlB stimulation.

c-MET phosphorylation in presence of ligand stimulus

Using our c-MET activation model (**Fig. 2.1**), we calculated the rate and magnitude of c-MET autophosphorylation and exogenous effector phosphorylation in response to added cognate extracellular ligand (**Fig. 4.2A & 4.2B**). Our model predicted that the concentration of total phosphorylated c-MET, defined as [pMET] + [pMET-Tyr] + [pMET-ATP] + [pMET-ATP-Tyr] + [$pMET_2$] + [$pMET_2$- Tyr] + [$pMET_2$-ATP] + [$pMET_2$-ATP-Tyr], was not linearly related to the concentration of added extracellular ligand (**Fig. 4.2A**). At low InlB concentrations (<5 nM), our model predicted that the phosphorylation of c-MET would reach a maximum steady-state level within seconds (**Fig. 4.2A**). In contrast, our model predicted that c-MET phosphorylation kinetics at higher InlB concentrations (>5 nM) would produce a rapid transient spike response followed by a steady-state phosphorylation level less than the maximum observed during the transient spike (**Fig. 4.2A**). The magnitude of the phosphorylated c-MET transient spike and steady-state levels were dependent on the concentration of added extracellular ligand.

These simulations were compared to data from cell culture experiments (**Fig. 4.3A**) to determine the accuracy and validity of our model. Predictions of c-MET phosphorylation were compared to c-MET phosphorylation levels measured in cultured Vero cells following different amounts of added InlB (1 nM, 5 nM and 20 nM) as c-MET agonist. Vero cells have been extensively used to characterize c-MET signaling following activation with HGF and InlB (Ireton *et al.* 1999; Seveau *et al.* 2004). We observed a ligand-dependent non-linear increase in c-MET phosphorylation in serum-starved Vero cells. In addition, a rapid transient spike in phosphorylated c-MET was observed at 20 nM InlB. Interestingly, an analogous transient spike response in phosphorylated EGFR was observed for cells stimulated with high EGF concentrations (Kholodenko *et al.* 1999). Our measured c-MET phosphorylation responses (**Fig. 4.3A**) were in very close agreement to our model predictions (**Fig. 4.2A**), implying our c-MET activation model was sufficient to accurately reproduce the salient features of c-MET activation. Unlike earlier modeling studies (Kholodenko *et al.* 1999), our activation model did not require the effector-bound state of the receptor to be "inaccessible" to cellular phosphatases in order to simulate the transient spike in receptor phosphorylation. Instead, the observed transient spike in phosphorylated receptor following stimulation with high ligand concentrations resulted from rapid c-MET autophosphorylation before cellular phosphatases reached full activity. In addition, our model interpreted the observed steady-state receptor phosphorylation levels as resulting from a dynamical balance between kinase and phosphatase kinetic reactions once a quasi-equilibrium state was reached. As discussed below, varying parameters associated with dimeric c-MET autophosphorylation (reaction 18) and dephosphorylation (reaction 25) reactions significantly modulated the shape and height of the phosphorylated c-MET transient spike that occurred following ligand stimulation. Our simulations accurately reproduced all tested cell culture observations, thus providing a significant validation of our activation model to further understand the dynamical processes that regulate c-MET activation.

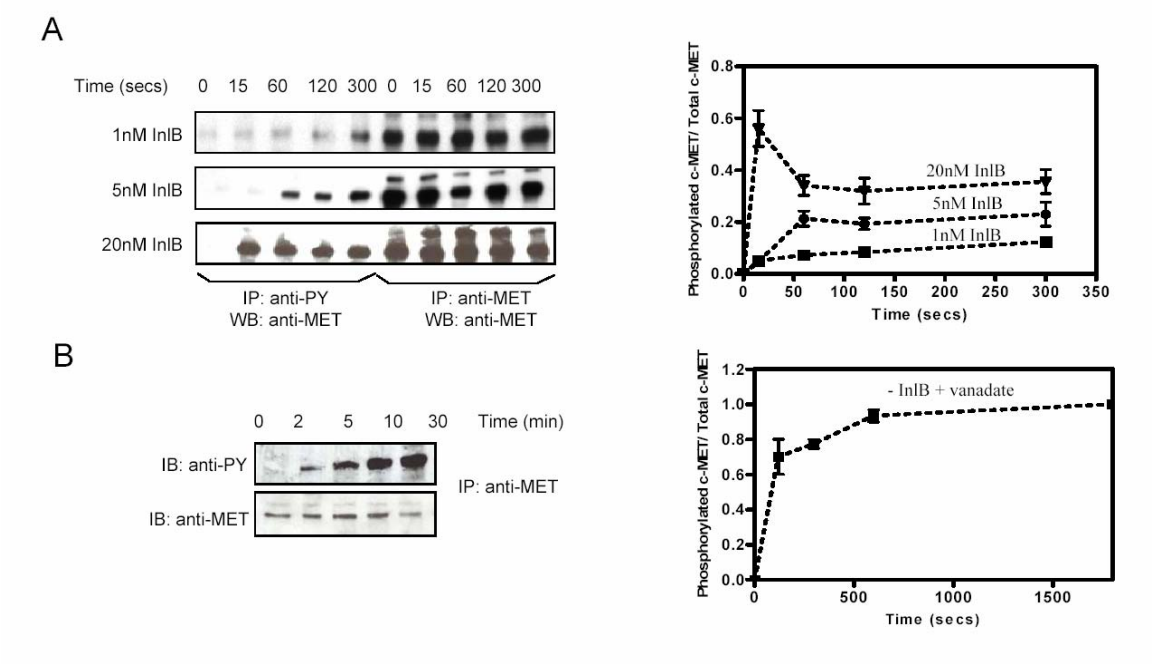

Fig. 4.3. Experimental validation of the activation model.
(**A**) Measured kinetics of c-MET phosphorylation in cultured Vero cells upon stimulation with different 1, 5 and 20nM lnlB. (**B**) Quantitative analyses of c-MET phosphorylation kinetics in presence of known PTP inhibitor pervanadate, and in absence of InlB. The data is presented as the mean of three different experiments with error bars representing standard error. The representative immunoblots for panels **A** and **B** are shown to the left of their respective graphs.

Computational analyses of effector binding and phosphorylation

Signaling from activated c-MET requires effectors bind to c-MET phosphotyrosines, after which the effector proteins become phosphorylated and/or activated (Birchmeier *et al.* 2003). Binding, phosphorylation, and dephosphorylation reactions of effectors that function as c-MET kinase substrates were included in our model. Although multiple effectors may interact with phosphorylated c-MET simultaneously, as a first approximation only one effector was included in our c-MET activation model. Subsequent complexities associated with multiple effector binding can be easily added to our model once the relevant experimental data becomes available. The time course for buildup of phosphorylated effector (pTyr) was simulated for a range of added extracellular ligand concentrations (**Fig. 4.2B**). At each extracellular ligand

concentration, our c-MET activation model showed pTyr levels would increase monotonically in response to ligand-induced dimerization; no transient spike was observed in pTyr levels. This pattern of effector phosphorylation was observed for Shc in the related EGFR RTK system (Kholodenko *et al.* 1999). In addition, our model predicted pTyr accumulated only after significant c-MET phosphorylation, resulting in a lag time between extracellular ligand stimulation and effector phosphorylation (**Fig. 4.2**). The rate of effector phosphorylation was biphasic (most clearly observed at high extracellular ligand concentrations), with a higher initial rate of effector phosphorylation followed by a slower rate of phosphorylation as the dynamical system reached steady-state (**Fig. 4.2B**). Finally, the amount of Tyr bound to the c-MET, defined as [MET-Tyr] + [MET-ATP-Tyr] + [pMET-Tyr] + [pMET-ATP-Tyr] + [MET_2-Tyr] + [MET_2-ATP-Tyr] + [$pMET_2$-Tyr)]+ [$pMET_2$-ATP-Tyr], correlated closely with the accumulation of phosphorylated c-MET. These observations implied c-MET phosphorylation was necessary for effective effector recruitment and/or phosphorylation.

Sensitivity of c-MET signaling to biochemical parameters

c-MET activation, described by the magnitude and specificity of c-MET and effector phosphorylation in response to extracellular ligand-mediated dimerization, is controlled by a variety of thermodynamic and kinetic parameters. The sensitivity of dimeric c-MET and effector phosphorylation to these different biochemical parameters was studied to understand their relative importance in c-MET activation. Sensitivity analysis of c-MET phosphorylation to kinase ATP and effector binding on and off rates showed that these parameters had little impact on the behavior of the c-MET activation model. In contrast, changing the kinetic parameters associated with dimeric c-MET phosphorylation and dephosphorylation had significant impact on c-MET activation as measured by buildup of phosphorylated dimeric c-MET and pTyr.

We systematically varied the kinetic parameters associated with dimeric c-MET autophosphorylation (k_{18}), dephosphorylation (V_{25}), and effector phosphorylation (k_{21}, k_{22}) to more completely understand the relative importance of these processes to c-MET

activation. **Fig. 4.4A** & **Fig. 4.4B** show the time-dependent accumulation of phosphorylated c-MET and pTyr as a function of dimer autophosphorylation k_{cat} (k_{18}) at saturating (i.e. 20 nM) extracellular ligand concentration. Clearly, the predicted rates of c-MET phosphorylation and steady-state levels of phosphorylated c-MET were dependent on c-MET dimer autophosphorylation values. Furthermore, by affecting the level of phosphorylated c-MET, the autophosphorylation k_{cat} significantly changed the rate of pTyr production (**Fig. 4.4B**). Thus, the c-MET activation response was sensitive to the dimer autophosphorylation rate. In contrast, changes to the effector phosphorylation $k_{cat,}$ (k_{21}, k_{22}) had little effect on the rate of buildup of phosphorylated c-MET (**Fig. 4.4C**). However, the rate of pTyr buildup was directly dependent upon the magnitude of the effector phosphorylation $k_{cat,}$ (**Fig. 4.4D**). Phosphorylated c-MET steady state levels and the rate of pTyr formation were significantly changed when the c-MET dephosphorylation V_{max} (V_{25}) was varied, implying cellular phosphatases also played a critical role in modulating c-MET signaling potential (**Fig. 4.4E & Fig. 4.4F**). Changes to the steady-state level of phosphorylated c-MET modified the sharpness of the phosphorylated c-MET transient spike observed at high extracellular ligand concentrations (**Fig. 4.4E**). Thus, the phosphatase-catalyzed dephosphorylation rates dictated the amplitude as well as duration of c-MET activation.

The above simulations evaluated the relative importance of kinetic and thermodynamic parameters associated with dimeric c-MET, the typical activated signaling species. A similar parameter sensitivity analysis was applied to monomeric (i.e., unstimulated) c-MET (**Appendix C)**. In this case, no significant differences were observed in the buildup of phosphorylated c-MET or pTyr by varying single thermodynamic or kinetic parameters (k_{17}, k_{19}, k_{20} and k_{26}). In contrast, as discussed in greater detail below, significant changes in the buildup of phosphorylated c-MET and pTyr were observed when several kinetic parameters for monomeric c-MET were simultaneously changed. Based on these results, it can be inferred that the kinetic parameters associated with c-MET have been tuned to render ligand-induced dimeric c-MET the active signaling state. Non-stimulated monomeric c-MET exists in a tightly

regulated inactive signaling state that is insensitive to individual changes to its kinetic and thermodynamic parameters.

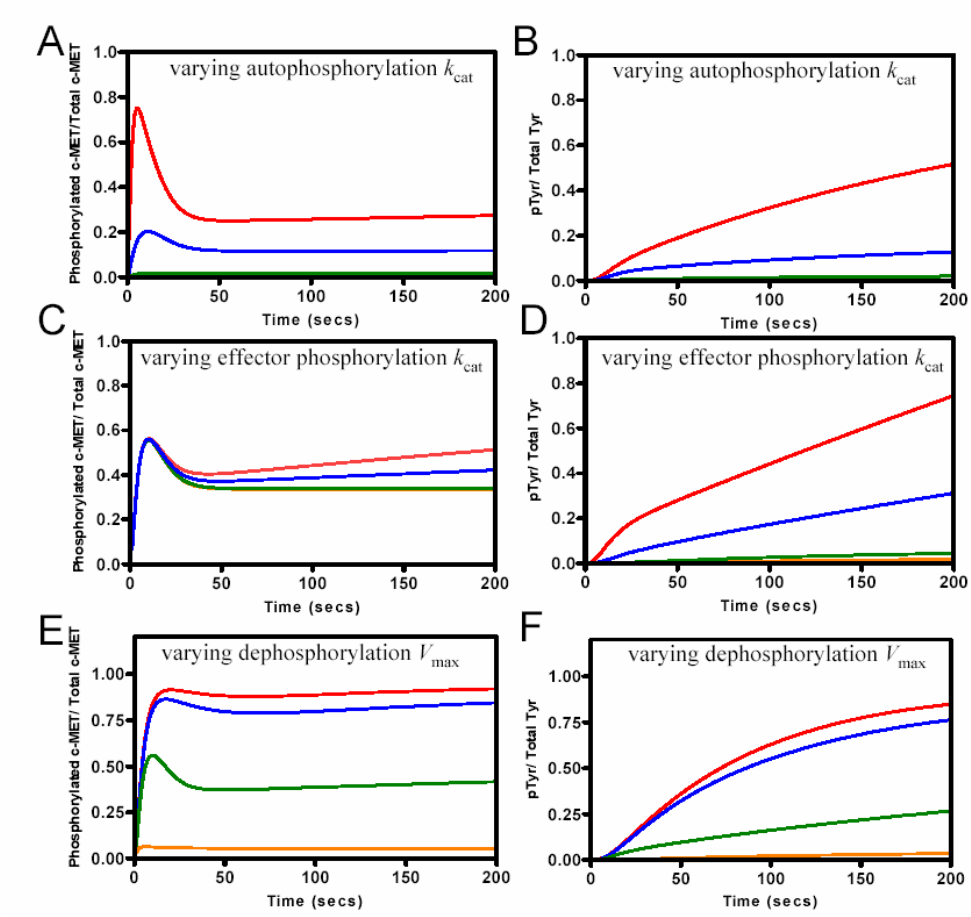

Fig. 4.4. Sensitivity of c-MET and Tyr phosphorylation kinetics to autophosphorylation, effector phosphorylation and PTP-catalyzed dephosphorylation.

(A, B) Predicted kinetics of c-MET (A) and Tyr (B) phosphorylation were calculated using kinase autophosphorylation kcat 0.0008 (orange), 0.008 (green), 0.08 (blue) and 0.8 s-1 (red). (C, D) Predicted kinetics of c-MET (C) and pTyr (D) phosphorylation at kinase effector phosphorylation kcat 0.00024 (orange), 0.0024 (green), 0.024 (blue) and 0.05 (red) s-1. (E, F) Predicted kinetics of c-MET (E) and pTyr (F) phosphorylation at dephosphorylation Vmax 0.00045 (red), 0.0045 (blue), 0.045 (green) and 0.45 (orange) μM·s-1. These simulations were carried out at saturating InlB concentration of 20nM, where all the c-MET species were dimeric.

Synergistic changes to c-MET biochemical properties

The k_{on} and k_{off} for the thermodynamic processes, the kinetic catalytic constants for autophosphorylation and effector phosphorylation, and c-MET dephosphorylation rates by phosphatases are the main biochemical parameters that differ between monomeric and dimeric c-MET. To better understand how oligomerization-induced changes to the thermodynamic, kinetic, and dephosphorylation properties of c-MET impact its activation, these properties were simultaneously varied for monomeric c-MET and the buildup of phosphorylated c-MET and pTyr monitored (**Table 4.1**). These modeling studies were normalized to baseline simulations that used monomeric and dimeric c-MET biochemical reaction parameters which were based on experimentally-determined values (as described above). c-MET activation in the absence of extracellular ligand stimulation (and hence, c-MET dimerization) was monitored by accumulation of phosphorylated monomeric c-MET and pTyr. For comparison, normalized values of phosphorylated c-MET and pTyr in presence of InlB are tabulated. As summarized in Table III, c-MET and effector phosphorylation levels did not significantly change relative to the baseline simulation unless a biochemical parameter changed >100-fold relative to its default value. However, small changes in two or more kinetic properties had significant synergistic effects on c-MET's signaling competence. For example, decreasing the dephosphorylation rate (V_{26}) by 10-fold and increasing autophosphorylation k_{cat} (k_{17}) and effector phosphorylation k_{cat} (k_{19} & k_{20}) 10-fold relative to the monomeric c-MET default parameters, resulted in a buildup of phosphorylated c-MET and pTyr comparable to that observed at 20 nM InlB (**Table 4.1**). An order of magnitude changes in the effector binding rate constants (k_2, k_3, k_6 and k_7) increased the basal levels of phosphorylated c-MET to ~ 0.5% of total c-MET, however, these levels were several-fold lower than that generated in presence of ligand. Thus, generation of an activated c-MET state appear to be dominated by synergistic effects

between dynamical processes regulating receptor kinase activity (autophosphorylation and effector phosphorylation), and dephosphorylation.

If oligomerization synergistically modifies multiple biochemical parameters to regulate c-the phosphorylation state and hence signaling activity of c-MET, does our model account for the constitutive activation from mutant c-MET receptors detected in several carcinomas (Jeffers *et al.* 1997)? As shown in Table III, it is clear that small synergistic changes in c-MET kinetic properties resulted in several-fold increased accumulation of phosphorylated c-MET and pTyr. Several point mutations (for e.g. D1228V, V1220I, Y1230H, Y1230C, D1228N, V1220I) in c-MET kinase domain have been identified that could potentially result in increased kinase activity of the receptor. Increased kinase activity of c-MET could directly impact the autophosphorylation (reaction 17) and effector phosphorylation (reactions 19 and 20) rates. If a c-MET point mutation increased the autophosphorylation (reaction 17) and effector phosphorylation (reactions 19 & 20) rates 10-fold relative to the wild-type monomeric receptor, our model predicted that the unstimulated c-MET mutant would have ~14-fold increased phosphorylated c-MET and ~130-fold increased pTyr levels relative to the unstimulated wild-type receptor. The pTyr levels predicted from the point-mutated receptor were quantitatively similar to the amount of pTyr generated by the wild-type receptor following stimulation with 3nM InlB (**Table 4.1**). c-MET point mutations that decrease the susceptibility of monomeric c-MET to dephosphorylation, and simultaneously increase the kinase autophosphorylation and effector phosphorylation catalytic efficiencies relative to wild-type c-MET, would produce a constitutively activate monomeric c-MET that produced phosphorylated c-MET and pTyr levels comparable to those observed from wild-type c-MET stimulated with saturating concentrations of extracellular ligand.

Table 4.1. Synergistic changes to c-MET biochemical properties are required for efficient and specific c-MET activation

Model prediction levels of pMET and pTyr at 100 sec post InlB stimulation. pMET and pTyr values normalized to the buildup observed at 0 nM ligand concentration

[InlB] nM	pMET	pTyr
0	1	1
1	127	59
3	278	155
20	566	421

Effect of incremental changes in the kinetic parameters associated with monomeric species on steady-state levels of phosphorylated c-MET and effector. The normalized values of 1 for k_{cat}, V_{max} and pMET and pTyr represent the monomeric basal parameters and phosphorylation of c-MET and Tyr in absence of ligand stimulation.

[InlB] nM	k_{17}	$k_{19,20}$	V_{26}	pMET	pTyr
0	1	1	1	1	1
0	10	1	1	13	1
0	100	1	1	484	20
0	1	10	1	1	1.7
0	1	100	1	1	84
0	1	1	1/10	12	1.7
0	1	1	1/100	832	141
0	1	10	1/10	12	17
0	10	1	1/10	598	110
0	10	10	1	14	129
0	10	10	1/10	604	345

DISCUSSION

The use of computer modeling to predict cellular responses to RTK activation has been widely studied in recent years (Kholodenko *et al.* 1999; Moehren *et al.* 2002; Posner *et al.* 1992; Sachs *et al.* 2002; Wiley *et al.* 2003). Much of this work has focused on

predicting downstream signal amplification and the flux through particular pathways in response to varying extracellular ligand stimulation. Unfortunately, until this current work, an adequate model that takes into account the feed-forward loop that exists between autophosphorylation, dephosphorylation and effector phosphorylation dynamical processes in the activation of RTKs has not been described.

The model presented here evaluated the relative importance of main regulatory processes that work in concert to sharply switch between an inactive and active c-MET state. This model also addressed the importance of dimerization-mediated changes in kinetic, biochemical, and dephosphorylation properties of c-MET in enabling activation specificity. Our model conclusively showed that ligand-stimulated c-MET was highly competent signaling species, which was sensitive to changes in its biochemical parameters. In contrast, unstimulated monomeric c-MET, although clearly an active kinase molecule, was incapable of existing in an activated (i.e., phosphorylated, signaling competent) state due to synergistic effects of the biochemical properties associated with the c-MET monomeric state. Thus, unstimulated monomeric c-MET was repressed in its ability to signal by virtue of its higher susceptibility to dephosphorylation and more inefficient thermodynamic and kinetic properties, relative to stimulated dimeric c-MET (**Fig. 4.5**). If the biochemical properties of monomeric c-MET were synergistically altered, our model predicted phosphorylated c-MET and pTyr could build to significant levels in the absence of extracellular ligand stimulation. Thus, the widespread use of the term "inactive" for monomeric unstimulated c-MET is not completely accurate, and may be misleading. c-MET "activation" in presence of extracellular cognate ligand is more appropriately viewed as the accumulation of dimeric receptors that are capable of sustaining a phosphorylated state and signaling due to synergistic effects of the biochemical properties associated with that state. This activation mechanism, based on the experimental data and modeling predictions, is shown in **Fig. 4.5**. This minimal activation model addresses the importance of oligomerization in the feed-forward activation process outlined in **Fig. 4.1**. Moreover, the development of rigorous models that accurately describe c-MET (and related RTK) activation allow the critical

determinants of receptor activation and signaling to be deconvoluted. Ultimately, these models could yield more complete understanding of cell signaling and novel therapeutic approaches to treat aberrant signaling.

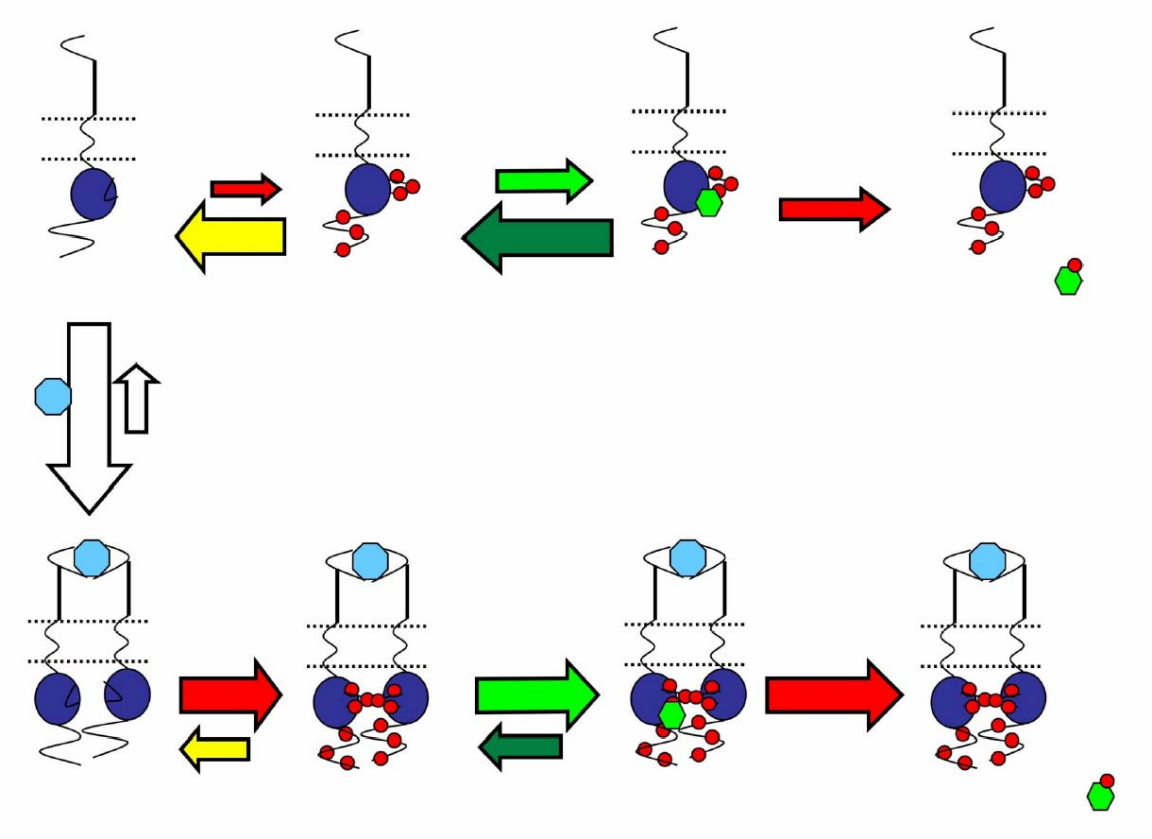

Fig. 4.5. Model for c-MET activation.
Shown is a model for c-MET activation based on experimental and modeling data. In the absence of extracellular ligand stimulus, monomeric c-MET is localized to cell surface, and exists as a kinase active, but unphosphorylated, receptor. Monomeric c-MET phosphorylation and signaling is repressed due to decreased kinetic and thermodynamic properties of monomeric c-MET and its high susceptibility to dephosphorylation by PTPs. c-MET dimerization, in presence of its cognate ligand, induces synergistic changes to the kinetic and thermodynamic properties of c-MET, which result in sustained c-MET autophosphorylation, effector recruitment and phosphorylation, and subsequent signaling.

CHAPTER 5:
CONCLUSIONS

Our work has conclusively shown that oligomerization in c-MET, and possibly in the other RTKs, is a key step that regulates, in addition to, and independent of the autophosphorylation reaction, the receptor's enzymatic activity and the receptor's susceptibility to dephosphorylation by cellular protein tyrosine phosphatases. Our studies conclusively show that the role of oligomerization is to trigger a feed-forward loop that is responsible for amplifying c-MET activation in presence of its ligand stimulus. Quantitative studies on the role of oligomerization-mediated changes in c-MET's kinetic, thermodynamic properties and dephosphorylation susceptibilities showed that these changes work synergistically to activate signaling from specific c-MET species (the ligand-bound dimer). Contrary to the classical model, the monomeric, unstimulated c-MET, is kinase active on cell-surface, but its phosphorylation is kept in check by the competing dephosphorylation reaction catalyzed by cellular phosphatases. The proposed feed-forward mechanism for c-MET activation successfully explains all the contradictory experimental data in the literature, and also serves as a model to understand oncogenic activation of c-MET by kinase domain mutations that are ligand-independent. This mechanism provides a dynamic snap-shot of the biochemical complexity of RTK activation and would be very useful in designing inhibitors targeting the abnormally activated RTKs.

CHAPTER 6:
FUTURE DIRECTIONS

TPR-MET STRUCTURAL STUDIES

Although we have conclusively shown that oligomerization in c-MET alters its biochemical properties and dephosphorylation susceptibilities, the structural basis of these changes is still elusive. The oligomerization-specific changes in the structural and dynamical properties of c-MET needs to be investigated for several reasons. The structure of a phosphorylated oligomeric form of a c-MET kinase domain would serve as a prototype to understand the structural basis of RTK activation. Furthermore, it can also serve as a template for structure-based drug design studies to identify inhibitors to a, possibly, more relevant conformation of RTKs for cancer therapeutics. TPR-MET serves as a good model to study the structural-basis of activation of c-MET by oligomerization. For several years, our structural studies on TPR-MET were hindered by low yields of TPR-MET in the Sf9 insect cell system. However, our recent studies using another insect cell system, the Hi5 cells, have shown promising TPR-MET expression that could be further pursued for producing mg quantities of the protein required for crystallization studies. Our preliminary studies have shown that TPR-MET expression in Hi5 cells was 5-10 fold greater than in the Sf9 cells. These studies provide the ground-work for further characterizing TPR-MET produced in Hi5 cells, with respect to its solubility, ease of purification, oligomerization and phosphorylation state. Once large quantities of TPR-MET can be purified to homogeneity, in addition to crystallization trials, the protein dynamics and solution properties could also be studied using a variety of biophysical techniques.

IDENTIFICATION OF PROTEIN-TYROSINE PHOSPHATASES (PTPS) THAT REGULATE C-MET PHOSPHORYLATION

Prior to our studies, the role of protein-tyrosine phosphatases in RTK regulation was largely elusive. While it was well-established that RTKs are dephosphorylated by cellular PTPs, how this reaction impacted the activation of RTKs in absence and/in presence of ligand was largely unknown. Using our kinetic model, we have been able to quantitatively characterize the role of dephosphorylation reaction in regulating the overall activation of c-MET in presence and absence of the ligand. Interestingly, our studies point to a multi-faceted role of PTPs in regulating c-MET activation. In absence of ligand, the PTP-catalyzed dephosphorylation is involved in a dynamic equilibrium between the competing autophosphorylation reactions. The role of PTPs, in absence of the ligand, is to push the equilibrium towards unphosphorylated c-MET, and thus maintain the receptor in a quiescent state in absence of a stimuli. However, in presence of a ligand, the dephosphorylation reaction serves to regulate the amplitude, and duration of the c-MET activation response, making the response 'switch-like'.

Thus, PTPs are critical determinants of c-MET activation response; however, much is yet to be known about the PTPs that specifically regulate c-MET phosphorylation. Multiple PTPs have been identified as key regulators of phosphorylation of IR, PDGFR, EGFR etc (Ostman and Bohmer 2001), however, relatively fewer studies have been focused on identifying PTPs that catalyze c-MET phosphorylation (Palka *et al.* 2003; Villa-Moruzzi *et al.* 1993). In order to identify cellular PTPs for c-MET, we have recently employed an in-gel phosphatase assay that can be used to identify PTPs that associate with c-MET (**Appendix A)** (Burridge and Nelson 1995). Our goal, using this assay, is to identify the PTP-activity (and molecular weight of the corresponding activity band) associated with c-MET immunoprecipitates from crude lysates. Once the molecular weight of PTPs that interact with c-MET are known, further identification of specific PTPs can be done by immunodepletion, siRNA and/or over expression studies in intact cells.

BIOCHEMICAL CHARACTERIZATION OF ONCOGENIC C-MET MUTANTS

Our studies have identified key parameters that are important regulators of c-MET activation potential. However, how these parameters are altered in cancer is yet unknown. Studies using mutants of c-MET that have shown oncogenic potential would be provide critical insights on the biochemical basis of aberrant c-MET regulation in tumorigenesis and metastasis. A long-term goal in the laboratory is, to biochemically and structurally characterize specific kinase domain mutant forms of c-MET that are oncogenic. Our hypothesis is that mutations alter c-MET biochemical properties and/or dephosphorylation susceptibilities such that the mutated c-MET has parameters that are similar to those seen for the dimeric form of c-MET. These alterations, depending on the parameters, would render the mutated c-MET to alter the dynamic equilibrium set by the competing autophosphorylation and dephosphorylation reactions favoring the buildup of phosphorylated c-MET, which could be capable of downstream signaling.

APPENDIX A

IN-GEL-PTP ASSAY PROTOCOL

Step 1: Prepare GST-FER tyrosine kinase

Day 1:

1. Innoculate 25 ml of LB-AMP (100ug/ml) with frozen stab of GST-FER bugs
2. Grow O/N @ 37C on shaker

Day 2:

1. Dilute 10 ml of O/N culture in 240 ml LB-AMP. Grow for 1 hour 45 min @ 37C on shaker
2. Add 1:1000 dilution of 100mM IPTG (0.1mM final conc) and induce at 30C for 2h
3. Spin 5000 RPM, 10 min, 4C, discharge supernatant
4. Resuspend pellet in 7 ml PBS + 10mM DTT on ice
5. Sonicate for 5 min (2 sec on/2 sec off)
6. Add 700 ul of 10% Triton X-100 and 20 ul of PMSF (10mg/ml). Rotate 30 mins @ 4C
7. Spin 27000 g (15,000 RPM) for 15 min
8. Collect supernatant and add 100 ul of 50% (v/v) glutathione sepharose beads. Rotate 30 min @ 4C
9. Wash beads 2 times 1ml with
    a. 50 mM Imidazole pH 7.2 (300 ul of 0.5M stock)
    b. 10mM DTT (30 ul of 1M stock)
    c. qs with 2670 ul dH2O

    with final wash, make 1:1 bed volume
10. Run 10 ul of beads on a 10% SDS-PAGE to check if purified
11. Use purified GST-FER immobilized on beads to phosphorylate poly glu-tyr (see below). Beads can also be stored at -20C in 50% glycerol for later use

Step 2: ^{32}P Labeling Reaction
Important: Before starting, thaw γ-^{32}P-ATP in fume hood behind a shield

1. Wash 50 ul GST-FER beads from above twice with 1 ml of
    50 mM imidazole pH 7.2 (200ul of 0.5 M stock)
    10 mM DTT (20 ul of 1M stock)
    0.1% β-mercaptoethanol (2 ul)

qs to 2 ml with dH2O

2. Transfer final wash to a screw cap tube (with O-ring)
   Aspirate all wash buffer

3. Add 250 ul 2X kinase buffer

   2X Kinase Buffer
   100 mM imidazole pH 7.2
   20 mM DTT
   60 mM MgCl2
   2 mM MnCl2
   0.1% Triton X-l00
   0.04 mM ATP
   2 mM Vandate

4. Set up the reaction as follows (in this order and in radioactive hood behind a shield)
   50 ul GST-FER beads
   250 ul of 2X kinase buffer
   _X_ ul dH2O
   _Y_ ul γ-32P ATP (250 uCi)
   50 ul poly glu-tyr (20 mg/ml in dH2O)

   Total Volume = 500 ul

Note: X+Y should be equal to 150 ul. Adjust the volume of water depending on activity of 32-P-ATP

5. Seal tube with parafilm. Rotate at room temp in fume hood behind shield O/N

Step 3: Running the G-25 column

1. Equilibrate G-25 column with 2 volumes 25mM Hepes, pH 7.3
2. Sediment GST-FER beads in the table top microcentrifuge
3. Transfer 'HOT' supernatant to screw cap tube containing 500 ul of 20% TCA
4. Precipitate on ice for 20 min
5. Spin in cold room, 12K RPM, 10 min
6. Remove supernatant to another tube→ LIQUID WASTE (Dispense in hot liquid waste receptacle)
7. Resuspend pellet in 100 ul of 2M Tris Base. Vortex to mix.
8. Apply to column (in fume hood, behind shield). Make sure column is clamped.
9. Rinse tube with 100 ul of 2M Tris base and apply to column
10. Run sample into column. Apply 400 ul of 25mM HEPES, pH 7.3 and run into column

11. Top off with 25 mM HEPES as needed
12. Collect 1 ml fractions into screw cap tubes
13. Count 2 ul of hottest fractions in 3 ml scintillation fluid
14. Freeze fractions with activity > 20,000 cpm/ul

Step 4: In-gel phosphatase assay

1. Cast an SDS-PAGE gel containing 10^5 cpm of labeled poly glu-tyr per 1 ml of gel solution. Add poly glu-tyr prior to addition of TEMED and APS
2. Run gel as usual
3. After gel is run incubate the gel in following solutions:

FIX: 1.5h-O/N	50 mM Tris pH 8.0 20% Isopropanol
WASH: 2 X 30 min	50mM Tris pH 8.0 0.3% β-mercaptoethanol
DENATURE: 1.5h	50mM Tris pH 8.0 6M Guanindine-HCl 0.3% β-mercaptoethanol
RENATURE: 3 X 1h	50mM Tris pH 8.0 1mM EDTA 0.3% β-mercaptoethanol 0.04% Tween-20
RENATURE: O/N	Above solutions + 4mM DTT

Coomassie stain and destain gel, and expose to X-ray film @ -70C

APPENDIX B

MATHEMATICA SCRIPT

```
Graphics`MultipleListPlot`
<< Graphics`Graphics`
<< Graphics`Legend`
<< Statistics`NormalDistribution`
<< Statistics`NonLinearFit`

monk1 = .01;
monk1r = .34;
monk2 = .00032;
monk2r = .096;
monk3 = .0015;
monk3r = .270;
monk4 = .01;
monk4r = .286;
monk5 = .01;
monk5r = .175;
monk6 = .032;
monk6r = .045;
monk7 = .15;
monk7r = .1014;
monk8 = .01;
monk8r = .143;
monKdATP = 34;
monKmATP = 60;
monKdPEP = 280;
monKdATPphos = 17.5;
monKdPEPphos = 143;
monKcat = 0.0008;
monKcatphos = 0.008;
KmPEPdephos = 0.1;
MET = 1;
monKmPdephos = 0.01;
VmaxPEPdephos = 0.001;
monVmaxPdephos = 0.45;
monKcatautophos = 0.0008;
monVmaxautophos = Kcatautophos * MET;
monα = .62;

dimk1 = .01;
dimk1r = .114;
dimk2 = .001;
dimk2r = .024;
dimk3 = .001;
dimk3r = .032;
dimk4 = .01;
dimk4r = .166;
dimk5 = .01;
dimk5r = .057;
dimk6 = .1;
dimk6r = .013;
dimk7 = .1;
dimk7r = .016;
dimk8 = .01;
dimk8r = .087;
dimKdATP = 11.4;
dimKmATP = 35;
dimKdPEP = 26.8;
dimKdATPphos = 5.7;
dimKdPEPphos = 15.9;
dimKcat = 0.0024;
dimKcatphos = 0.024;
dimKmPEPdephos = 0.1;
TPRMET = 1;
dimKmPdephos = 0.1;
dimVmaxPEPdephos = 0.001;
dimVmaxPdephos = 0.045;
dimKcatautophos = 0.24;
dimVmaxautophos = Kcatautophos * TPRMET;
dimα = .62;
```

Slope = 1;

WashTime = 8000;

$$mon[t\_] = \left(\frac{1}{\left(1 + e^{\left(\frac{WashTime - t}{Slope} \right)} \right)} \right)$$

$$dim[t\_] = \left(\frac{e^{\left(\frac{WashTime - t}{Slope} \right)}}{\left(1 + e^{\left(\frac{WashTime - t}{Slope} \right)} \right)} \right)$$

$$GF[t\_] = .100 - \left(\frac{.100}{\left(1 + e^{\left(\frac{WashTime - t}{Slope} \right)} \right)} \right)$$

$$GF75[t\_] = .003 - \left(\frac{.003}{\left(1 + e^{\left(\frac{WashTime - t}{Slope} \right)} \right)} \right)$$

$$GF50[t\_] = .001 - \left(\frac{.001}{\left(1 + e^{\left(\frac{WashTime - t}{Slope} \right)} \right)} \right)$$

$$GF25[t\_] = .00033 - \left(\frac{.00033}{\left(1 + e^{\left(\frac{WashTime - t}{Slope} \right)} \right)} \right)$$

GF0 = 0;

GFon = 10;

GFoff = .01;

$$\partial_t \text{monP}[t] == \text{monk1r} * \text{monPA}[t] + \text{monk2r} * \text{monPL}[t] + ((\text{monVmaxPdephos} * \text{monPphos}[t]) / (\text{monKmPdephos} + \text{monPphos}[t])) + \text{GFoff} * \text{dimP}[t] - \text{monk1} * A[t] * \text{monP}[t] - \text{monk2} * \text{monP}[t] * L[t] - \text{GFon} * \text{GF}[t] * \text{monP}[t] + \text{monKcat} * \text{monPAL}[t]$$

$$\partial_t A[t] == \text{monk1r} * \text{monPA}[t] + \text{monk5r} * \text{monPphosA}[t] + \text{monk4r} * \text{monPAL}[t] + \text{monk8r} * \text{monPphosAL}[t] - \text{monk1} * \text{monP}[t] * A[t] - \text{monk4} * \text{monPL}[t] * A[t] - \text{monk5} * \text{monPphos}[t] * A[t] - \text{monk8} * \text{monPphosL}[t] * A[t] - \text{monKcat} * \text{monPAL}[t] - \text{monKcatphos} * \text{monPphosAL}[t] - \text{monKcatautophos} * \text{monPA}[t] + \text{dimk1r} * \text{dimPA}[t] + \text{dimk5r} * \text{dimPphosA}[t] + \text{dimk4r} * \text{dimPAL}[t] + \text{dimk8r} * \text{dimPphosAL}[t] - \text{dimk1} * \text{dimP}[t] * A[t] - \text{dimk4} * \text{dimPL}[t] * A[t] - \text{dimk5} * \text{dimPphos}[t] * A[t] - \text{dimk8} * \text{dimPphosL}[t] * A[t] - \text{dimKcat} * \text{dimPAL}[t] - \text{dimKcatphos} * \text{dimPphosAL}[t] - \text{dimKcatautophos} * \text{dimPA}[t]$$

$$\partial_t L[t] == \text{monk2r} * \text{monPL}[t] + \text{monk3r} * \text{monPAL}[t] + \text{monk6r} * \text{monPphosL}[t] + \text{monk7r} * \text{monPphosAL}[t] + ((\text{VmaxPEPdephos} * \text{Lphos}[t]) / (\text{KmPEPdephos} + \text{Lphos}[t])) - \text{monk2} * \text{monP}[t] * L[t] - \text{monk3} * \text{monPA}[t] * L[t] - \text{monk6} * \text{monPphos}[t] * L[t] - \text{monk7} * \text{monPphosA}[t] * L[t] + \text{dimk2r} * \text{dimPL}[t] + \text{dimk3r} * \text{dimPAL}[t] + \text{dimk6r} * \text{dimPphosL}[t] + \text{dimk7r} * \text{dimPphosAL}[t] + ((\text{dimVmaxPEPdephos} * \text{Lphos}[t]) / (\text{dimKmPEPdephos} + \text{Lphos}[t])) - \text{dimk2} * \text{dimP}[t] * L[t] - \text{dimk3} * \text{dimPA}[t] * L[t] - \text{dimk6} * \text{dimPphos}[t] * L[t] - \text{dimk7} * \text{dimPphosA}[t] * L[t]$$

$$\partial_t \text{monPA}[t] == \text{monk1} * \text{monP}[t] * A[t] + \text{monk3r} * \text{monPAL}[t] + ((\text{monVmaxPdephos} * \text{monPphosA}[t]) / (\text{monKmPdephos} + \text{monPphosA}[t])) - \text{monk1r} * \text{monPA}[t] - \text{monk3} * \text{monPA}[t] * L[t] - \text{monKcatautophos} * \text{monPA}[t] + \text{GFoff} * \text{dimPA}[t] - \text{GFon} * \text{monPA}[t] * \text{GF}[t]$$

$$\partial_t \text{monPL}[t] == \text{monk2} * \text{monP}[t] * L[t] + \text{monk4r} * \text{monPAL}[t] + ((\text{monVmaxPdephos} * \text{monPphosL}[t]) / (\text{monKmPdephos} + \text{monPphosL}[t])) - \text{monk2r} * \text{monPL}[t] - \text{monk4} * \text{monPL}[t] * A[t] + \text{GFoff} * \text{dimPL}[t] - \text{GFon} * \text{monPL}[t] * \text{GF}[t]$$

$$\partial_t \text{monPAL}[t] == \text{monk3} * \text{monPA}[t] * L[t] + \text{monk4} * \text{monPL}[t] * A[t] + ((\text{monVmaxPdephos} * \text{monPphosAL}[t]) / (\text{monKmPdephos} + \text{monPphosAL}[t])) - \text{monk3r} * \text{monPAL}[t] - \text{monk4r} * \text{monPAL}[t] - \text{monKcat} * \text{monPAL}[t] - \text{GFon} * \text{monPAL}[t] * \text{GF}[t] + \text{GFoff} * \text{dimPAL}[t]$$

$$\partial_t \text{monPphos}[t] == \text{monk5r} * \text{monPphosA}[t] + \text{monk6r} * \text{monPphosL}[t] + \text{monKcatautophos} * \text{monPA}[t] - \text{monk5} * \text{monPphos}[t] * A[t] - \text{monk6} * \text{monPphos}[t] * L[t] - ((\text{monVmaxPdephos} * \text{monPphos}[t]) / (\text{monKmPdephos} + \text{monPphos}[t])) + \text{monKcatphos} * \text{monPphosAL}[t] + \text{GFoff} * \text{dimPphos}[t] - \text{GFon} * \text{GF}[t] * \text{monPphos}[t]$$

$$\partial_t \text{monPphosA}[t] == \text{monk5} * \text{monPphos}[t] * A[t] + \text{monk7r} * \text{monPphosAL}[t] - \text{monk5r} * \text{monPphosA}[t] - \text{monk7} * \text{monPphosA}[t] * L[t] - ((\text{monVmaxPdephos} * \text{monPphosA}[t]) / (\text{monKmPdephos} + \text{monPphosA}[t])) + \text{GFoff} * \text{dimPphosA}[t] - \text{GFon} * \text{GF}[t] * \text{monPphosA}[t]$$

$$\partial_t \text{monPphosL}[t] == \text{monk6} * \text{monPphos}[t] * L[t] + \text{monk8r} * \text{monPphosAL}[t] - \text{monk6r} * \text{monPphosL}[t] - \text{monk8} * \text{monPphosL}[t] * A[t] - ((\text{monVmaxPdephos} * \text{monPphosL}[t]) / (\text{monKmPdephos} + \text{monPphosL}[t])) + \text{GFoff} * \text{dimPphosL}[t] - \text{GFon} * \text{GF}[t] * \text{monPphosL}[t]$$

$$\partial_t \text{monPphosAL}[t] == \text{monk8} * \text{monPphosL}[t] * A[t] + \text{monk7} * \text{monPphosA}[t] * L[t] - \text{monk7r} * \text{monPphosAL}[t] - \text{monk8r} * \text{monPphosAL}[t] - \text{monKcatphos} * \text{monPphosAL}[t] - ((\text{monVmaxPdephos} * \text{monPphosAL}[t]) / (\text{monKmPdephos} + \text{monPphosAL}[t])) + \text{GFoff} * \text{dimPphosAL}[t] - \text{GFon} * \text{GF}[t] * \text{monPphosAL}[t]$$

$$\partial_t \text{monPpTot}[t] == \text{monPphos}[t] + \text{monPphosA}[t] + \text{monPphosL}[t] + \text{monPphosAL}[t]$$

$$\partial_t \text{Lphos}[t] == \text{monKcat} * \text{monPAL}[t] + \text{monKcatphos} * \text{monPphosAL}[t] - ((\text{VmaxPEPdephos} * \text{Lphos}[t]) / (\text{KmPEPdephos} + \text{Lphos}[t])) + \text{dimKcat} * \text{dimPAL}[t] + \text{dimKcatphos} * \text{dimPphosAL}[t]$$

$$\partial_t \text{dimP}[t] == \text{dimk1r} * \text{dimPA}[t] + \text{dimk2r} * \text{dimPL}[t] + ((\text{dimVmaxPdephos} * \text{dimPphos}[t]) / (\text{dimKmPdephos} + \text{dimPphos}[t])) - \text{dimk1} * A[t] * \text{dimP}[t] - \text{dimk2} * L[t] * \text{dimP}[t] + \text{dimKcat} * \text{dimPAL}[t] + \text{GFon} * \text{monP}[t] * \text{GF}[t] - \text{GFoff} * \text{dimP}[t]$$

$$\partial_t \text{dimPA}[t] == \text{dimk1} * \text{dimP}[t] * A[t] + \text{dimk3r} * \text{dimPAL}[t] + ((\text{dimVmaxPdephos} * \text{dimPphosA}[t]) / (\text{dimKmPdephos} + \text{dimPphosA}[t])) - \text{dimk1r} * \text{dimPA}[t] - \text{dimk3} * \text{dimPA}[t] * L[t] - \text{dimKcatautophos} * \text{dimPA}[t] + \text{GFon} * \text{monPA}[t] * \text{GF}[t] - \text{GFoff} * \text{dimPA}[t]$$

$$\partial_t \text{dimPL}[t] == \text{dimk2} * \text{dimP}[t] * L[t] + \text{dimk4r} * \text{dimPAL}[t] + ((\text{dimVmaxPdephos} * \text{dimPphosL}[t]) / (\text{dimKmPdephos} + \text{dimPphosL}[t])) - \text{dimk2r} * \text{dimPL}[t] - \text{dimk4} * \text{dimPL}[t] * A[t] + \text{GFon} * \text{monPL}[t] * \text{GF}[t] - \text{GFoff} * \text{dimPL}[t]$$

$$\partial_t \text{dimPAL}[t] == \text{dimk3} * \text{dimPA}[t] * L[t] + \text{dimk4} * \text{dimPL}[t] * A[t] + ((\text{dimVmaxPdephos} * \text{dimPphosAL}[t]) / (\text{dimKmPdephos} + \text{dimPphosAL}[t])) - \text{dimk3r} * \text{dimPAL}[t] - \text{dimk4r} * \text{dimPAL}[t] - \text{dimKcat} * \text{dimPAL}[t] + \text{GFon} * \text{monPAL}[t] * \text{GF}[t] - \text{GFoff} * \text{dimPAL}[t]$$

$$\partial_t \text{dimPphos}[t] == \text{dimk5r} * \text{dimPphosA}[t] + \text{dimk6r} * \text{dimPphosL}[t] + \text{dimKcatautophos} * \text{dimPA}[t] - \text{dimk5} * \text{dimPphos}[t] * A[t] - \text{dimk6} * \text{dimPphos}[t] * L[t] - ((\text{dimVmaxPdephos} * \text{dimPphos}[t]) / (\text{dimKmPdephos} + \text{dimPphos}[t])) + \text{dimKcatphos} * \text{dimPphosAL}[t] + \text{GFon} * \text{monPphos}[t] * \text{GF}[t] - \text{GFoff} * \text{dimPphos}[t]$$

$$\partial_t \text{dimPphosA}[t] == \text{dimk5} * \text{dimPphos}[t] * A[t] + \text{dimk7r} * \text{dimPphosAL}[t] - \text{dimk5r} * \text{dimPphosA}[t] - \text{dimk7} * \text{dimPphosA}[t] * L[t] - ((\text{dimVmaxPdephos} * \text{dimPphosA}[t]) / (\text{dimKmPdephos} + \text{dimPphosA}[t])) + \text{GFon} * \text{monPphosA}[t] * \text{GF}[t] - \text{GFoff} * \text{dimPphosA}[t]$$

$$\partial_t \text{dimPphosL}[t] == \text{dimk6} * \text{dimPphos}[t] * L[t] + \text{dimk8r} * \text{dimPphosAL}[t] - \text{dimk6r} * \text{dimPphosL}[t] - \text{dimk8} * \text{dimPphosL}[t] * A[t] - ((\text{dimVmaxPdephos} * \text{dimPphosL}[t]) / (\text{dimKmPdephos} + \text{dimPphosL}[t])) + \text{GFon} * \text{monPphosL}[t] * \text{GF}[t] - \text{GFoff} * \text{dimPphosL}[t]$$

```
∂t dimPphosAL[t] == dimk8 * dimPphosL[t] * A[t] + dimk7 * dimPphosA[t] * L[t] - dimk7r * dimPphosAL[t] -
    dimk8r * dimPphosAL[t] - dimKcatphos * dimPphosAL[t] -
    ((dimVmaxPdephos * dimPphosAL[t]) / (dimKmPdephos + dimPphosAL[t])) + GFon * monPphosAL[t] * GF[t] -
    GFoff * dimPphosAL[t]
∂t dimPpTot[t] == dimPphos[t] + dimPphosA[t] + dimPphosL[t] + dimPphosAL[t]
∂t dimerMET[t] == dimP[t] + dimPA[t] + dimPL[t] + dimPAL[t] + dimPphos[t] + dimPphosA[t] + dimPphosL[t] + dimPphosAL[t]
∂t monomerMET[t] == monP[t] + monPA[t] + monPL[t] + monPAL[t] + monPphos[t] + monPphosA[t] + monPphosL[t] + monPphosAL[t]


ndsolutioncombined =
  NDSolve[
    {∂t monP[t] == monk1r * monPA[t] + monk2r * monPL[t] + ((monVmaxPdephos * monPphos[t]) / (monKmPdephos + monPphos[t])) +
        GFoff * dimP[t] - monk1 * A[t] * monP[t] - monk2 * monP[t] * L[t] - GFon * GF[t] * monP[t] + monKcat * monPAL[t],
     ∂t A[t] == monk1r * monPA[t] + monk5r * monPphosA[t] + monk4r * monPAL[t] + monk8r * monPphosAL[t] -
        monk1 * monP[t] * A[t] - monk4 * monPL[t] * A[t] - monk5 * monPphos[t] * A[t] - monk8 * monPphosL[t] * A[t] -
        monKcat * monPAL[t] - monKcatphos * monPphosAL[t] - monKcatautophos * monPA[t] + dimk1r * dimPA[t] +
        dimk5r * dimPphosA[t] + dimk4r * dimPAL[t] + dimk8r * dimPphosAL[t] - dimk1 * dimP[t] * A[t] -
        dimk4 * dimPL[t] * A[t] - dimk5 * dimPphos[t] * A[t] - dimk8 * dimPphosL[t] * A[t] - dimKcat * dimPAL[t] -
        dimKcatphos * dimPphosAL[t] - dimKcatautophos * dimPA[t],
     ∂t L[t] == monk2r * monPL[t] + monk3r * monPAL[t] + monk6r * monPphosL[t] + monk7r * monPphosAL[t] -
        monk2 * monP[t] * L[t] - monk3 * monPA[t] * L[t] - monk6 * monPphos[t] * L[t] - monk7 * monPphosA[t] * L[t] +
        dimk2r * dimPL[t] + dimk3r * dimPAL[t] + dimk6r * dimPphosL[t] + dimk7r * dimPphosAL[t] +
        ((dimVmaxPEPdephos * Lphos[t]) / (dimKmPEPdephos + Lphos[t])) - dimk2 * dimP[t] * L[t] - dimk3 * dimPA[t] * L[t] -
        dimk6 * dimPphos[t] * L[t] - dimk7 * dimPphosA[t] * L[t],
     ∂t monPA[t] == monk1 * monP[t] * A[t] + monk3r * monPAL[t] +
        ((monVmaxPdephos * monPphosA[t]) / (monKmPdephos + monPphosA[t])) - monk1r * monPA[t] -
        monk3 * monPA[t] * L[t] - monKcatautophos * monPA[t] + GFoff * dimPA[t] - GFon * monPA[t] * GF[t],
     ∂t monPL[t] == monk2 * monP[t] * L[t] + monk4r * monPAL[t] +
        ((monVmaxPdephos * monPphosL[t]) / (monKmPdephos + monPphosL[t])) - monk2r * monPL[t] -
        monk4 * monPL[t] * A[t] + GFoff * dimPL[t] - GFon * monPL[t] * GF[t],
     ∂t monPAL[t] == monk3 * monPA[t] * L[t] + monk4 * monPL[t] * A[t] +
        ((monVmaxPdephos * monPphosAL[t]) / (monKmPdephos + monPphosAL[t])) - monk3r * monPAL[t] -
        monk4r * monPAL[t] - monKcat * monPAL[t] - GFon * monPAL[t] * GF[t] + GFoff * dimPAL[t],
     ∂t monPphos[t] == monk5r * monPphosA[t] + monk6r * monPphosL[t] + monKcatautophos * monPA[t] -
        monk5 * monPphos[t] * A[t] - monk6 * monPphos[t] * L[t] -
        ((monVmaxPdephos * monPphos[t]) / (monKmPdephos + monPphos[t])) + monKcatphos * monPphosAL[t] +
        GFoff * dimPphos[t] - GFon * GF[t] * monPphos[t],
     ∂t monPphosA[t] == monk5 * monPphos[t] * A[t] + monk7r * monPphosAL[t] - monk5r * monPphosA[t] -
        monk7 * monPphosA[t] * L[t] - ((monVmaxPdephos * monPphosA[t]) / (monKmPdephos + monPphosA[t])) +
        GFoff * dimPphosA[t] - GFon * GF[t] * monPphosA[t],
     ∂t monPphosL[t] == monk6 * monPphos[t] * L[t] + monk8r * monPphosAL[t] - monk6r * monPphosL[t] -
        monk8 * monPphosL[t] * A[t] - ((monVmaxPdephos * monPphosL[t]) / (monKmPdephos + monPphosL[t])) +
        GFoff * dimPphosL[t] - GFon * GF[t] * monPphosL[t],
     ∂t monPphosAL[t] == monk8 * monPphosL[t] * A[t] + monk7 * monPphosA[t] * L[t] - monk7r * monPphosAL[t] -
        monk8r * monPphosAL[t] - monKcatphos * monPphosAL[t] -
        ((monVmaxPdephos * monPphosAL[t]) / (monKmPdephos + monPphosAL[t])) + GFoff * dimPphosAL[t] -
        GFon * GF[t] * monPphosAL[t],
     ∂t monPpTot[t] == ∂t monPphos[t] + ∂t monPphosA[t] + ∂t monPphosL[t] + ∂t monPphosAL[t],
     ∂t Lphos[t] == monKcat * monPAL[t] + monKcatphos * monPphosAL[t] -
        ((VmaxPEPdephos * Lphos[t]) / (KmPEPdephos + Lphos[t])) + dimKcat * dimPAL[t] + dimKcatphos * dimPphosAL[t],
     ∂t dimP[t] == dimk1r * dimPA[t] + dimk2r * dimPL[t] + ((dimVmaxPdephos * dimPphos[t]) / (dimKmPdephos + dimPphos[t])) -
        dimk1 * A[t] * dimP[t] - dimk2 * L[t] * dimP[t] + dimKcat * dimPAL[t] + GFon * monP[t] * GF[t] - GFoff * dimP[t],
```

```
∂t dimPA[t] == dimk1 * dimP[t] * A[t] + dimk3r * dimPAL[t] +
    ((dimVmaxPdephos * dimPphosA[t]) / (dimKmPdephos + dimPphosA[t])) - dimk1r * dimPA[t] - dimk3 * dimPA[t] * L[t] -
    dimKcatautophos * dimPA[t] + GFon * monPA[t] * GF[t] - GFoff * dimPA[t],
∂t dimPL[t] == dimk2 * dimP[t] * L[t] + dimk4r * dimPAL[t] +
    ((dimVmaxPdephos * dimPphosL[t]) / (dimKmPdephos + dimPphosL[t])) - dimk2r * dimPL[t] - dimk4 * dimPL[t] * A[t] +
    GFon * monPL[t] * GF[t] - GFoff * dimPL[t],
∂t dimPAL[t] == dimk3 * dimPA[t] * L[t] + dimk4 * dimPL[t] * A[t] +
    ((dimVmaxPdephos * dimPphosAL[t]) / (dimKmPdephos + dimPphosAL[t])) - dimk3r * dimPAL[t] -
    dimk4r * dimPAL[t] - dimKcat * dimPAL[t] + GFon * monPAL[t] * GF[t] - GFoff * dimPAL[t],
∂t dimPphos[t] == dimk5r * dimPphosA[t] + dimk6r * dimPphosL[t] + dimKcatautophos * dimPA[t] -
    dimk5 * dimPphos[t] * A[t] - dimk6 * dimPphos[t] * L[t] - ((dimVmaxPdephos * dimPphos[t]) / (dimKmPdephos + dimPphos[t])) +
    dimKcatphos * dimPphosAL[t] + GFon * monPphos[t] * GF[t] - GFoff * dimPphos[t],
∂t dimPphosA[t] == dimk5 * dimPphos[t] * A[t] + dimk7r * dimPphosAL[t] - dimk5r * dimPphosA[t] -
    dimk7 * dimPphosA[t] * L[t] - ((dimVmaxPdephos * dimPphosA[t]) / (dimKmPdephos + dimPphosA[t])) +
    GFon * monPphosA[t] * GF[t] - GFoff * dimPphosA[t],
∂t dimPphosL[t] == dimk6 * dimPphos[t] * L[t] + dimk8r * dimPphosAL[t] - dimk6r * dimPphosL[t] -
    dimk8 * dimPphosL[t] * A[t] - ((dimVmaxPdephos * dimPphosL[t]) / (dimKmPdephos + dimPphosL[t])) +
    GFon * monPphosL[t] * GF[t] - GFoff * dimPphosL[t],
∂t dimPphosAL[t] == dimk8 * dimPphosL[t] * A[t] + dimk7 * dimPphosA[t] * L[t] - dimk7r * dimPphosAL[t] -
    dimk8r * dimPphosAL[t] - dimKcatphos * dimPphosAL[t] -
    ((dimVmaxPdephos * dimPphosAL[t]) / (dimKmPdephos + dimPphosAL[t])) + GFon * monPphosAL[t] * GF[t] -
    GFoff * dimPphosAL[t],
∂t dimPpTot[t] == ∂t dimPphos[t] + ∂t dimPphosA[t] + ∂t dimPphosL[t] + ∂t dimPphosAL[t],
∂t dimerMET[t] == ∂t dimP[t] + ∂t dimPA[t] + ∂t dimPL[t] + ∂t dimPAL[t] + ∂t dimPphos[t] + ∂t dimPphosA[t] +
    ∂t dimPphosL[t] + ∂t dimPphosAL[t],
∂t monomerMET[t] == ∂t monP[t] + ∂t monPA[t] + ∂t monPL[t] + ∂t monPAL[t] + ∂t monPphos[t] + ∂t monPphosA[t] +
    ∂t monPphosL[t] + ∂t monPphosAL[t],
dimP[0] == 0, A[0] == 1000, L[0] == 3, dimPA[0] == 0, dimPL[0] == 0, dimPAL[0] == 0, dimPphos[0] == 0,
dimPphosA[0] == 0, dimPphosL[0] == 0, dimPphosAL[0] == 0, dimPpTot[0] == 0, Lphos[0] == 0, monP[0] == 1,
monPA[0] == 0, monPL[0] == 0, monPAL[0] == 0, monPphos[0] == 0, monPphosA[0] == 0, monPphosL[0] == 0,
monPphosAL[0] == 0, monPpTot[0] == 0, monomerMET[0] == 1, dimerMET[0] == 0},
{dimP, A, L, dimPA, dimPL, dimPAL, dimPphos, dimPphosA, dimPphosL, dimPphosAL, dimPpTot, Lphos, monP,
  monPA, monPL, monPAL, monPphos, monPphosA, monPphosL, monPphosAL, monPpTot, monomerMET, dimerMET},
{t, 0, 2000}, MaxSteps → 10000]
```

```
ndsolutioncombined75 =
  NDSolve[
   {∂t monP[t] == monk1r * monPA[t] + monk2r * monPL[t] + ((monVmaxPdephos * monPphos[t]) / (monKmPdephos + monPphos[t])) +
        GFoff * dimP[t] - monk1 * A[t] * monP[t] - monk2 * monP[t] * L[t] - GFon * GF75[t] * monP[t] + monKcat * monPAL[t],
    ∂t A[t] == monk1r * monPA[t] + monk5r * monPphosA[t] + monk4r * monPAL[t] + monk8r * monPphosAL[t] -
        monk1 * monP[t] * A[t] - monk4 * monPL[t] * A[t] - monk5 * monPphos[t] * A[t] - monk8 * monPphosL[t] * A[t] -
        monKcat * monPAL[t] - monKcatphos * monPphosAL[t] - monKcatautophos * monPA[t] + dimk1r * dimPA[t] +
        dimk5r * dimPphosA[t] + dimk4r * dimPAL[t] + dimk8r * dimPphosAL[t] - dimk1 * dimP[t] * A[t] -
        dimk4 * dimPL[t] * A[t] - dimk5 * dimPphos[t] * A[t] - dimk8 * dimPphosL[t] * A[t] - dimKcat * dimPAL[t] -
        dimKcatphos * dimPphosAL[t] - dimKcatautophos * dimPA[t],
    ∂t L[t] == monk2r * monPL[t] + monk3r * monPAL[t] + monk6r * monPphosL[t] + monk7r * monPphosAL[t] -
        monk2 * monP[t] * L[t] - monk3 * monPA[t] * L[t] - monk6 * monPphos[t] * L[t] - monk7 * monPphosA[t] * L[t] +
        dimk2r * dimPL[t] + dimk3r * dimPAL[t] + dimk6r * dimPphosL[t] + dimk7r * dimPphosAL[t] +
        ((dimVmaxPEPdephos * Lphos[t]) / (dimKmPEPdephos + Lphos[t])) - dimk2 * dimP[t] * L[t] - dimk3 * dimPA[t] * L[t] -
        dimk6 * dimPphos[t] * L[t] - dimk7 * dimPphosA[t] * L[t],
    ∂t monPA[t] == monk1 * monP[t] * A[t] + monk3r * monPAL[t] +
        ((monVmaxPdephos * monPphosA[t]) / (monKmPdephos + monPphosA[t])) - monk1r * monPA[t] -
        monk3 * monPA[t] * L[t] - monKcatautophos * monPA[t] + GFoff * dimPA[t] - GFon * monPA[t] * GF75[t],
    ∂t monPL[t] == monk2 * monP[t] * L[t] + monk4r * monPAL[t] +
        ((monVmaxPdephos * monPphosL[t]) / (monKmPdephos + monPphosL[t])) - monk2r * monPL[t] -
        monk4 * monPL[t] * A[t] + GFoff * dimPL[t] - GFon * monPL[t] * GF75[t],
    ∂t monPAL[t] == monk3 * monPA[t] * L[t] + monk4 * monPL[t] * A[t] +
        ((monVmaxPdephos * monPphosAL[t]) / (monKmPdephos + monPphosAL[t])) - monk3r * monPAL[t] -
        monk4r * monPAL[t] - monKcat * monPAL[t] - GFon * monPAL[t] * GF75[t] + GFoff * dimPAL[t],
    ∂t monPphos[t] == monk5r * monPphosA[t] + monk6r * monPphosL[t] + monKcatautophos * monPA[t] -
        monk5 * monPphos[t] * A[t] - monk6 * monPphos[t] * L[t] -
        ((monVmaxPdephos * monPphos[t]) / (monKmPdephos + monPphos[t])) + monKcatphos * monPphosAL[t] +
        GFoff * dimPphos[t] - GFon * GF75[t] * monPphos[t],
    ∂t monPphosA[t] == monk5 * monPphos[t] * A[t] + monk7r * monPphosAL[t] - monk5r * monPphosA[t] -
        monk7 * monPphosA[t] * L[t] - ((monVmaxPdephos * monPphosA[t]) / (monKmPdephos + monPphosA[t])) +
        GFoff * dimPphosA[t] - GFon * GF75[t] * monPphosA[t],
    ∂t monPphosL[t] == monk6 * monPphos[t] * L[t] + monk8r * monPphosAL[t] - monk6r * monPphosL[t] -
        monk8 * monPphosL[t] * A[t] - ((monVmaxPdephos * monPphosL[t]) / (monKmPdephos + monPphosL[t])) +
        GFoff * dimPphosL[t] - GFon * GF75[t] * monPphosL[t],
    ∂t monPphosAL[t] == monk8 * monPphosL[t] * A[t] + monk7 * monPphosA[t] * L[t] - monk7r * monPphosAL[t] -
        monk8r * monPphosAL[t] - monKcatphos * monPphosAL[t] -
        ((monVmaxPdephos * monPphosAL[t]) / (monKmPdephos + monPphosAL[t])) + GFoff * dimPphosAL[t] -
        GFon * GF75[t] * monPphosAL[t],
    ∂t monPpTot[t] == ∂t monPphos[t] + ∂t monPphosA[t] + ∂t monPphosL[t] + ∂t monPphosAL[t],
    ∂t Lphos[t] == monKcat * monPAL[t] + monKcatphos * monPphosAL[t] -
        ((VmaxPEPdephos * Lphos[t]) / (KmPEPdephos + Lphos[t])) + dimKcat * dimPAL[t] + dimKcatphos * dimPphosAL[t],
    ∂t dimP[t] == dimk1r * dimPA[t] + dimk2r * dimPL[t] + ((dimVmaxPdephos * dimPphos[t]) / (dimKmPdephos + dimPphos[t])) -
        dimk1 * A[t] * dimP[t] - dimk2 * L[t] * dimP[t] + dimKcat * dimPAL[t] + GFon * monP[t] * GF75[t] - GFoff * dimP[t],
    ∂t dimPA[t] == dimk1 * dimP[t] * A[t] + dimk3r * dimPAL[t] +
        ((dimVmaxPdephos * dimPphosA[t]) / (dimKmPdephos + dimPphosA[t])) - dimk1r * dimPA[t] - dimk3 * dimPA[t] * L[t] -
        dimKcatautophos * dimPA[t] + GFon * monPA[t] * GF75[t] - GFoff * dimPA[t],
    ∂t dimPL[t] == dimk2 * dimP[t] * L[t] + dimk4r * dimPAL[t] +
        ((dimVmaxPdephos * dimPphosL[t]) / (dimKmPdephos + dimPphosL[t])) - dimk2r * dimPL[t] - dimk4 * dimPL[t] * A[t] +
        GFon * monPL[t] * GF75[t] - GFoff * dimPL[t],
```

```
    ∂t dimPAL[t] == dimk3 * dimPA[t] * L[t] + dimk4 * dimPL[t] * A[t] +
       ((dimVmaxPdephos * dimPphosAL[t]) / (dimKmPdephos + dimPphosAL[t])) - dimk3r * dimPAL[t] -
       dimk4r * dimPAL[t] - dimKcat * dimPAL[t] + GFon * monPAL[t] * GF75[t] - GFoff * dimPAL[t],
    ∂t dimPphos[t] == dimk5r * dimPphosA[t] + dimk6r * dimPphosL[t] + dimKcatautophos * dimPA[t] -
       dimk5 * dimPphos[t] * A[t] - dimk6 * dimPphos[t] * L[t] - ((dimVmaxPdephos * dimPphos[t]) / (dimKmPdephos + dimPphos[t])) +
       dimKcatphos * dimPphosAL[t] + GFon * monPphos[t] * GF75[t] - GFoff * dimPphos[t],
    ∂t dimPphosA[t] == dimk5 * dimPphos[t] * A[t] + dimk7r * dimPphosAL[t] - dimk5r * dimPphosA[t] -
       dimk7 * dimPphosA[t] * L[t] - ((dimVmaxPdephos * dimPphosA[t]) / (dimKmPdephos + dimPphosA[t])) +
       GFon * monPphosA[t] * GF75[t] - GFoff * dimPphosA[t],
    ∂t dimPphosL[t] == dimk6 * dimPphos[t] * L[t] + dimk8r * dimPphosAL[t] - dimk6r * dimPphosL[t] -
       dimk8 * dimPphosL[t] * A[t] - ((dimVmaxPdephos * dimPphosL[t]) / (dimKmPdephos + dimPphosL[t])) +
       GFon * monPphosL[t] * GF75[t] - GFoff * dimPphosL[t],
    ∂t dimPphosAL[t] == dimk8 * dimPphosL[t] * A[t] + dimk7 * dimPphosA[t] * L[t] - dimk7r * dimPphosAL[t] -
       dimk8r * dimPphosAL[t] - dimKcatphos * dimPphosAL[t] -
       ((dimVmaxPdephos * dimPphosAL[t]) / (dimKmPdephos + dimPphosAL[t])) + GFon * monPphosAL[t] * GF75[t] -
       GFoff * dimPphosAL[t],
    ∂t dimPpTot[t] == ∂t dimPphos[t] + ∂t dimPphosA[t] + ∂t dimPphosL[t] + ∂t dimPphosAL[t],
    ∂t dimerMET[t] == ∂t dimP[t] + ∂t dimPA[t] + ∂t dimPL[t] + ∂t dimPAL[t] + ∂t dimPphos[t] + ∂t dimPphosA[t] +
       ∂t dimPphosL[t] + ∂t dimPphosAL[t],
    ∂t monomerMET[t] == ∂t monP[t] + ∂t monPA[t] + ∂t monPL[t] + ∂t monPAL[t] + ∂t monPphos[t] + ∂t monPphosA[t] +
       ∂t monPphosL[t] + ∂t monPphosAL[t],
    dimP[0] == 0, A[0] == 1000, L[0] == 3, dimPA[0] == 0, dimPL[0] == 0, dimPAL[0] == 0, dimPphos[0] == 0,
    dimPphosA[0] == 0, dimPphosL[0] == 0, dimPphosAL[0] == 0, dimPpTot[0] == 0, Lphos[0] == 0, monP[0] == 1,
    monPA[0] == 0, monPL[0] == 0, monPAL[0] == 0, monPphos[0] == 0, monPphosA[0] == 0, monPphosL[0] == 0,
    monPphosAL[0] == 0, monPpTot[0] == 0, monomerMET[0] == 1, dimerMET[0] == 0},
   {dimP, A, L, dimPA, dimPL, dimPAL, dimPphos, dimPphosA, dimPphosL, dimPphosAL, dimPpTot, Lphos, monP,
    monPA, monPL, monPAL, monPphos, monPphosA, monPphosL, monPphosAL, monPpTot, monomerMET, dimerMET},
   {t, 0, 2000}, MaxSteps → 10000]

dsolutioncombined50 =
  NDSolve[
   {∂t monP[t] == monk1r * monPA[t] + monk2r * monPL[t] + ((monVmaxPdephos * monPphos[t]) / (monKmPdephos + monPphos[t])) +
      GFoff * dimP[t] - monk1 * A[t] * monP[t] - monk2 * monP[t] * L[t] - GFon * GF50[t] * monP[t] + monKcat * monPAL[t],
    ∂t A[t] == monk1r * monPA[t] + monk5r * monPphosA[t] + monk4r * monPAL[t] + monk8r * monPphosAL[t] -
      monk1 * monP[t] * A[t] - monk4 * monPL[t] * A[t] - monk5 * monPphos[t] * A[t] - monk8 * monPphosL[t] * A[t] -
      monKcat * monPAL[t] - monKcatphos * monPphosAL[t] - monKcatautophos * monPA[t] + dimk1r * dimPA[t] +
      dimk5r * dimPphosA[t] + dimk4r * dimPAL[t] + dimk8r * dimPphosAL[t] - dimk1 * dimP[t] * A[t] -
      dimk4 * dimPL[t] * A[t] - dimk5 * dimPphos[t] * A[t] - dimk8 * dimPphosL[t] * A[t] - dimKcat * dimPAL[t] -
      dimKcatphos * dimPphosAL[t] - dimKcatautophos * dimPA[t],
    ∂t L[t] == monk2r * monPL[t] + monk3r * monPAL[t] + monk6r * monPphosL[t] + monk7r * monPphosAL[t] -
      monk2 * monP[t] * L[t] - monk3 * monPA[t] * L[t] - monk6 * monPphos[t] * L[t] - monk7 * monPphosA[t] * L[t] +
      dimk2r * dimPL[t] + dimk3r * dimPAL[t] + dimk6r * dimPphosL[t] + dimk7r * dimPphosAL[t] +
      ((dimVmaxPEPdephos * Lphos[t]) / (dimKmPEPdephos + Lphos[t])) - dimk2 * dimP[t] * L[t] - dimk3 * dimPA[t] * L[t] -
      dimk6 * dimPphos[t] * L[t] - dimk7 * dimPphosA[t] * L[t],
    ∂t monPA[t] == monk1 * monP[t] * A[t] + monk3r * monPAL[t] +
      ((monVmaxPdephos * monPphosA[t]) / (monKmPdephos + monPphosA[t])) - monk1r * monPA[t] -
      monk3 * monPA[t] * L[t] - monKcatautophos * monPA[t] + GFoff * dimPA[t] - GFon * monPA[t] * GF50[t],
    ∂t monPL[t] == monk2 * monP[t] * L[t] + monk4r * monPAL[t] +
      ((monVmaxPdephos * monPphosL[t]) / (monKmPdephos + monPphosL[t])) - monk2r * monPL[t] -
      monk4 * monPL[t] * A[t] + GFoff * dimPL[t] - GFon * monPL[t] * GF50[t],
    ∂t monPAL[t] == monk3 * monPA[t] * L[t] + monk4 * monPL[t] * A[t] +
      ((monVmaxPdephos * monPphosAL[t]) / (monKmPdephos + monPphosAL[t])) - monk3r * monPAL[t] -
      monk4r * monPAL[t] - monKcat * monPAL[t] - GFon * monPAL[t] * GF50[t] + GFoff * dimPAL[t],
```

```
  ∂t monPphos[t] == monk5r * monPphosA[t] + monk6r * monPphosL[t] + monKcatautophos * monPA[t] -
      monk5 * monPphos[t] * A[t] - monk6 * monPphos[t] * L[t] -
      ((monVmaxPdephos * monPphos[t]) / (monKmPdephos + monPphos[t])) + monKcatphos * monPphosAL[t] +
      GFoff * dimPphos[t] - GFon * GF50[t] * monPphos[t],
  ∂t monPphosA[t] == monk5 * monPphos[t] * A[t] + monk7r * monPphosAL[t] - monk5r * monPphosA[t] -
      monk7 * monPphosA[t] * L[t] - ((monVmaxPdephos * monPphosA[t]) / (monKmPdephos + monPphosA[t])) +
      GFoff * dimPphosA[t] - GFon * GF50[t] * monPphosA[t],
  ∂t monPphosL[t] == monk6 * monPphos[t] * L[t] + monk8r * monPphosAL[t] - monk6r * monPphosL[t] -
      monk8 * monPphosL[t] * A[t] - ((monVmaxPdephos * monPphosL[t]) / (monKmPdephos + monPphosL[t])) +
      GFoff * dimPphosL[t] - GFon * GF50[t] * monPphosL[t],
  ∂t monPphosAL[t] == monk8 * monPphosL[t] * A[t] + monk7 * monPphosA[t] * L[t] - monk7r * monPphosAL[t] -
      monk8r * monPphosAL[t] - monKcatphos * monPphosAL[t] -
      ((monVmaxPdephos * monPphosAL[t]) / (monKmPdephos + monPphosAL[t])) + GFoff * dimPphosAL[t] -
      GFon * GF50[t] * monPphosAL[t],
  ∂t monPpTot[t] == ∂t monPphos[t] + ∂t monPphosA[t] + ∂t monPphosL[t] + ∂t monPphosAL[t],
  ∂t Lphos[t] == monKcat * monPAL[t] + monKcatphos * monPphosAL[t] -
      ((VmaxPEPdephos * Lphos[t]) / (KmPEPdephos + Lphos[t])) + dimKcat * dimPAL[t] + dimKcatphos * dimPphosAL[t],
  ∂t dimP[t] == dimk1r * dimPA[t] + dimk2r * dimPL[t] + ((dimVmaxPdephos * dimPphos[t]) / (dimKmPdephos + dimPphos[t])) -
      dimk1 * A[t] * dimP[t] - dimk2 * L[t] * dimP[t] + dimKcat * dimPAL[t] + GFon * monP[t] * GF50[t] - GFoff * dimP[t],
  ∂t dimPA[t] == dimk1 * dimP[t] * A[t] + dimk3r * dimPAL[t] +
      ((dimVmaxPdephos * dimPphosA[t]) / (dimKmPdephos + dimPphosA[t])) - dimk1r * dimPA[t] - dimk3 * dimPA[t] * L[t] -
      dimKcatautophos * dimPA[t] + GFon * monPA[t] * GF50[t] - GFoff * dimPA[t],
  ∂t dimPL[t] == dimk2 * dimP[t] * L[t] + dimk4r * dimPAL[t] +
      ((dimVmaxPdephos * dimPphosL[t]) / (dimKmPdephos + dimPphosL[t])) - dimk2r * dimPL[t] - dimk4 * dimPL[t] * A[t] +
      GFon * monPL[t] * GF50[t] - GFoff * dimPL[t],
  ∂t dimPAL[t] == dimk3 * dimPA[t] * L[t] + dimk4 * dimPL[t] * A[t] +
      ((dimVmaxPdephos * dimPphosAL[t]) / (dimKmPdephos + dimPphosAL[t])) - dimk3r * dimPAL[t] -
      dimk4r * dimPAL[t] - dimKcat * dimPAL[t] + GFon * monPAL[t] * GF50[t] - GFoff * dimPAL[t],
  ∂t dimPphos[t] == dimk5r * dimPphosA[t] + dimk6r * dimPphosL[t] + dimKcatautophos * dimPA[t] -
      dimk5 * dimPphos[t] * A[t] - dimk6 * dimPphos[t] * L[t] - ((dimVmaxPdephos * dimPphos[t]) / (dimKmPdephos + dimPphos[t])) +
      dimKcatphos * dimPphosAL[t] + GFon * monPphos[t] * GF50[t] - GFoff * dimPphos[t],
  ∂t dimPphosA[t] == dimk5 * dimPphos[t] * A[t] + dimk7r * dimPphosAL[t] - dimk5r * dimPphosA[t] -
      dimk7 * dimPphosA[t] * L[t] - ((dimVmaxPdephos * dimPphosA[t]) / (dimKmPdephos + dimPphosA[t])) +
      GFon * monPphosA[t] * GF50[t] - GFoff * dimPphosA[t],
  ∂t dimPphosL[t] == dimk6 * dimPphos[t] * L[t] + dimk8r * dimPphosAL[t] - dimk6r * dimPphosL[t] -
      dimk8 * dimPphosL[t] * A[t] - ((dimVmaxPdephos * dimPphosL[t]) / (dimKmPdephos + dimPphosL[t])) +
      GFon * monPphosL[t] * GF50[t] - GFoff * dimPphosL[t],
  ∂t dimPphosAL[t] == dimk8 * dimPphosL[t] * A[t] + dimk7 * dimPphosA[t] * L[t] - dimk7r * dimPphosAL[t] -
      dimk8r * dimPphosAL[t] - dimKcatphos * dimPphosAL[t] -
      ((dimVmaxPdephos * dimPphosAL[t]) / (dimKmPdephos + dimPphosAL[t])) + GFon * monPphosAL[t] * GF50[t] -
      GFoff * dimPphosAL[t],
  ∂t dimPpTot[t] == ∂t dimPphos[t] + ∂t dimPphosA[t] + ∂t dimPphosL[t] + ∂t dimPphosAL[t],
  ∂t dimerMET[t] == ∂t dimP[t] + ∂t dimPA[t] + ∂t dimPL[t] + ∂t dimPAL[t] + ∂t dimPphos[t] + ∂t dimPphosA[t] +
      ∂t dimPphosL[t] + ∂t dimPphosAL[t],
  ∂t monomerMET[t] == ∂t monP[t] + ∂t monPA[t] + ∂t monPL[t] + ∂t monPAL[t] + ∂t monPphos[t] + ∂t monPphosA[t] +
      ∂t monPphosL[t] + ∂t monPphosAL[t],
  dimP[0] == 0, A[0] == 1000, L[0] == 3, dimPA[0] == 0, dimPL[0] == 0, dimPAL[0] == 0, dimPphos[0] == 0,
  dimPphosA[0] == 0, dimPphosL[0] == 0, dimPphosAL[0] == 0, dimPpTot[0] == 0, Lphos[0] == 0, monP[0] == 1,
  monPA[0] == 0, monPL[0] == 0, monPAL[0] == 0, monPphos[0] == 0, monPphosA[0] == 0, monPphosL[0] == 0,
  monPphosAL[0] == 0, monPpTot[0] == 0, monomerMET[0] == 1, dimerMET[0] == 0},
{dimP, A, L, dimPA, dimPL, dimPAL, dimPphos, dimPphosA, dimPphosL, dimPphosAL, dimPpTot, Lphos, monP,
  monPA, monPL, monPAL, monPphos, monPphosA, monPphosL, monPphosAL, monPpTot, monomerMET, dimerMET},
{t, 0, 2000}, MaxSteps → 10000]
```

```
ndsolutioncombined25 =
  NDSolve[
   {∂t monP[t] == monk1r * monPA[t] + monk2r * monPL[t] + ((monVmaxPdephos * monPphos[t]) / (monKmPdephos + monPphos[t])) +
       GFoff * dimP[t] − monk1 * A[t] * monP[t] − monk2 * monP[t] * L[t] − GFon * GF25[t] * monP[t] + monKcat * monPAL[t],
    ∂t A[t] == monk1r * monPA[t] + monk5r * monPphosA[t] + monk4r * monPAL[t] + monk8r * monPphosAL[t] −
       monk1 * monP[t] * A[t] − monk4 * monPL[t] * A[t] − monk5 * monPphos[t] * A[t] − monk8 * monPphosL[t] * A[t] −
       monKcat * monPAL[t] − monKcatphos * monPphosAL[t] − monKcatautophos * monPA[t] + dimk1r * dimPA[t] +
       dimk5r * dimPphosA[t] + dimk4r * dimPAL[t] + dimk8r * dimPphosAL[t] − dimk1 * dimP[t] * A[t] −
       dimk4 * dimPL[t] * A[t] − dimk5 * dimPphos[t] * A[t] − dimk8 * dimPphosL[t] * A[t] − dimKcat * dimPAL[t] −
       dimKcatphos * dimPphosAL[t] − dimKcatautophos * dimPA[t],
    ∂t L[t] == monk2r * monPL[t] + monk3r * monPAL[t] + monk6r * monPphosL[t] + monk7r * monPphosAL[t] −
       monk2 * monP[t] * L[t] − monk3 * monPA[t] * L[t] − monk6 * monPphos[t] * L[t] − monk7 * monPphosA[t] * L[t] +
       dimk2r * dimPL[t] + dimk3r * dimPAL[t] + dimk6r * dimPphosL[t] + dimk7r * dimPphosAL[t] +
       ((dimVmaxPEPdephos * Lphos[t]) / (dimKmPEPdephos + Lphos[t])) − dimk2 * dimP[t] * L[t] − dimk3 * dimPA[t] * L[t] −
       dimk6 * dimPphos[t] * L[t] − dimk7 * dimPphosA[t] * L[t],
    ∂t monPA[t] == monk1 * monP[t] * A[t] + monk3r * monPAL[t] +
       ((monVmaxPdephos * monPphosA[t]) / (monKmPdephos + monPphosA[t])) − monk1r * monPA[t] −
       monk3 * monPA[t] * L[t] − monKcatautophos * monPA[t] + GFoff * dimPA[t] − GFon * monPA[t] * GF25[t],
    ∂t monPL[t] == monk2 * monP[t] * L[t] + monk4r * monPAL[t] +
       ((monVmaxPdephos * monPphosL[t]) / (monKmPdephos + monPphosL[t])) − monk2r * monPL[t] −
       monk4 * monPL[t] * A[t] + GFoff * dimPL[t] − GFon * monPL[t] * GF25[t],
    ∂t monPAL[t] == monk3 * monPA[t] * L[t] + monk4 * monPL[t] * A[t] +
       ((monVmaxPdephos * monPphosAL[t]) / (monKmPdephos + monPphosAL[t])) − monk3r * monPAL[t] −
       monk4r * monPAL[t] − monKcat * monPAL[t] − GFon * monPAL[t] * GF25[t] + GFoff * dimPAL[t],
    ∂t monPphos[t] == monk5r * monPphosA[t] + monk6r * monPphosL[t] + monKcatautophos * monPA[t] −
       monk5 * monPphos[t] * A[t] − monk6 * monPphos[t] * L[t] −
       ((monVmaxPdephos * monPphos[t]) / (monKmPdephos + monPphos[t])) + monKcatphos * monPphosAL[t] +
       GFoff * dimPphos[t] − GFon * GF25[t] * monPphos[t],
    ∂t monPphosA[t] == monk5 * monPphos[t] * A[t] + monk7r * monPphosAL[t] − monk5r * monPphosA[t] −
       monk7 * monPphosA[t] * L[t] − ((monVmaxPdephos * monPphosA[t]) / (monKmPdephos + monPphosA[t])) +
       GFoff * dimPphosA[t] − GFon * GF25[t] * monPphosA[t],
    ∂t monPphosL[t] == monk6 * monPphos[t] * L[t] + monk8r * monPphosAL[t] − monk6r * monPphosL[t] −
       monk8 * monPphosL[t] * A[t] − ((monVmaxPdephos * monPphosL[t]) / (monKmPdephos + monPphosL[t])) +
       GFoff * dimPphosL[t] − GFon * GF25[t] * monPphosL[t],
    ∂t monPphosAL[t] == monk8 * monPphosL[t] * A[t] + monk7 * monPphosA[t] * L[t] − monk7r * monPphosAL[t] −
       monk8r * monPphosAL[t] − monKcatphos * monPphosAL[t] −
       ((monVmaxPdephos * monPphosAL[t]) / (monKmPdephos + monPphosAL[t])) + GFoff * dimPphosAL[t] −
       GFon * GF25[t] * monPphosAL[t],
    ∂t monPpTot[t] == ∂t monPphos[t] + ∂t monPphosA[t] + ∂t monPphosL[t] + ∂t monPphosAL[t],
    ∂t Lphos[t] == monKcat * monPAL[t] + monKcatphos * monPphosAL[t] −
       ((VmaxPEPdephos * Lphos[t]) / (KmPEPdephos + Lphos[t])) + dimKcat * dimPAL[t] + dimKcatphos * dimPphosAL[t],
    ∂t dimP[t] == dimk1r * dimPA[t] + dimk2r * dimPL[t] + ((dimVmaxPdephos * dimPphos[t]) / (dimKmPdephos + dimPphos[t])) −
       dimk1 * A[t] * dimP[t] − dimk2 * L[t] * dimP[t] + dimKcat * dimPAL[t] + GFon * monP[t] * GF25[t] − GFoff * dimP[t],
    ∂t dimPA[t] == dimk1 * dimP[t] * A[t] + dimk3r * dimPAL[t] +
       ((dimVmaxPdephos * dimPphosA[t]) / (dimKmPdephos + dimPphosA[t])) − dimk1r * dimPA[t] − dimk3 * dimPA[t] * L[t] −
       dimKcatautophos * dimPA[t] + GFon * monPA[t] * GF25[t] − GFoff * dimPA[t],
    ∂t dimPL[t] == dimk2 * dimP[t] * L[t] + dimk4r * dimPAL[t] +
       ((dimVmaxPdephos * dimPphosL[t]) / (dimKmPdephos + dimPphosL[t])) − dimk2r * dimPL[t] − dimk4 * dimPL[t] * A[t] +
       GFon * monPL[t] * GF25[t] − GFoff * dimPL[t],
```

```
    ∂t dimPAL[t] == dimk3 * dimPA[t] * L[t] + dimk4 * dimPL[t] * A[t] +
      ((dimVmaxPdephos * dimPphosAL[t]) / (dimKmPdephos + dimPphosAL[t])) - dimk3r * dimPAL[t] -
      dimk4r * dimPAL[t] - dimKcat * dimPAL[t] + GFon * monPAL[t] * GF25[t] - GFoff * dimPAL[t],
    ∂t dimPphos[t] == dimk5r * dimPphosA[t] + dimk6r * dimPphosL[t] + dimKcatautophos * dimPA[t] -
      dimk5 * dimPphos[t] * A[t] - dimk6 * dimPphos[t] * L[t] - ((dimVmaxPdephos * dimPphos[t]) / (dimKmPdephos + dimPphos[t])) +
      dimKcatphos * dimPphosAL[t] + GFon * monPphos[t] * GF25[t] - GFoff * dimPphos[t],
    ∂t dimPphosA[t] == dimk5 * dimPphos[t] * A[t] + dimk7r * dimPphosAL[t] - dimk5r * dimPphosA[t] -
      dimk7 * dimPphosA[t] * L[t] - ((dimVmaxPdephos * dimPphosA[t]) / (dimKmPdephos + dimPphosA[t])) +
      GFon * monPphosA[t] * GF25[t] - GFoff * dimPphosA[t],
    ∂t dimPphosL[t] == dimk6 * dimPphos[t] * L[t] + dimk8r * dimPphosAL[t] - dimk6r * dimPphosL[t] -
      dimk8 * dimPphosL[t] * A[t] - ((dimVmaxPdephos * dimPphosL[t]) / (dimKmPdephos + dimPphosL[t])) +
      GFon * monPphosL[t] * GF25[t] - GFoff * dimPphosL[t],
    ∂t dimPphosAL[t] == dimk8 * dimPphosL[t] * A[t] + dimk7 * dimPphosA[t] * L[t] - dimk7r * dimPphosAL[t] -
      dimk8r * dimPphosAL[t] - dimKcatphos * dimPphosAL[t] -
      ((dimVmaxPdephos * dimPphosAL[t]) / (dimKmPdephos + dimPphosAL[t])) + GFon * monPphosAL[t] * GF25[t] -
      GFoff * dimPphosAL[t],
    ∂t dimPpTot[t] == ∂t dimPphos[t] + ∂t dimPphosA[t] + ∂t dimPphosL[t] + ∂t dimPphosAL[t],
    ∂t dimerMET[t] == ∂t dimP[t] + ∂t dimPA[t] + ∂t dimPL[t] + ∂t dimPAL[t] + ∂t dimPphos[t] + ∂t dimPphosA[t] +
      ∂t dimPphosL[t] + ∂t dimPphosAL[t],
    ∂t monomerMET[t] == ∂t monP[t] + ∂t monPA[t] + ∂t monPL[t] + ∂t monPAL[t] + ∂t monPphos[t] + ∂t monPphosA[t] +
      ∂t monPphosL[t] + ∂t monPphosAL[t],
    dimP[0] == 0, A[0] == 1000, L[0] == 3, dimPA[0] == 0, dimPL[0] == 0, dimPAL[0] == 0, dimPphos[0] == 0,
    dimPphosA[0] == 0, dimPphosL[0] == 0, dimPphosAL[0] == 0, dimPpTot[0] == 0, Lphos[0] == 0, monP[0] == 1,
    monPA[0] == 0, monPL[0] == 0, monPAL[0] == 0, monPphos[0] == 0, monPphosA[0] == 0, monPphosL[0] == 0,
    monPphosAL[0] == 0, monPpTot[0] == 0, monomerMET[0] == 1, dimerMET[0] == 0},
   {dimP, A, L, dimPA, dimPL, dimPAL, dimPphos, dimPphosA, dimPphosL, dimPphosAL, dimPpTot, Lphos, monP,
    monPA, monPL, monPAL, monPphos, monPphosA, monPphosL, monPphosAL, monPpTot, monomerMET, dimerMET},
   {t, 0, 2000}, MaxSteps → 10000]

ndsolutioncombined0 =
  NDSolve[
   {∂t monP[t] == monk1r * monPA[t] + monk2r * monPL[t] + ((monVmaxPdephos * monPphos[t]) / (monKmPdephos + monPphos[t])) +
      GFoff * dimP[t] - monk1 * A[t] * monP[t] - monk2 * monP[t] * L[t] - GFon * GF0 * monP[t] + monKcat * monPAL[t],
    ∂t A[t] == monk1r * monPA[t] + monk5r * monPphosA[t] + monk4r * monPAL[t] + monk8r * monPphosAL[t] -
      monk1 * monP[t] * A[t] - monk4 * monPL[t] * A[t] - monk5 * monPphos[t] * A[t] - monk8 * monPphosL[t] * A[t] -
      monKcat * monPAL[t] - monKcatphos * monPphosAL[t] - monKcatautophos * monPA[t] + dimk1r * dimPA[t] +
      dimk5r * dimPphosA[t] + dimk4r * dimPAL[t] + dimk8r * dimPphosAL[t] - dimk1 * dimP[t] * A[t] -
      dimk4 * dimPL[t] * A[t] - dimk5 * dimPphos[t] * A[t] - dimk8 * dimPphosL[t] * A[t] - dimKcat * dimPAL[t] -
      dimKcatphos * dimPphosAL[t] - dimKcatautophos * dimPA[t],
    ∂t L[t] == monk2r * monPL[t] + monk3r * monPAL[t] + monk6r * monPphosL[t] + monk7r * monPphosAL[t] -
      monk2 * monP[t] * L[t] - monk3 * monPA[t] * L[t] - monk6 * monPphos[t] * L[t] - monk7 * monPphosA[t] * L[t] +
      dimk2r * dimPL[t] + dimk3r * dimPAL[t] + dimk6r * dimPphosL[t] + dimk7r * dimPphosAL[t] +
      ((dimVmaxPEPdephos * Lphos[t]) / (dimKmPEPdephos + Lphos[t])) - dimk2 * dimP[t] * L[t] - dimk3 * dimPA[t] * L[t] -
      dimk6 * dimPphos[t] * L[t] - dimk7 * dimPphosA[t] * L[t],
    ∂t monPA[t] == monk1 * monP[t] * A[t] + monk3r * monPAL[t] +
      ((monVmaxPdephos * monPphosA[t]) / (monKmPdephos + monPphosA[t])) - monk1r * monPA[t] -
      monk3 * monPA[t] * L[t] - monKcatautophos * monPA[t] + GFoff * dimPA[t] - GFon * monPA[t] * GF0,
```

$$\partial_t \text{monPL}[t] == \text{monk2} * \text{monP}[t] * \text{L}[t] + \text{monk4r} * \text{monPAL}[t] + ((\text{monVmaxPdephos} * \text{monPphosL}[t]) / (\text{monKmPdephos} + \text{monPphosL}[t])) - \text{monk2r} * \text{monPL}[t] - \text{monk4} * \text{monPL}[t] * \text{A}[t] + \text{GFoff} * \text{dimPL}[t] - \text{GFon} * \text{monPL}[t] * \text{GF0},$$

$$\partial_t \text{monPAL}[t] == \text{monk3} * \text{monPA}[t] * \text{L}[t] + \text{monk4} * \text{monPL}[t] * \text{A}[t] + ((\text{monVmaxPdephos} * \text{monPphosAL}[t]) / (\text{monKmPdephos} + \text{monPphosAL}[t])) - \text{monk3r} * \text{monPAL}[t] - \text{monk4r} * \text{monPAL}[t] - \text{monKcat} * \text{monPAL}[t] - \text{GFon} * \text{monPAL}[t] * \text{GF0} + \text{GFoff} * \text{dimPAL}[t],$$

$$\partial_t \text{monPphos}[t] == \text{monk5r} * \text{monPphosA}[t] + \text{monk6r} * \text{monPphosL}[t] + \text{monKcatautophos} * \text{monPA}[t] - \text{monk5} * \text{monPphos}[t] * \text{A}[t] - \text{monk6} * \text{monPphos}[t] * \text{L}[t] - ((\text{monVmaxPdephos} * \text{monPphos}[t]) / (\text{monKmPdephos} + \text{monPphos}[t])) + \text{monKcatphos} * \text{monPphosAL}[t] + \text{GFoff} * \text{dimPphos}[t] - \text{GFon} * \text{GF0} * \text{monPphos}[t],$$

$$\partial_t \text{monPphosA}[t] == \text{monk5} * \text{monPphos}[t] * \text{A}[t] + \text{monk7r} * \text{monPphosAL}[t] - \text{monk5r} * \text{monPphosA}[t] - \text{monk7} * \text{monPphosA}[t] * \text{L}[t] - ((\text{monVmaxPdephos} * \text{monPphosA}[t]) / (\text{monKmPdephos} + \text{monPphosA}[t])) + \text{GFoff} * \text{dimPphosA}[t] - \text{GFon} * \text{GF0} * \text{monPphosA}[t],$$

$$\partial_t \text{monPphosL}[t] == \text{monk6} * \text{monPphos}[t] * \text{L}[t] + \text{monk8r} * \text{monPphosAL}[t] - \text{monk6r} * \text{monPphosL}[t] - \text{monk8} * \text{monPphosL}[t] * \text{A}[t] - ((\text{monVmaxPdephos} * \text{monPphosL}[t]) / (\text{monKmPdephos} + \text{monPphosL}[t])) + \text{GFoff} * \text{dimPphosL}[t] - \text{GFon} * \text{GF0} * \text{monPphosL}[t],$$

$$\partial_t \text{monPphosAL}[t] == \text{monk8} * \text{monPphosL}[t] * \text{A}[t] + \text{monk7} * \text{monPphosA}[t] * \text{L}[t] - \text{monk7r} * \text{monPphosAL}[t] - \text{monk8r} * \text{monPphosAL}[t] - \text{monKcatphos} * \text{monPphosAL}[t] - ((\text{monVmaxPdephos} * \text{monPphosAL}[t]) / (\text{monKmPdephos} + \text{monPphosAL}[t])) + \text{GFoff} * \text{dimPphosAL}[t] - \text{GFon} * \text{GF0} * \text{monPphosAL}[t],$$

$$\partial_t \text{monPpTot}[t] == \partial_t \text{monPphos}[t] + \partial_t \text{monPphosA}[t] + \partial_t \text{monPphosL}[t] + \partial_t \text{monPphosAL}[t],$$

$$\partial_t \text{Lphos}[t] == \text{monKcat} * \text{monPAL}[t] + \text{monKcatphos} * \text{monPphosAL}[t] - ((\text{VmaxPEPdephos} * \text{Lphos}[t]) / (\text{KmPEPdephos} + \text{Lphos}[t])) + \text{dimKcat} * \text{dimPAL}[t] + \text{dimKcatphos} * \text{dimPphosAL}[t],$$

$$\partial_t \text{dimP}[t] == \text{dimk1r} * \text{dimPA}[t] + \text{dimk2r} * \text{dimPL}[t] + ((\text{dimVmaxPdephos} * \text{dimPphos}[t]) / (\text{dimKmPdephos} + \text{dimPphos}[t])) - \text{dimk1} * \text{A}[t] * \text{dimP}[t] - \text{dimk2} * \text{L}[t] * \text{dimP}[t] + \text{dimKcat} * \text{dimPAL}[t] + \text{GFon} * \text{monP}[t] * \text{GF0} - \text{GFoff} * \text{dimP}[t],$$

$$\partial_t \text{dimPA}[t] == \text{dimk1} * \text{dimP}[t] * \text{A}[t] + \text{dimk3r} * \text{dimPAL}[t] + ((\text{dimVmaxPdephos} * \text{dimPphosA}[t]) / (\text{dimKmPdephos} + \text{dimPphosA}[t])) - \text{dimk1r} * \text{dimPA}[t] - \text{dimk3} * \text{dimPA}[t] * \text{L}[t] - \text{dimKcatautophos} * \text{dimPA}[t] + \text{GFon} * \text{monPA}[t] * \text{GF0} - \text{GFoff} * \text{dimPA}[t],$$

$$\partial_t \text{dimPL}[t] == \text{dimk2} * \text{dimP}[t] * \text{L}[t] + \text{dimk4r} * \text{dimPAL}[t] + ((\text{dimVmaxPdephos} * \text{dimPphosL}[t]) / (\text{dimKmPdephos} + \text{dimPphosL}[t])) - \text{dimk2r} * \text{dimPL}[t] - \text{dimk4} * \text{dimPL}[t] * \text{A}[t] + \text{GFon} * \text{monPL}[t] * \text{GF0} - \text{GFoff} * \text{dimPL}[t],$$

$$\partial_t \text{dimPAL}[t] == \text{dimk3} * \text{dimPA}[t] * \text{L}[t] + \text{dimk4} * \text{dimPL}[t] * \text{A}[t] + ((\text{dimVmaxPdephos} * \text{dimPphosAL}[t]) / (\text{dimKmPdephos} + \text{dimPphosAL}[t])) - \text{dimk3r} * \text{dimPAL}[t] - \text{dimk4r} * \text{dimPAL}[t] - \text{dimKcat} * \text{dimPAL}[t] + \text{GFon} * \text{monPAL}[t] * \text{GF0} - \text{GFoff} * \text{dimPAL}[t],$$

$$\partial_t \text{dimPphos}[t] == \text{dimk5r} * \text{dimPphosA}[t] + \text{dimk6r} * \text{dimPphosL}[t] + \text{dimKcatautophos} * \text{dimPA}[t] - \text{dimk5} * \text{dimPphos}[t] * \text{A}[t] - \text{dimk6} * \text{dimPphos}[t] * \text{L}[t] - ((\text{dimVmaxPdephos} * \text{dimPphos}[t]) / (\text{dimKmPdephos} + \text{dimPphos}[t])) + \text{dimKcatphos} * \text{dimPphosAL}[t] + \text{GFon} * \text{monPphos}[t] * \text{GF0} - \text{GFoff} * \text{dimPphos}[t],$$

$$\partial_t \text{dimPphosA}[t] == \text{dimk5} * \text{dimPphos}[t] * \text{A}[t] + \text{dimk7r} * \text{dimPphosAL}[t] - \text{dimk5r} * \text{dimPphosA}[t] - \text{dimk7} * \text{dimPphosA}[t] * \text{L}[t] - ((\text{dimVmaxPdephos} * \text{dimPphosA}[t]) / (\text{dimKmPdephos} + \text{dimPphosA}[t])) + \text{GFon} * \text{monPphosA}[t] * \text{GF0} - \text{GFoff} * \text{dimPphosA}[t],$$

$$\partial_t \text{dimPphosL}[t] == \text{dimk6} * \text{dimPphos}[t] * \text{L}[t] + \text{dimk8r} * \text{dimPphosAL}[t] - \text{dimk6r} * \text{dimPphosL}[t] - \text{dimk8} * \text{dimPphosL}[t] * \text{A}[t] - ((\text{dimVmaxPdephos} * \text{dimPphosL}[t]) / (\text{dimKmPdephos} + \text{dimPphosL}[t])) + \text{GFon} * \text{monPphosL}[t] * \text{GF0} - \text{GFoff} * \text{dimPphosL}[t],$$

$$\partial_t \text{dimPphosAL}[t] == \text{dimk8} * \text{dimPphosL}[t] * \text{A}[t] + \text{dimk7} * \text{dimPphosA}[t] * \text{L}[t] - \text{dimk7r} * \text{dimPphosAL}[t] - \text{dimk8r} * \text{dimPphosAL}[t] - \text{dimKcatphos} * \text{dimPphosAL}[t] - ((\text{dimVmaxPdephos} * \text{dimPphosAL}[t]) / (\text{dimKmPdephos} + \text{dimPphosAL}[t])) + \text{GFon} * \text{monPphosAL}[t] * \text{GF0} - \text{GFoff} * \text{dimPphosAL}[t],$$

```
    ∂t dimPpTot[t] == ∂t dimPphos[t] + ∂t dimPphosA[t] + ∂t dimPphosL[t] + ∂t dimPphosAL[t],
    ∂t dimerMET[t] == ∂t dimP[t] + ∂t dimPA[t] + ∂t dimPL[t] + ∂t dimPAL[t] + ∂t dimPphos[t] + ∂t dimPphosA[t] +
      ∂t dimPphosL[t] + ∂t dimPphosAL[t],
    ∂t monomerMET[t] == ∂t monP[t] + ∂t monPA[t] + ∂t monPL[t] + ∂t monPAL[t] + ∂t monPphos[t] + ∂t monPphosA[t] +
      ∂t monPphosL[t] + ∂t monPphosAL[t],
    dimP[0] == 0, A[0] == 1000, L[0] == 3, dimPA[0] == 0, dimPL[0] == 0, dimPAL[0] == 0, dimPphos[0] == 0,
    dimPphosA[0] == 0, dimPphosL[0] == 0, dimPphosAL[0] == 0, dimPpTot[0] == 0, Lphos[0] == 0, monP[0] == 1,
    monPA[0] == 0, monPL[0] == 0, monPAL[0] == 0, monPphos[0] == 0, monPphosA[0] == 0, monPphosL[0] == 0,
    monPphosAL[0] == 0, monPpTot[0] == 0, monomerMET[0] == 1, dimerMET[0] == 0},
  {dimP, A, L, dimPA, dimPL, dimPAL, dimPphos, dimPphosA, dimPphosL, dimPphosAL, dimPpTot, Lphos, monP,
    monPA, monPL, monPAL, monPphos, monPphosA, monPphosL, monPphosAL, monPpTot, monomerMET, dimerMET},
  {t, 0, 2000}, MaxSteps → 10000]

Plot[{mon[t], dim[t]}, {t, 0, 1000}, PlotStyle → {RGBColor[1, 0, 0], RGBColor[0, 1, 0]}, PlotRange → {{0, 1000}, {−0.10, 1.1}},
  Frame → True,
  PlotLabel → StyleForm[StyleForm["Monomer", FontColor → RGBColor[1, 0, 0]] StyleForm["Dimer", FontColor → RGBColor[0, 1, 0]]]]
```

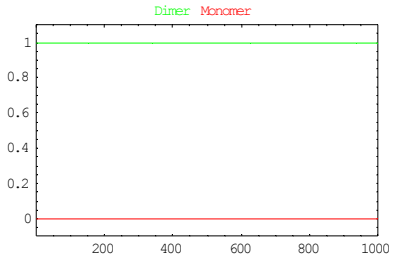


```
Plot[{GF[t], GF75[t], GF50[t], GF25[t]}, {t, 0, 1000},
  PlotStyle → {RGBColor[1, 0, 0], RGBColor[0, 1, 0], RGBColor[0, 0, 1], RGBColor[1, 0, 1]}, PlotRange → {{775, 825}, {−0.0010, .11}},
  PlotLabel → StyleForm["GF 100%", FontColor → RGBColor[1, 0, 0]] StyleForm["GF 75%", FontColor → RGBColor[0, 1, 0]]
    StyleForm["GF 50% ", FontColor → RGBColor[0, 0, 1]] StyleForm["GF 25%", FontColor → RGBColor[1, 0, 1]]]
```

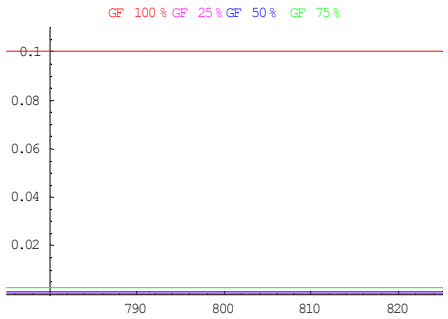

```
METPphosTot = {monPpTot[t] /. ndsolutioncombined};
TPRMETPphosTot = {dimPpTot[t] /. ndsolutioncombined};
TPRMETtotal = {dimerMET[t] /. ndsolutioncombined};
cytoMETtotal = {monomerMET[t] /. ndsolutioncombined};
ATP = {A[t] /. ndsolutioncombined};
Tyr = {L[t] /. ndsolutioncombined};
METfree = {monP[t] /. ndsolutioncombined};
METATP = {monPA[t] /. ndsolutioncombined};
METTyr = {monPL[t] /. ndsolutioncombined};
METTyrATP = {monPAL[t] /. ndsolutioncombined};
pMET = {monPphos[t] /. ndsolutioncombined};
pMETATP = {monPphosA[t] /. ndsolutioncombined};
pMETTyr = {monPphosL[t] /. ndsolutioncombined};
pMETTyrATP = {monPphosAL[t] /. ndsolutioncombined};
TPRMETfree = {dimP[t] /. ndsolutioncombined};
TPRMETATP = {dimPA[t] /. ndsolutioncombined};
TPRMETTyr = {dimPL[t] /. ndsolutioncombined};
TPRMETTyrATP = {dimPAL[t] /. ndsolutioncombined};
pTPRMET = {dimPphos[t] /. ndsolutioncombined};
pTPRMETATP = {dimPphosA[t] /. ndsolutioncombined};
pTPRMETTyr = {dimPphosL[t] /. ndsolutioncombined};
pTPRMETTyrATP = {dimPphosAL[t] /. ndsolutioncombined};
pTyr = {Lphos[t] /. ndsolutioncombined};
METPphosTot75 = {monPpTot[t] /. ndsolutioncombined75};
TPRMETPphosTot75 = {dimPpTot[t] /. ndsolutioncombined75};
TPRMETtotal75 = {dimerMET[t] /. ndsolutioncombined75};
cytoMETtotal75 = {monomerMET[t] /. ndsolutioncombined75};
pTyr75 = {Lphos[t] /. ndsolutioncombined75};
METPphosTot50 = {monPpTot[t] /. ndsolutioncombined50};
TPRMETPphosTot50 = {dimPpTot[t] /. ndsolutioncombined50};
TPRMETtotal50 = {dimerMET[t] /. ndsolutioncombined50};
cytoMETtotal50 = {monomerMET[t] /. ndsolutioncombined50};
pTyr50 = {Lphos[t] /. ndsolutioncombined50};
METPphosTot25 = {monPpTot[t] /. ndsolutioncombined25};
TPRMETPphosTot25 = {dimPpTot[t] /. ndsolutioncombined25};
TPRMETtotal25 = {dimerMET[t] /. ndsolutioncombined25};
cytoMETtotal25 = {monomerMET[t] /. ndsolutioncombined25};
pTyr25 = {Lphos[t] /. ndsolutioncombined25};
METPphosTot0 = {monPpTot[t] /. ndsolutioncombined0};
TPRMETPphosTot0 = {dimPpTot[t] /. ndsolutioncombined0};
TPRMETtotal0 = {dimerMET[t] /. ndsolutioncombined0};
cytoMETtotal0 = {monomerMET[t] /. ndsolutioncombined0};
pTyr0 = {Lphos[t] /. ndsolutioncombined0};
```

```
Plot[{TPRMETPphosTot0, TPRMETPphosTot, TPRMETPphosTot75, TPRMETPphosTot50}, {t, 0, 1000},
  PlotRange → {{0, 600}, {−.05, 1}}, Frame → True]
```

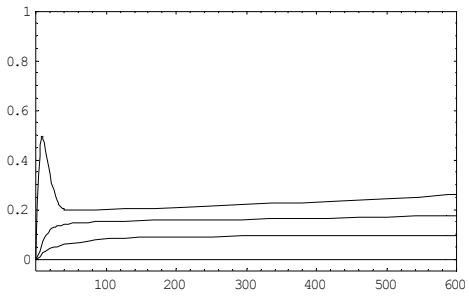


```
Plot[{pTyr, pTyr75, pTyr50, pTyr0}, {t, 0, 2000}, PlotRange → {{0, 600}, {−0.0001, .015}}, Frame → True]
```

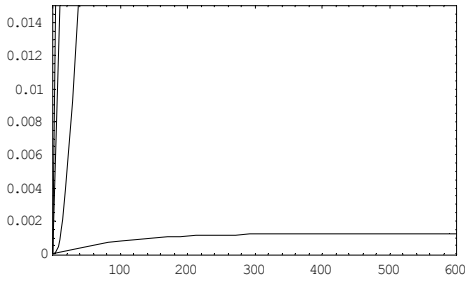


```
Plot[{pTPRMETTyrATP, TPRMETTyrATP}, {t, 0, 2000}, PlotRange → {{0, 800}, {0, .5}}, Frame → True]
```

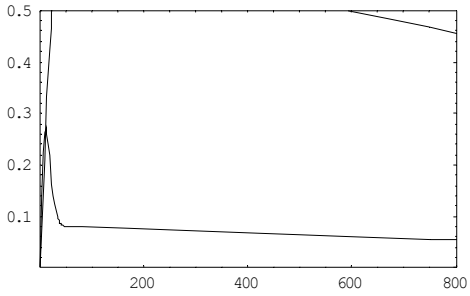

APPENDIX C

PARAMETER SENSITIVITY ANALYSES

Sensitivity analyses provide valuable information at understanding the behavior of the system being modeled. In order to probe the effects of individual parameters on the overall c-MET activation, we performed detailed sensitivity analyses for three different parameters (the autophosphorylation k_{cat}, the dephosphorylation V_{max} and substrate phosphorylation k_{cat}). The analyses were carried out for ligand-stimulated dimeric c-MET and unstimulated monomeric c-MET for comparison. For the analyses, for each parameter, a value range was defined and for different values within the range, the c-MET activation output (the buildup of phosphorylated c-MET (pMET) and Tyr (pTyr)) was measured. In absence of ligand stimulus, the c-MET activation output showed sensitivity to the changes in the monomer autophosphorylation k_{cat} **(Fig. AC.2**). However, the levels of buildup of pTyr and pMET seen in the parameter range defined (0 to 0.8) were yet several fold lower (~100-fold lower for k_{cat} autophosphorylation (monomer)= 0.8, which is 100 fold higher than the estimated monomer autophosphorylation k_{cat} = 0.08) than that for the stimulated dimeric c-MET **(Figs. AC.1 and AC.2**). Thus, changes to autophosphorylation $k_{cat,,}$ unless 100-fold or more, would not render monomeric c-MET to signal comparable to the dimeric c-MET. c-MET activation, in presence of ligand, was highly sensitive to the autophosphorylation k_{cat} of the dimeric c-MET (**Fig. AC.2**). Similar effects on c-MET activation response were seen by varying the dephosphorylation V_{max}. While, the dimeric stimulated c-MET was very sensitive to the PTP-catalyzed dephosphorylation parameters, not a significant difference in the overall levels of buildup of pMET and pTyr were seen if the corresponding parameter for the monomeric c-MET was varied **(Figs. AC.1 and AC.2**). Varying the substrate phosphorylation k_{cat} showed that this parameter was important for pTyr buildup and the dimeric c-MET showed high sensitivity to this parameter for c-MET activation. These analyses indicated that the parameters in the dimeric (ligand-stimulated) c-MET

are optimized to provide maximum sensitivity and output. However, the monomer parameters are tuned in a way such that changes to individual parameters are optimized to minimize sensitivity and output.

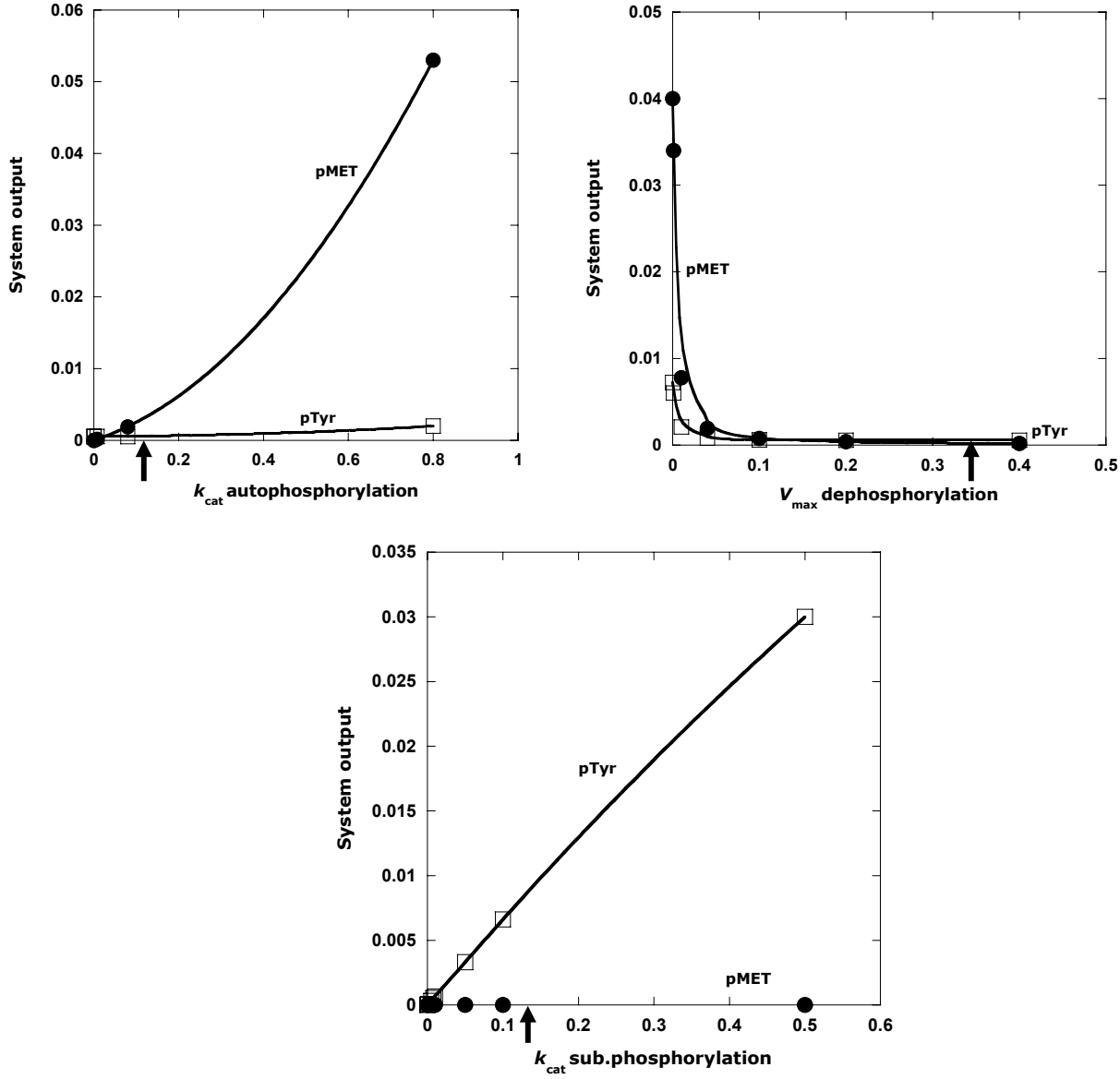

Fig. AC.1. Parameter Sensitivity Analyses on unstimulated monomeric c-MET.
Shown are the effects of varying k_{cat} autophosphorylation (top left), V_{max} dephosphorylation (top right) and k_{cat} substrate phosphorylation (bottom) on the output from unstimulated c-MET. Although varying these parameters render increased c-MET activation in absence of ligand, the levels of pMET and pTyr generated are significantly lower that the levels seen in presence of the

stimulated c-MET (Fig. AC.2). The parameter values that were used for the monomeric c-MET in the model are shown on X-axis.

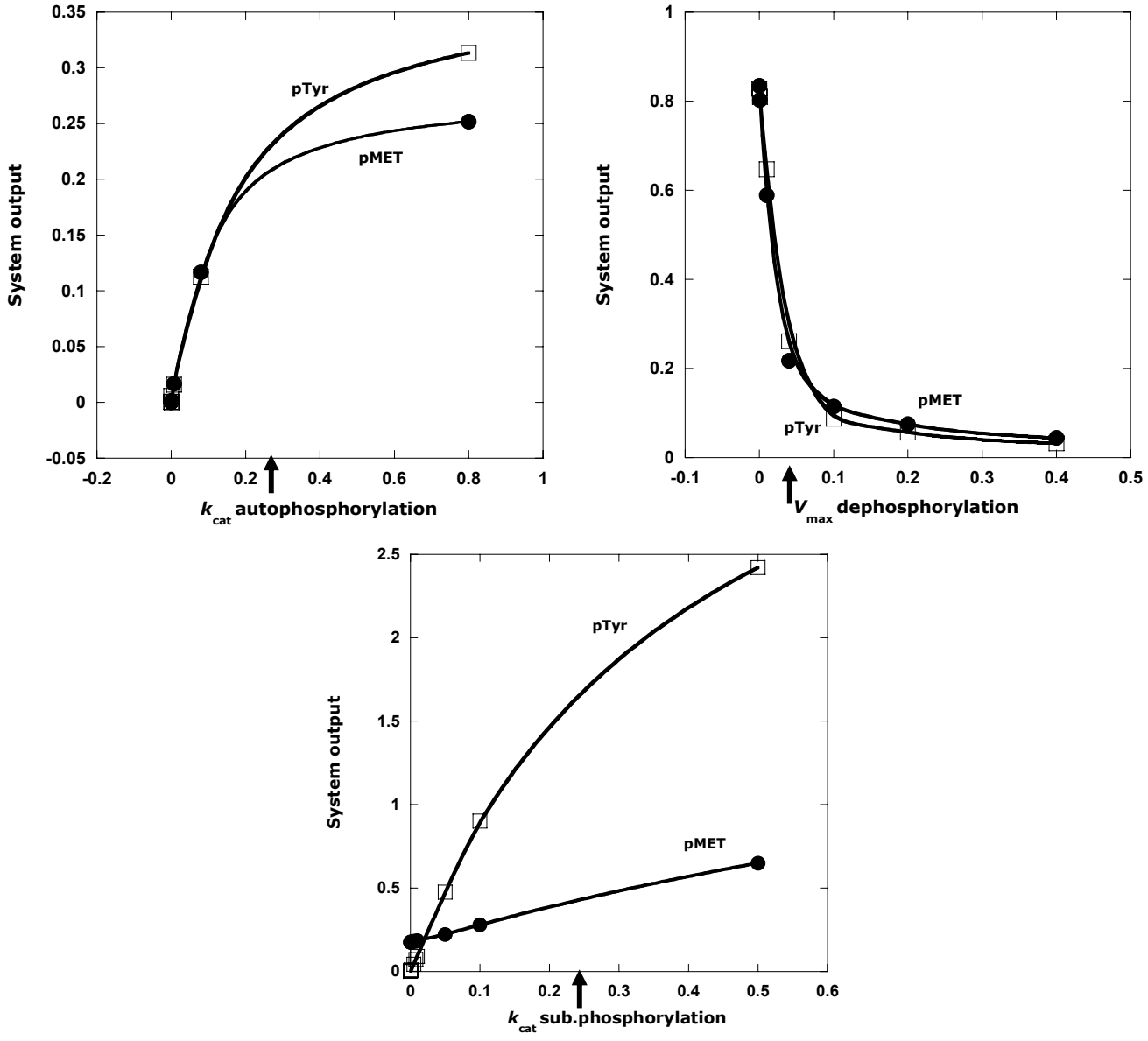

Fig. AC.2. Parameter Sensitivity Analyses on stimulated dimeric c-MET.
Shown are the effects of varying k_{cat} autophosphorylation (top left), V_{max} dephosphorylation (top right) and k_{cat} substrate phosphorylation (bottom) on the output from stimulated c-MET. The c-MET activation in presence of ligand is highly sensitive to changes in these parameters. The parameter values that were used for the monomeric c-MET in the model are shown on X-axis.

REFERENCES

Angeles TS, Yang SX, Steffler C, Dionne CA. 1998. Kinetics of trkA tyrosine kinase activity and inhibition by K-252a. Arch. Biochem. Biophys. 349(2):267-74.

Asthagiri AR, Lauffenburger DA. 2000. Bioengineering models of cell signaling. Annu. Rev. Biomed. Eng. 02:31-53.

Baer K, Al-Hasani H, Parvaresch S, Corona T, Rufer A, Nolle V, Bergschneider E, Klein HW. 2001. Dimerization-induced activation of soluble insulin/IGF-1 receptor kinases: an alternative mechanism of activation. Biochemistry 40(47):14268-78.

Basile JR, Afkhami T, Gutkind JS. 2005. Semaphorin 4D/plexin-B1 induces endothelial cell migration through activation of PYK2, Src, and the phosphatidylinositol 3-kinase-Akt pathway. Mol. Cell. Biol. 25(16):6889-6998.

Baxter RM, Secrist JP, Vaillancourt RR, Kazlauskas A. 1998. Full activation of the platelet-derived growth factor beta-receptor kinase involves multiple events. J. Biol. Chem. 273(27):17050-5.

Bertics PJ, Weber W, Cochet C, Gill GN. 1985. Regulation of the epidermal growth factor receptor by phosphorylation. J. Cell Biochem. 29(3):195-208.

Bertotti A, Comoglio PM. 2003. Tyrosine kinase signal specificity: lessons from the HGF receptor. Trends Biochem Sci 28(10):527-533.

Birchmeier C, Birchmeier W, Gherardi E, Vande Woude GF. 2003. Met, metastasis, motility and more. Nat. Rev. Mol. Cell Biol. 4:915-925.

Biswas R, Basu M, Sen-Majumdar A, Das M. 1985. Intrapeptide autophosphorylation of the epidermal growth factor receptor: regulation of kinase catalytic function by receptor dimerization. Biochemistry 24(14):3795-802.

Bladt F, Riethmacher D, Isenmann S, Aguzzi A, Birchmeier C. 1995. Essential role for the c-MET receptor in the migration of myogenic precursor cells into the limb bud. Nature 376(6543):768-771.

Blume-Jensen P, Hunter T. 2001. Oncogenic kinase signaling. Nature 411(6835):355-65.

Boccaccio C, Ando M, Tamagnone L, Bardelli A, Michieli P, Battistini C, Comoglio PM. 1998. Induction of epithelial tubules by growth factor HGF depends on the STAT pathway. Nature 391(6664):285-288.

Bohmer FD, Bohmer A, Obermeier A, Ullrich A. 1995. Use of selective tyrosine kinase blockers to monitor growth factor receptor dephosphorylation in intact cells. Anal. Biochem. 228:267-273.

Bork P, Doerks T, Springer TA, Snel B. 1999. Domains in plexins: links to integrins and transcription factors. Trends Biochem Sci 24:261-63.

Bottaro DB, Rubin JS, Faletto DL, Chan AM, Kmeicik TE, Vande Woude GF, Aaronson SA. 1992. Identification of the hepatocyte growth factor receptor as the c-met proto-oncogene product. *Science* 251:802-804.

Burridge K, Nelson A. 1995. An in-gel assay for protein tyrosine phosphatase activity: detection of widespread distribution in cells and tissues. Anal. Chem. 232:56-64.

Campbell SL, Khosravi-Far R, Rossman KL, Clark GJ, Der CJ. 1998. Increasing complexity of Ras signaling. Oncogene 17(11):1395-1413.

Carrollo M, Giordano S, Cabrita-Santos L, Corso S, Vigario AM, Silva S, Leiriao P, Carapau D, Armas-Portela R, Comoglio PM and others. 2003. Hepatocyte growth factor and its receptor are required for malaria infection. Nat. Med. 9(11):1363-1369.

Cheng K, Koland JG. 1996. Nucleotide binding by the epidermal growth factor receptor protein-tyrosine kinase. Trinitrophenyl-ATP as a spectroscopic probe. J. Biol. Chem. 271(1):311-8.

Cho H, Krishnaraj R, Itoh M, Kitas E, Bannwarth W, Saito H, Walsh CT. 1993. Substrate specificities of catalytic fragments of protein tyrosine phosphatases (HPTPb, LAR, and CD45) towards phosphotyrosylpeptide substrates and thiophosphotyrosylated peptides as inhibitors. Protein Sci. 2:977-984.

Churin Y, Al-Ghoul L, Kepp O, Meyer TF, Birchmeier W, Naumann M. 2003. Helicobacter pylori CagA protein targets the c-MET receptor and enhances the motogenic response. J. Cell Biol. 161(2):249-55.

Cobb MH, Sang BC, Gonzalez R, Goldsmith E, Ellis L. 1989. Autophosphorylation activates the soluble cytoplasmic domain of the insulin receptor in an intermolecular reaction. J. Biol. Chem. 264(31):18701-18706.

Cooper CS, Park M, Blair DG, Tainsky MA, Huebner K, Croce CM, Vande Woude GF. 1984. Molecular cloning of a new transforming gene from a chemically transformed human cell line. Nature 311(5981):29-33.

Danilkovitch-Miagkova A, Zbar B. 2002. Dysregulation of Met receptor tyrosine kinase activity in invasive tumors. J. Clin. Invest. 109(7):863-867.

DiGabriele AD, Lax I, Chen DI, Svahn CM, Jaye M, Schlessinger J, Hendrickson WA. 1998. Structure of a heparin-linked biologically active dimer of fibroblast growth factor. Nature 393(6687):812-817.

Fischer EH, Krebs EG. 1955. Conversion of phosphorylase b to phosphorylase a in muscle extracts. J. Biol. Chem. 216(1):121-32.

Fukuda T, Ichimura E, Shinozaki T, Sano T, Kashiwabara K, Oyama T, Nakajima T, Nakamura T. 1998. Coexpression of HGF and c-MET/HGF receptor in human bone and soft tissue tumors. Pathol. Int. 48(10):757-762.

Gherardi E, Youles ME, Miguel RN, Blundell TL, Iamele L, Gough J, Bandyopadhyay A, Hartmann G, Butler PJ. 2003. Functional map and domain structure of MET, the product of the c-*met* proto-oncogene and receptor for hepatocyte growth factor/scatter factor. Proc. Natl. Acad. Sci. U S A 100(12):12039-12044.

Giordano S, Corso S, Conrotto P, Artigiani S, Gilestro G, Barberis D, Tamagnone L, Comoglio PM. 2002. The semaphorin 4D receptor controls invasive growth by coupling with Met. Nat Cell Biol. 4(9):720-724.

Graveel C, Su Y, Koeman J, Wang LM, Tessarollo L, Fiscella M, Birchmeier C, Swiatek P, Bronson R, Vande Woude G. 2004. Activating met mutations produce unique tumor profiles in mice with selective duplication of the mutant allele. Proc. Natl. Acad. Sci. U S A 101(49):17198-203.

Gu H, Neel BG. 2003. The "Gab" in signal transduction. Trends Cell Biol 13(3):122-30.

Gual P, Giordano S, Williams TA, Rocchi S, Van Obberghen E, Comoglio PM. 2000. Sustained recruitment of phospholipase C-gamma to Gab1 is required for HGF-induced branching tubulogenesis. Oncogene 19(12):1509-1518.

Hammond DE, Carter S, Clague ME. 2004. Met receptor dynamics and signaling. Curr Top Microbiol Immunol 286:21-44.

Hammond DE, Carter S, McCullough J, Urbe S, Vande Woude GF, Clague ME. 2003. Endosomal dynamics of met determines signaling output. Mol. Cell. Biol. 14(4):1346-54.

Hartmann G, Prospero T, Brinkmann V, Ozcelik C, Winter G, Hepple J, Batley S, Bladt F, Sachs M, Birchmeier C and others. 1998. Engineered mutants of HGF/SF with reduced binding to heparan sulfate proteoglycans, decreased clearance and enhanced activity in vivo. Curr Biol. 8(3):125-134.

Hays JL, Watowich SJ. 2003. Oligomerization-induced modulation of TPR-MET tyrosine kinase activity. J. Biol. Chem. 278(30):27456-27463.

Hays JL, Watowich SJ. 2004. Oligomerization-dependent changes in the thermodynamic properties of the TPR-MET receptor tyrosine kinase. Biochemistry 43:10570-10578.

Hendrix MJ, Seftor EA, Seftor RE, Kirschmann DA, Gardner LM, Boldt HC, Meyer M, Pe'er J, Folberg R. 1998. Regulation of uveal melanoma interconverted phenotype by hepatocyte growth factor/scatter factor (HGF/SF). Am. J. Pathol. 152(4):855-863.

Holgado-Madruga M, Emlet DR, Moscatello DK, Godwin AK, Wong AJ. 1996. A Grb2-associated docking protein in EGF- and insulin-receptor signaling. Nature 379(6565):560-564.

Hubbard SR. 1997. Crystal structure of the activated insulin receptor tyrosine kinase in complex with peptide substrate and ATP analog. EMBO J. 16(18):5572-81.

Hubbard SR, Mohammadi M, Schlessinger J. 1998. Autoregulatory mechanisms of protein-tyrosine kinases. J. Biol. Chem. 273(20):11987-90.

Hubbard SR, Till JH. 2000. Protein tyrosine kinase structure and function. Annu. Rev. Biochem. 69:373-398.

Hubbard SR, Wei L, Ellis L, Hendrickson WA. 1994. Crystal structure of the tyrosine kinase domain of the human insulin receptor. Nature 372(6508):746-54.

Huff JL, Jelinek MA, Borgman CA, Lansing TJ, Parsons JT. 1993. The proto-oncogene c-sea encodes a transmembrane protein-tyrosine kinase related to the Met/hepatocyte growth factor/scatter factor receptor. Proc. Natl. Acad. Sci. U S A 90(13):6140-6144.

Hunter T. 1997. Oncoprotein networks. Cell. 88(3):333-46.

Ireton K, Payrastre B, Cossart P. 1999. The *Listeria monocytogenes* protein InlB is an agonist of mammalian phosphoinositide 3-kinase. J. Biol. Chem. 274(24):17025-32.

Iwasaki Y, Nishiyama H, Suzuki K, Koizumi S. 1997. Sequential cis/trans autophosphorylation in TrkB tyrosine kinase. Biochemistry 36(9):2694-2700.

Jeffers M, Schmidt L, Nakaigawa N, Webb CP, Weirich G, Kishida T, Zbar B, Vande Woude GF. 1997. Activating mutations for the met tyrosine kinase receptor in human cancer. Proc. Natl. Acad. Sci. U S A 94(21):11445-50.

Kholodenko BN, Demin OV, Moehren G, Hoek JB. 1999. Quantification of short term signaling by epidermal growth factor receptor. J. Biol. Chem. 274(42):30169-81.

Khwaja A, Lehmann K, Marte BM, Downward J. 1998. Phosphoinositide 3-kinase induces scattering and tubulogenesis in epithelial cells through a novel pathway. J. Biol. Chem. 273(30):18793-18801.

Kohanski RA. 1993a. Insulin receptor autophosphorylation. I. Autophosphorylation kinetics of the native receptor and its cytoplasmic kinase domain. Biochemistry 32(22):5766-5772.

Kohanski RA. 1993b. Insulin receptor autophosphorylation. I. Autophosphorylation kinetics of the native receptor and its cytoplasmic kinase domain. Biochemistry 32(22):5766-72.

Koochekpour S, Jeffers M, Rulong S, Taylor G, Klineberg E, Hudson EA, Resau JH, Vande Woude GF. 1997. Met and hepatocyte growth factor/scatter factor expression in human gliomas. Cancer Res. 57(23):5391-5398.

Kozlov G, Perreault A, Schrag JD, Park M, Cygler M, Gehring K, Ekiel I. 2004. Insights into function of PSI domains from structure of the Met receptor PSI domain. Biochem Biophy Res Commun 321(1):234-40.

Kulas DT, Goldstein BJ, Mooney RA. 1996. The transmembrane protein-tyrosine phosphatase LAR modulates signaling by multiple receptor tyrosine kinases. J. Biol. Chem. 271(2):748-754.

Lee JH, Han SU, Cho H, Jennings B, Gerrard B, Dean M, Schmidt L, Zbar B, Vande Woude GF. 2000. A novel germ line juxtamembrane Met mutation in human gastric cancer. Oncogene 19(43):4947-4953.

Li N, Xiang GS, Dokainish H, Ireton K, Elferink LA. 2005. The Listeria protein InlB mimics hepatocyte growth factor-induced receptor trafficking. Traffic 6(6):459-473.

Lietha D, Chirgadze DY, Mulloy B, Blundell TL, Gherardi E. 2001. Crystal structure of NK1-heparin complexes reveal the basis for NK1 activity and enable engineering of potent agonists of the MET receptor. EMBO J. 20(20):5543-5555.

Lock LS, Royal I, Naujokas MA, Park M. 2000. Identification of an atypical Grb2 carboxy-terminal SH3 domain binding site in Gab docking proteins reveals Grb2-dependent and -independent recruitment of Gab1 to receptor tyrosine kinases. J. Biol. Chem. 275(40):31536-31545.

Lokker NA, Mark MR, Luis EA, Bennett GL, Robbins KA, Baker JB, Godowski PJ. 1992. Structure-function analysis of hepatocyte growth factor: identification of

variants that lack mitogenic activity yet retain high affinity receptor binding. EMBO J. 11(7):2503-2510.

Ma PC, Kijima T, Maulik G, Fox EA, Sattler M, Griffin JD, Johnson BE, Salgia R. 2003. c-MET mutational analysis in small lung cancer: novel juxtamembrane domain mutations regulating cytoskeletal functions. Cancer Res. 63(19):6272-6281.

Machner MP, Frese S, Schubert W, Orian-Rousseau V, Gherardi E, Wehland J, Niemann HH, Heinz DW. 2003. Aromatic amino acids at the surface of InlB are essential for host cell invasion by *Listeria* monocytogenes. Mol. Microbiol. 48(6):1525-1536.

Maroun CR, Holgado-Madruga M, Royal I, Naujokas MA, Fournier TM, Wong AJ, Park M. 1999. The Gab1 PH domain is required for localization of Gab1 at sites of cell-cell contact and epithelial morphogenesis downstream from the met receptor tyrosine kinase. Mol Cell Biol. 19(3):1784-99.

Maroun CR, Naujokas MA, Holgado-Madruga M, Wong AJ, Park M. 2000. The tyrosine phosphatase SHP-2 is required for sustained activation of extracellular signal-regulated kinase and epithelial morphogenesis downstream from the met receptor tyrosine kinase. Mol Cell Biol. 20(22):8513-8525.

Matsumoto K, Nakamura T. 2001. Hepatocyte growth factor: renotropic and potential therapeutics for renal diseases. Kidney Int. 59(6):2023-2038.

Michalopoulos GK, DeFrances MC. 1997. Liver regeneration. Science 276(5309):60-66.

Moehren G, Markevich N, Demin O, Kiyatkin A, Goryanin I, Hoek JB, Kholodenko BN. 2002. Temperature dependence of the epidermal growth factor receptor signaling network can be accounted for by a kinetic model. Biochemistry 41(1):306-20.

Mohammadi M, Froum S, Hamby JM, Schroeder MC, Panek RL, Lu GH, Eliseenkova AV, Green D, Schlessinger J, Hubbard SR. 1998. Crystal structure of an angiogenesis inhibitor bound to the FGF receptor tyrosine kinase domain. EMBO J. 17(20):5896-904.

Mohammadi M, Olsen SK, Goetz R. 2005. A protein canyon in the FGF-FGF receptor dimer selects from an a la carte menu of heparan sulfate motifs. Curr. Opin. Struct. Biol. 15:506-516.

Mohammadi M, Schlessinger J, Hubbard SR. 1996. Structure of the FGF receptor tyrosine kinase domain reveals a novel autoinhibitory mechanism. Cell 86(4):577-87.

Murray BW, Padrique ES, Pinko C, McTigue MA. 2001. Mechanistic effects of autophosphorylation on receptor tyrosine kinase catalysis: enzymatic characterization of Tie2 and phospho-Tie2. Biochemistry 40(34):10243-53.

Nakamura T, Nishizawa T, Hagiya M, Seki T, Shimonishi M, Sugimura A, Tashiro K, Shimizu S. 1989. Molecular cloning and expression of human hepatocyte growth factor. Nature 342(6248):440-443.

Naldini L, Vigna E, Ferracini R, Longati P, Gandino L, Prat M, Comoglio PM. 1991a. The tyrosine kinase encoded by the MET proto-oncogene is activated by autophosphorylation. Mol. Cell. Biol. 11(4):1793-803.

Naldini L, Vigna E, Narsimhan RP, Gaudino G, R. Z, Michalopoulos GK, Comoglio PM. 1991b. Hepatocyte growth factor (HGF) stimulates the tyrosine kinase activity of the receptor encoded by the proto-oncogene c-MET. Oncogene 6(4):501-4.

Naldini L, Weidner MK, Vigna E, Gaudino G, Bardelli A, Ponzetto C, Narsimhan RP, Hartmann G, Zarnegar R, Michalopoulos GK and others. 1991c. Scatter factor and hepatocyte growth factor are indistinguishable ligands for the MET receptor. EMBO J. 10(10):2867-78.

Offterdinger M, Georget V, Girod A, Bastiaens PI, H. 2004. Imaging phosphorylation dynamics of the epidermal growth factor receptor. J. Biol. Chem. 279(35):36972-36981.

Ogiso H, Ishitani R, Nureki O, Fukai S, Yamanaka M, Kim JH, Saito K, Sakamoto A, Inoue M, Shirouzu M and others. 2002. Crystal structure of the complex of human epidermal growth factor and receptor extracellular domains. Cell 110:775-87.

Ohta K, Mizutani A, Kawakami A, Murakami Y, Kasuya Y, Takagi S, Tanaka H, Fujisawa H. 1995. Plexins: a novel neuronal cell surface molecule that mediates cell adhesion via a homopholic binding mechanism in the presence of calcium ions. Neuron 14:1189-1199.

Orian-Rousseau V, Chen L, Sleeman JP, Herrlich P, Ponta H. 2002. CD44 is required for two consecutive steps in HGF/c-MET signaling. Genes Dev. 16(23):3074-3086.

Osawa M, Itoh S, Ohta S, Huang Q, Berk BC, Marmarosh NL, Che W, Ding B, Yan C, Abe J. 2004. ERK1/2 associates with the c-MET binding domain of growth factor receptor-bound protein 2 (Grb2)-associated binder-1 (Gab1): role in ERK1/2 and early growth response factor-1 (Egr-1) nuclear accumulation. J. Biol. Chem. 279(28):29691-29699.

Ostman A, Bohmer FD. 2001. Regulation of receptor tyrosine kinase signaling by protein tyrosine phosphatases. Trends Cell Biol 11(6):258-66.

Palka HL, Park M, Tonks NK. 2003. Hepatocyte growth factor receptor tyrosine kinase met is a substrate of the receptor protein-tyrosine phosphatase DEP-1. J. Biol. Chem. 278(8):5728-5735.

Parast CV, Mroczkowski B, Pinko C, Misialek S, Khambatta G, Appelt K. 1998. Characterization and kinetic mechanism of catalytic domain of human vascular endothelial growth factor receptor-2 tyrosine kinase (VEGFR2 TK), a key enzyme in angiogenesis. Biochemistry 37(47):16788-801.

Pazin MJ, Williams LT. 1992. Triggering signaling cascades by receptor tyrosine kinases. Trends. Biochem. Sci. 17:374-378.

Pelicci G, Giordano S, Zhen Z, Salcini AE, Lanfrancone L, Bardelli A, Panayotou G, Waterfield MD, Ponzetto C, Pelicci PGea. 1995. The motogenic and mitogenic responses to HGF are amplified by the Shc adapter protein. Oncogene 10(8):1631-1638.

Ponzetto C, Bardelli A, Maina F, Longati P, Panayotou G, Dhand R, Waterfield MD, Comoglio PM. 1993. A novel recognition motif for phosphatidylinositol 3-kinase binding mediates its association with the hepatocyte growth factor/scatter factor receptor. Mol. Cell. Biol. 13:4600-4608.

Ponzetto C, Bardelli A, Zhen Z, Maina F, dalla Zonca P, Giordano S, Graziani A, Panayouto G, Comoglio PM. 1994. A multifunctional docking site mediates signaling and transformation by the hepatocyte growth factor/scatter factor receptor family. Cell 77(2):261-271.

Posner BI, Faure R, Burgess JW, Bevan AP, Lachance D, Zhang-Sun G, Fantus IG, Ng JB, Hall DA, Lum BS and others. 1994. Peroxovanadium compounds. A new class of potent phosphotyrosine phosphatase inhibitors which are insulin mimetics. J. Biol. Chem. 269(6):4596-604.

Posner I, Engel M, Levitzki A. 1992. Kinetic model of the epidermal growth factor (EGF) receptor tyrosine kinase and a possible mechanism of its activation by EGF. J. Biol. Chem. 267(29):20638-47.

Potempa S, Ridley AJ. 1998. Activation of both MAP kinase and phosphatidylinositide 3-kinase by Ras is required for hepatocyte growth factor/scatter factor-induced adherens junction disassembly. Mol. Biol. Cell. 9(8):2185-2200.

Prat M, Crepaldi T, Pennacchietti S, Bussolino F, Comoglio PM. 1998. Agonistic monoclonal antibodies against the Met receptor dissect the biological responses to HGF. J. Cell Sci. 111(Pt 2):237-247.

Preschard P, Fournier TM, Lamorte L, Naujokas MA, Band H, Langdon WY, Park M. 2001. Mutation of the c-Cbl TKB domain binding site on the Met receptor tyrosine kinase converts it into a transforming protein. Mol Cell 8(5):995-1004.

Preschard P, Noboru I, Tong L, Lipkowitz S, Park M. 2004. A conserved DpYR motif in the juxtamembrane domain of Met receptor family form an atypical c-Cbl/Cbl-b tyrosine kinase binding domain binding site required for suppression of oncogenic activation. J. Biol. Chem. 279(28):29565-29571.

Rahimi N, Hung W, Tremblay E, Saulnier R, Elliott B. 1998. c-Src kinase activity is required for hepatocyte growth factor-induced motility and anchorage-independent growth of mammary carcinoma cells. J. Biol. Chem. 273(50):33714-33721.

Rodrigues GA, Park M. 1993. Dimerization mediated through a leucine zipper activates the oncogenic potential of the met receptor tyrosine kinase. Mol. Cell. Biol. 13(11):6711-22.

Rodrigues GA, Park M. 1994. Autophosphorylation modulates the kinase activity and oncogenic potential of the Met receptor tyrosine kinase. Oncogene 9(7):2019-27.

Rong S, Segal S, Anver M, Resau JH, Vande Woude GF. 1994. Invasiveness and metastasis of NIH 3T3 cells induced by Met-hepatocyte growth factor/scatter factor autocrine stimulation. Proc. Natl. Acad. Sci. U S A 91(11):4731-4735.

Ronsin C, Muscatelli F, Mattei MG, Breathnach R. 1993. A novel putative receptor protein tyrosine kinase of the met family. Oncogene 8(5):1195-1202.

Royal I, Fournier TM, Park M. 1997. Differential requirement of Grb2 and PI3-kinase in HGF/SF-induced cell motility and tubulogenesis. J. Cell Physiol 173(2):196-201.

Royal I, Park M. 1995. Hepatocyte growth factor-induced scatter of Maldin-Darby canine kidney cells requires phosphatidylinositol 3-kinase. J. Biol. Chem. 270(46):27780-27787.

Sachs K, Gifford D, Jaakkola T, Sorger P, Lauffenburger DA. 2002. Bayesian network approach to cell signaling pathway modeling. Sci STKE 148:PE38.

Sachs M, Brohmann H, Zechner D, Muller T, Hulsken J, Walther I, Schaeper U, Birchmeier C, Birchmeier W. 2000. Essential role of Gab1 for signaling by the c-MET receptor in vivo. J. Cell Biol. 150(6):1375-1384.

Schaeper U, Gehring NH, Fuchs KP, Sachs M, Kempkes B, Birchmeier W. 2000. Coupling of Gab1 to c-MET, Grb2, and Shp2 mediated biological responses. J. Cell Biol. 149(7):1419-1432.

Schiering N, Knapp S, Marconi M, Flocco MM, Cui J, Perego R, Rusconi L, Cristiani C. 2003. Crystal structure of the tyrosine kinase domain of the hepatocyte growth factor c-MET and its complex with the microbial alkaloid K-252a. Proc. Natl. Acad. Sci. U S A 100(22):12654-12659.

Schlessinger J. 2000. Cell signaling by receptor tyrosine kinases. Cell 103(2):211-25.

Schlessinger J, Plotnikov AN, Ibrahimi OA, Eliseenkova AV, Yeh BK, Yayon A, Linhardt RJ, Mohammadi M. 2000. Crystal structure of a ternary FGF-FGFR-heparin complex reveals a dual role for heparin in FGFR binding and dimerization. Mol. Cell. 6:743-750.

Schlessinger J, Ullrich A. 1992. Growth factor signaling by receptor tyrosine kinases. *Neuron* 9(3):383-91.

Schmidt C, Bladt F, Goedecke S, Brinkmann V, Zschiesche W, Sharpe M, Gherardi E, Birchmeier C. 1995. Scatter factor/hepatocyte growth factor is essential for liver development. Nature 373(6516):699-702.

Seveau S, Bierne H, Giroux S, Prevost M-C, Cossart P. 2004. Role of lipid rafts in E-cadherin-and HGF-R/Met-mediated entry in Listeria moncytogenes into host cells. J. Cell Biol. 166(5):743-753.

Shen Y, Naujokas MA, Park M, Ireton K. 2000. InlB-dependent internalization of *Listeria* is mediated by the Met receptor tyrosine kinase. Cell 103:501-510.

Sherrill JM. 1997. Self-phosphorylation of epidermal growth factor receptor is an intermolecular reaction. Biochemistry 36(42):12890-6.

Sheth PR, Watowich SJ. 2005. Oligomerization-induced differential dephosphorylation of c-MET receptor tyrosine kinase. Biochemistry 44(33):10984-93.

Shimizu A, Persson C, Heldin CH, Ostman A. 2001. Ligand stimulation reduces platelet-derived growth factor beta-receptor susceptibility to tyrosine dephosphorylation. J. Biol. Chem. 276(30):27749-27752.

Stamos J, Lazarus RA, Yao X, Kirchhofer D, Wiesmann C. 2004. Crystal structure of the HGF beta-chain in complex with Sema domain of the Met receptor. EMBO J. 23(12):2325-2335.

Stoker M, Gherardi E, Perryman M, Gray J. 1987. Scatter factor is a fibroblast-derived modulator of epithelial cell mobility. Nature 327(6119):239-242.

Stoker M, Perryman M. 1985. An epithelial scatter factor released by embryo fibroblasts. J. Cell. Sci. 77:209-223.

Treadway JL, Morrison BD, Soos MA, Siddle K, Olefsky J, Ullrich A, McClain DA, Pessin JE. 1991. Transdominant inhibition of tyrosine kinase activity in mutant insulin/insulin-like growth factor I hybrid receptors. Proc. Natl. Acad. Sci. U S A 88(1):214-218.

Trusolino L, Bertotti A, Comoglio PM. 2001. A signaling adapter function for alpha6beta4 integrin in the control of HGF-dependent invasive growth. Cell 107(5):643-654.

Trusolino L, Comoglio PM. 2002. Scatter-factor and semaphorin receptors: cell signaling for invasive growth. Nat. Rev. Cancer. 4:289-300.

Uehara Y, Minowa O, Mori C, Shiota K, Kuno J, Noda T, Kitamura N. 1995. Placental defect and embryonic lethality in mice lacking hepatocyte growth factor/scatter factor. Nature 373(6516):702-705.

Ullrich A, Schlessinger J. 1990. Signal transduction by receptors with tyrosine kinase activity. Cell 61:203-212.

Ultsch M, Lokker NA, Godowski PJ, deVos AM. 1998. Crystal structure of the NK1 fragment of human hepatocyte growth factor at 2.0 A resolution. Structure 6(11):1383-1393.

van der Voort R, Taher TE, Derksen PW, Spaargaren M, van der Neut R, Pals ST. 2000. The hepatocyte growth factor/Met Pathway in development, tumorigenesis, and B-cell differentiation. Adv. Cancer Res. 79:39-90.

Villalba M, Wente SR, Russell DS, Ahn JC, Reichelderfer CF, Rosen OM. 1989. Another version of the human receptor kinase domain: expression, purification and characterization. Proc. Natl. Acad. Sci. U S A 86(20):7848-7852.

Villa-Moruzzi E, Lapi S, Prat M, Gaudino G, Comoglio PM. 1993. A protein tyrosine phosphatase activity associated with the hepatocyte growth factor/scatter factor receptor. J. Biol. Chem. 268(24):18176-18180.

Villa-Moruzzi E, Puntoni F, Bardelli A, Vigna E, De Rosa S, Comoglio PM. 1998. Protein tyrosine phosphatase PTP-S binds to the juxtamembrane region of the hepatocyte growth factor receptor Met. Biochem. J. 336:235-239.

Walker DH, Kuppuswamy D, Visvanathan A, Pike LJ. 1987. Substrate specificity and kinetic mechanism of human placental insulin receptor/kinase. Biochemistry 26(5):1428-33.

Ward WH, Cook PN, Slater AM, Davies DH, Holdgate GA, Green LR. 1994. Epidermal growth factor receptor tyrosine kinase. Investigation of catalytic mechanism, structure-based searching and discovery of a potent inhibitor. Biochem. Pharmacol. 48(4):659-666.

Weber W, Bertics PJ, Gill GN. 1984. Immunoaffinity purification of the epidermal growth factor receptor. Stoichiometry of binding and kinetics of self-phosphorylation. J. Biol. Chem. 259(23):14631-14636.

Weidner KM, Sachs M, Riethmacher D, Birchmeier W. 1995. Mutation of juxtamembrane tyrosine residue 1001 suppresses loss-of-function mutations of the met receptor in epithelial cells. Proc. Natl. Acad. Sci. U S A 92:2597-2601.

Wiesmann C, Fuh G, Christinger HW, Eigenbrot C, Wells JA, de Vos AM. 1997. Crystal structure at 1.7 A resolution of VEGF in complex with domain 2 of the Flt-1 receptor. Cell 91(5):695-704.

Wiley HS, Shvartsman SY, Lauffenburger DA. 2003. Computational modeling of the EGF-receptor system: a paradigm for systems biology. Trends Cell Biol. 13(1):43-50.

Winberg ML, Noordermeer JN, Tamagnone L, Comoglio PM, Spriggs MK, Tessier-Lavigne M, Goodman CS. 1998. Plexin A is neuronal semaphorin receptor that controls axon guidance. Cell. 95:903-916.

Wong TW, Goldberg AR. 1984. Kinetics and mechanism of angiotensin phosphorylation by the transforming gene product of Rous sarcoma virus. J. Biol. Chem. 259(5):3127-3131.

Xiao GH, Jeffers M, Bellacosa A, Mitsuuchi Y, Vande Woude GF, Testa JR. 2001. Anti-apoptotic signaling by hepatocyte growth factor/Met via the phosphatidylinositol 3-kinase/Akt and mitogen-activated protein kinase pathways. Proc. Natl. Acad. Sci. U S A 98(1):247-252.

Yarden Y, Schlessinger J. 1987. Epidermal growth factor induces rapid, reversible aggregation of the purified epidermal growth factor receptor. Biochemistry 26(5):1443-1451.

Yuan CJ, Jakes S, Elliott S, Graves DJ. 1990. A rationale for the design of an inhibitor for tyrosyl kinase. J. Biol. Chem. 265(27):16205-9.

Zhang YW, Graveel C, Shinomiya N, Vande Woude GF. 2004. Met decoys: will cancer take the bait? Cancer Cell. 6(1):5-6.

Zhang YW, Wang LM, Jove R, Vande Woude GF. 2002. Requirement of Stat3 signaling for HGF/SF-Met mediated tumorigenesis. Oncogene 21(2):217-226.

VITA

Payal Sheth was born on July 2nd, 1979, in Mumbai, India. After attending the University of Mumbai for her Bachelor's degree, Payal matriculated at the University of Texas Medical Branch. In 2005, Payal was awarded the James W. McLaughlin predoctoral fellowship. During her graduate tenure, Payal also attended several international conferences in her field including the FASEB summer research conference- Growth factor receptor tyrosine kinases in mitogenesis, morphogenesis and tumorigenesis at Tuscon, AZ, the Keystone Symposia on Cancer and Kinases- Lessons from the clinics at Santa Fe, NM and Protein Kinase Resource Workshop at Monterey, CA, where she presented posters. Based on her research, she was awarded travel awards for two of the above mentioned international conferences - Protein Kinase Resource Travel Award in 2003 and Keystone Symposia Student Travel grant in 2005. She was also received several awards for poster presentations at intramural scientific meetings including McLaughlin Symposium in 2006, Biochemistry and Molecular Biology Orientation in 2005, and 2004 and the 12th Annual Science Forum in 2004.

Education

B.E., Chemical Engineering, July 2001, University of Mumbai, India

Publications

Sheth, P. R., Watowich S.J. 2006. Biochemical ground-rules regulating c-MET receptor tyrosine kinase activation. *Cancer Therapy*. 4(A)- 1-15

Sheth, P. R., Watowich S.J. 2005. Oligomerization-induced differential dephosphorylation of c-MET receptor tyrosine kinase. *Biochemistry*. 44(33)-10984-93

Sheth, P. R., Hays, J. L., Elferink, L. A., Watowich S.J. 2006. A feed-forward loop provides a functional switch for c-MET activation (*Submitted*)

Sheth, P. R., Watowich, S. J. 2006. Structure-based design of receptor tyrosine kinase inhibitors (In preparation)